Paleokarst reservoir modelling - A concept-driven approach

Bjarte Lønøy

Thesis for the degree of Philosophiae Doctor (PhD)
University of Bergen, Norway
2021

UNIVERSITY OF BERGEN

Paleokarst reservoir modelling - A concept-driven approach

Bjarte Lønøy

Thesis for the degree of Philosophiae Doctor (PhD)
at the University of Bergen

Date of defense: 20.08.2021

Year: 2021

Title: Paleokarst reservoir modelling - A concept-driven approach

Name: Bjarte Lønøy

Print: Skipnes Kommunikasjon / University of Bergen

PALEOKARST RESERVOIR MODELLING

A concept-driven approach

Bjarte Lønøy

Dissertation for the degree Philosophiae Doctor (PhD)

NORCE – Norwegian Research Centre AS, Bergen, Norway

Energy

University of Bergen, Bergen, Norway

Department of Earth Science

University of Bristol, Bristol, UK

Dedication

This thesis is dedicated to my grandfather Norvald Lønøy (1925-2020), who sadly passed away during the completion of my doctorate. He has been a great inspiration and one of the reasons why I found interest in natural sciences.

Acknowledgements

Although I have declared that most of the thesis work was conducted by myself, the research would not be possible without the loving support of many great people.

First, I would like to express great gratitude to my principal supervisor Jan Tveranger (NORCE - Norwegian Research Centre AS) for believing in me and giving me the chance to pursue my dream of a PhD within carbonates, and more specifically within karst/paleokarst. His ability to share his extensive knowledge in an educational and welcoming manner is admirable. Although his office door was often closed due to a busy schedule, I always felt I could run down his door for a discussion. Jan has become not only a good colleague but also a friend and I hope that I will adopt many of the strong characteristics of Jan as a fantastic leader, researcher, and human.

What could potentially be more rewarding than having one outstanding principal supervisor? The short answer is having additional four excellent supervisors: Prof. Stein-Erik Lauritzen (University of Bergen), Assoc. Prof. Isabelle Lecomte (University of Bergen), Dr. Øystein Pettersen (NORCE) and Prof. Fiona Whitaker (University of Bristol). I am truly grateful for all your support throughout my PhD. A special thanks go to Fiona Whitaker, who took great care of my family and me during my research stay at the University of Bristol. She has been a great inspiration and a fantastic supervisor and friend.

Postdoc Christos Pennos has been a fantastic colleague, co-author and "partner in crime". He has also functioned as a mentor, willingly sharing his extensive caving skills and karst knowledge. We became good friends at an early stage, and through time the friendship has become stronger and highly valued.

Another project member that is highly valued is Kristian Jensen. He has been a great motivator and colleague throughout the PhD period. Kristians' ability to converse about all and nothing have resulted in many great discussions on and off-topic. He also contributed to the initial fieldwork in Greece and assisted with the ERT survey. Kristian is an amazing geophysicist that I hope to work with in the future.

In the absence of useful cave data in the initial phase of the research, Jim Coke offered to share his cave survey. The comprehensive dataset provided was unfortunately in a format I couldn't use. However, his willingness to share years and years of hard work with a "total stranger" shows what a great man he is. I will always appreciate his kindness and respect him for his offer. Many thanks, Jim.

At NORCE, I´ve had many great colleagues throughout my doctorate, and all are highly valued. A special thanks go to Bartek Florczyk Vik, Edin Alagic, Eivind Bastesen, Walter Wheeler, Beate Hovland, Audun Libak, Tove Leiknes Eide, Rikke Helen Ulvøen, Simon Johan Buckley, Nicole Naumann, Kari Ringdal, Nicole Dopffel, Benjamin Dolva, Anita Torabi and Tobias Herbert Kurz. Also, I have had the pleasure to get to know many fantastic fellow PhD students and colleagues from the University of Bergen: Thomas Thuesen, Dr. Björn Nyberg, Dr. Casey Nixon, Assoc. Prof. Christian Eide, Dr. Isabelle "Izzy" Edmundson, May Britt Kjærevik Zachariah, Dr. Sofia Pechlivanidou, Vilde Dimmen, Prof. Atle Rotevatn, Dr. Leif-Erik Rydland Pedersen, Linn Merethe Olsen, and Albina Gilmullina.

During my research stay at the University of Bristol, Dr. Rattana Thirathititham, Rungroj Benjakul, Joao Paulo Gomes and Otávio August took great care of me. They showed me around the campus and city, and generously invited me into their "group". We have become good friends and I hope our paths will cross again and that I´ll have the pleasure of working alongside these great people in the future.

I would also like to express my outermost gratitude to Assoc. Prof. Gunnar Sælen. In addition to be a fantastic supervisor during my MSc research, he has been a great inspiration, a good friend and colleague throughout the years.

Throughout the doctorate, many great researchers have provided crucial input to my work, eventually improving the final research. In particular: Gordon Coy, Mateu Esteban Cerdá, Pedro Augustin Robledo Ardila, Luis Pomar and Maurice Tucker have contributed with scientific discussions and suggestions. Many thanks for all your help.

The Maaras Tourist Centre by Nikos "Tom Cruise of Prosotani" Diafas and Dimitris Stergiakos, are recognised for offering facilities to prepare for fieldwork and delicious

coffee in the morning. The Hellenic Ministry of culture is acknowledged for granting access to the caves.

Experiencing the wonderful caves of Greece would not be the same without some native caving buddies. Eugenia Kiourexidou, Stavros Zachariadis, Tasos Polihroniadis and Yorgos Sotiriadis, many thanks for some fun caving memories.

Finally, the completion of the doctorate would not have been possible without the strong backing from my family. My fantastic partner Marion Rodgers Løseth has gone that extra mile to support me through challenging times, and I feel lucky to have her as a partner and mother to my children. My precious children Olava and Leon have helped me keep the spirit up and brought happiness being loving and kind. My parents, Doris Iren Fyllingen and Arve Lønøy, and my stepmom Elena Kuzmina have assisted me with babysitting and daily chores so that I could work extra hours. My father has also contributed to scientific discussions and proofreading, which have been very useful and improved my work. My "mother in law" Nina Rodgers has assisted by babysitting Olava and cooking dinner, and for that, I am truly grateful.

Bjarte Lønøy Bergen, December 2020

Bjarte Lønøy

Preface

Scientific environment

The work presented in this PhD thesis was initially undertaken at the Centre for Integrated Petroleum Research (Uni CIPR, division of Uni Research) and the Department of Earth Science at the University of Bergen. The former research company (Uni Research) later merged with several other research institutions to form NORCE – Norwegian Research Centre AS and is where the research was finalised. A research stay was carried out in 2018 at the School of Earth Science, University of Bristol, UK. The research stay was supervised by Professor Fiona Whitaker. Substantial fieldwork was carried out in northern Greece.

Main supervisor:

Dr. Jan Tveranger (NORCE – Norwegian Research Centre AS)

Co-supervisors:

Professor Stein-Erik Lauritzen (University of Bergen)

Associate Professor Isabelle Lecomte (University of Bergen)

Dr. Øystein Pettersen (NORCE – Norwegian Research Centre AS)

Professor Fiona Whitaker (University of Bristol)

Project Information & funding

This three-year PhD project was financed by the Norwegian Research Council's PETROMAKS2 program and is part of the FOPAK project initiated by Jan Tveranger in 2016 ("FOPAK – Forecasting of architecture, seismic characteristics, and flow behavior in paleokarst reservoirs" - project number: 267634). The project includes four supervisory professors: Dr. Jan Tveranger (research leader and principal supervisor), Dr. Stein-Erik Lauritzen (co-supervisor), Dr. Isabelle Lecomte (co-supervisor), Dr. Øystein Pettersen (co-supervisor) and Dr. Fiona Whitaker (co-supervisor), one postdoc: Dr. Christos Pennos, two PhD candidates: Bjarte Lønøy (myself) and Kristian Jensen, and a couple of master students: Martin Kyrkjebø Johansen, Tor Jarle Grimstad, and Mustaqim Balyesiima. This thesis constitutes one of multiple work packages within the FOPAK research project and was primarily supervised by Jan Tveranger.

A World University Networks (WUN) researcher mobility grant was awarded in 2018 and funded the University of Bristol research stay. Conference attendance and associated travel cost were mainly financed by the project (Norwegian Research Council project funding). The Academia agreement awarded additional funding for attending the AGU 100 Fall Meeting and for inviting guest researcher Dr. Mateu Esteban Cédra to Bergen. Dr. Esteban was invited to give a presentation on paleokarst reservoirs at the University of Bergen (hosted by NGF) and Equinor, and to contribute to the ongoing FOPAK project. In 2019, Bjarte Lønøy was one of the plenary speakers at the "Bathurst Meeting of Carbonate Sedimentologist 2019". This conference attendance was partially funded by "The Paul Milroy carbonate award" awarded early 2019.

Software and data access

Academic software licenses were kindly provided by ROXAR – EMERSON (RMS™), ArcGIS (ArcMAP™), MathWorks (MATLAB™) and Google (Google Earth Pro™ & Google Earth Studio™). Permission to access the studied caves were generously provided to Christos Pennos by The Hellenic Ministry of Culture (reference number: ΥΠΠΟΑ/ΓΔΑΠΚ/ΕΠΣ/ΤΑΠΠΠ/307618/181597/5084/2126). The Microsoft 365™ apps were used to generate plots and graphs, and to develop the forward collapse

modelling tool. All caves surveys applied in this thesis was provided by Dr. Christos Pennos. Dr. Pennos was either the principal surveyor or part of the team conducting the surveys. All cave survey data was provided in a *.top-file format, and PocketTopo (Heeb, 2010) was used to export the data to suitable file formats. 2D maps and 3D "exoskeleton" models of the caves were constructed using the free open-source software Therion (Budaj and Mudrák, 2008; Budaj and Stacho, 2019). Point-cloud generation of the karst/paleokarst systems (pre-/post-collapse) was generated using a MATLAB™ algorithm developed by Dr. Christos Pennos. Most maps were made in ArcGIS except some of the maps included in Paper III which were constructed using the free and open-source software QGIS™.

Note that other software combinations may achieve similar results to those presented here, and that the proposed workflows may not be limited to the software combination mentioned above.

Thesis structure

A short introduction of the thesis structure is provided for readers accustomed to a monographic dissertation. This article-based dissertation comprises two main parts and an appendix:

Part I – Background and synthesis: The first part introduces the scientific objectives of the research and provides a short introduction to various cross-disciplinary topics addressed in this work. The main results are synthesized in Part I and addressed in depth in the various papers.

Part II – Papers: This section presents an assembly of the three research articles which make up the bulk of work conducted during the PhD study.

Appendix: The appendix list selected conference abstracts and poster presentations (A4 scale to fit the thesis format) presented or co-authored during the PhD study.

Scientific manuscripts and contributions

The following manuscripts are in included in this PhD dissertation and are reproduced in Part II. Other scientific contributions not included in the thesis are summarised below.

Paper I

Lønøy, B., Tveranger, J., Pennos, C., Whitaker, F., & Lauritzen, S. E. (2020). *Geocellular rendering of cave surveys in paleokarst reservoir models. Marine and Petroleum Geology, 122, 104652.*

Paper II

Lønøy, B., Pennos, C., Tveranger, J., Fikos, I., Vargemezis, G., & Lauritzen, S. E. (2021). *Delimiting morphological and volumetric elements of cave surveys as analogues for paleokarst reservoir modelling – A case study from the Maaras cave system, northern Greece. Marine and Petroleum Geology (In press).*

Paper III

Lønøy, B., Pennos, C., Tveranger, J., Fikos, I., Vargemezis, G., & Lauritzen, S. E. *A concept-driven approach to paleokarst reservoir modelling. To be submitted to The American Association of Petroleum Geologists Bulletin (AAPG).*

Other scientific contributions:

2019

Fikos, Ilias; Vargemezis, George; Pennos, Christos; Lønøy, Bjarte; Jensen, Kristian; Tveranger, Jan.
Processing 2D ERT-data in 3D environment: A case study inside a karstic cave in North Greece. EAGE Near Surface Geoscience; 8-13. September

Lønøy, Bjarte; Pennos, Christos; Tveranger, Jan; Fikos, Ilias; Vargemezis, George; Jensen, Kristian; Lauritzen, Stein-Erik.
Sediment accumulations in paleokarst reservoirs - Analogues from an active cave system. Bathurst Meeting of Carbonate Sedimentologists; 5-13. July.

Lønøy, Bjarte; Pennos, Christos; Tveranger, Jan; Lauritzen, Stein-Erik; Furnée, Jon Petter; Ledsaak, Karina.
Paleokarst reservoir modelling based on active cave system analogs - implementing cave survey data in geocellular reservoir models. NGF Winter conference; 7-9. January.

Lønøy, Bjarte; Pennos, Christos; Tveranger, Jan; Lauritzen, Stein-Erik; Furnée, Jon Petter; Ledsaak, Karina.
Paleokarst reservoir modelling based on recent cave system analogs - A novel methodology for importing geometrically complex geobodies into geocellular reservoir models. AGU Fall Meeting; 9-13. December.

Tveranger, Jan; Kaschwich, Tina; Lauritzen, Stein-Erik; Lecomte, Isabelle; Lønøy, Bjarte; Pennos, Christos; Pettersen, Øystein.
A genetic approach for characterising paleokarst reservoirs. NGF Winter Meeting; 7-9. January.

2018

Pennos, Christos; Lauritzen, Stein-Erik; Lønøy, Bjarte; Tveranger, Jan.
A 3D model of a cave collapse from Peristerionas cave, northern Greece. EGU General Assembly; 8-13. April.

Authorship and workload of the thesis

Bjarte Lønøy is the sole author of Part I of this PhD thesis, and the principal author of all manuscripts reproduced in Part II. The approximate contribution to each manuscript is tabulated below.

Paper I: Geocellular rendering of cave surveys in paleokarst reservoir models	
Principal Author	Bjarte Lønøy
Co-authors	Jan Tveranger, Christos Pennos, Fiona Whitaker & Stein-Erik Lauritzen
Text	Lønøy, Tveranger, Pennos and Whitaker
Figures/Tables	Lønøy
Fieldwork and sampling	Pennos + associated surveyors (cave survey)
Data processing	Lønøy (reservoir modelling & methodology) Pennos (MATLAB point cloud algorithm and methodology) Tveranger (reservoir modelling QC & methodology) Lauritzen (methodology
Discussion and revision	Lønøy, Pennos, Tveranger, Whitaker & Lauritzen
Approximate total contribution	Lønøy: 50% Tveranger: 20% Pennos: 20% Remaining co-authors: 10% in total
Status of manuscript	Published in Marine and Petroleum Geology

Paper II: Delimiting morphological and volumetric elements of cave surveys as analogues for paleokarst reservoir modelling – A case study from the Maaras cave system, northern Greece	
Principal Author	Bjarte Lønøy
Co-authors	Christos Pennos, Jan Tveranger, Ilias Fikos, George Vargemezis & Stein-Erik Lauritzen
Text	Lønøy, Pennos, Tveranger, Fikos and Lauritzen
Figures/Tables	Lønøy and Fikos
Fieldwork and sampling	Lønøy (stratigraphic logging, sediment sampling, tallus mapping & electrical resistivity tomography) Pennos (stratigraphic logging, sediment sampling, tallus mapping, electrical resistivity tomography & cave survey) Fikos (electrical resistivity tomography) Vargemezis (electrical resistivity tomography) Stavros Zachariadis (assisted stratigraphic logging & sediment sampling)
Data processing	Fikos & Vargemezis (electrical resistivity data) Lønøy (grain size analysis) Pennos (grain size analysis)
Discussion and revision	Lønøy, Pennos, Tveranger, Fikos, Vargemezis & Lauritzen
Approximate total contribution	Lønøy: 55% Pennos: 15% Tveranger: 15% Remaining co-authors: 15% in total
Status of manuscript	In press: Marine and Petroleum Geology

Paper III: A concept-driven approach to paleokarst reservoir modelling	
Principal Author	Bjarte Lønøy
Co-authors	Christos Pennos, Jan Tveranger, Ilias Fikos, George Vargemezis & Stein-Erik Lauritzen
Text	Lønøy and Tveranger
Figures/Tables	Lønøy, Fikos (ERT)
Fieldwork and sampling	Lønøy (structural measurements, field reconnaissance) Pennos (cave survey, structural measurements, field reconnaissance)
Data processing	Lønøy (forward collapse modelling tool, data structuring, methodology, reservoir modelling) Pennos (methodology) Tveranger (reservoir modelling QC & methodology) Fikos (electrical resistivity tomography) Vargemezis (electrical resistivity tomography)
Discussion and revision	Lønøy, Pennos, Tveranger, Fikos, Vargemezis & Lauritzen
Approximate total contribution	Lønøy: 70% Pennos: 10% Tveranger: 10% Remaining co-authors: 10% in total
Status of manuscript	To be submitted to The American Association of Petroleum Geologists (AAPG)

Abstract

A significant proportion of the world's hydrocarbon production comes from paleokarst reservoirs. Although these reservoirs boast some of the most productive wells in oil history, the recovery factor is relatively low (RF_{mean}: 32%) compared to other carbonate reservoirs (RF_{mean}: 37 - 51%). The low recovery could relate to current reservoir modelling approaches potentially yielding inaccurate resource estimates or early water-breakthrough. Conventional industry-standard reservoir modelling software suites do not have dedicated workflows or add-ins for handling the complex morphologies commonly associated with paleokarst. Current modelling approaches are often data-driven (conditioned on available seismic and well data) and employ adapted or modified versions of stochastic reservoir modelling workflows used for siliciclastic and carbonate reservoirs. However, many paleokarst features are below seismic resolution, and the representativity of individual well data is often challenging to assess. Consequently, data-driven models often fail to render the connectivity, geometry, and volume of karst features. Karst is the predecessor to paleokarst, and therefore a genetic approach employing existent information from recent karst systems may be a good starting point for generating analogues to paleokarst reservoirs. A concept-driven approach, in combination with current data-driven modelling approaches, may enable model rendering that more closely echoes actual paleokarst reservoir architectures. However, only a few conceptual modelling methods are publicly available and described in the literature. The drawbacks with the available methods are that they under-/overestimate the cave volumes, fail to provide realistic cave morphologies, and forecast clastic sediment infill, and do not differentiate between preserved and collapsed caverns. Consequently, post-collapse reservoir morphologies, volumes and facies distributions may be rendered inaccurately. This thesis aims to address the shortcomings of currently available conceptual methods and present a novel concept-driven workflow for paleokarst reservoir modelling.

A novel methodology for geocellular rendering of karst systems is presented in this thesis. The method utilizes modern cave-survey data to generate dense, equally spaced point-clouds (infilling the cave periphery). These point clouds can be used to discretize

the karst systems in a geocellular framework by geometrical modelling. The volumetric and geometric rendering of the method is compared with two pre-established methods and benchmarked against the cave survey. The results show that the new method offers improved volumetric and geometric geocellular rendering compared to the pre-established methods and are comparable to that of the cave survey.

A pilot study using a well-known and pre-established geophysical method, electrical resistivity tomography (ERT), was carried out in the Maaras cave system in northern Greece to evaluate the large-scale volumetric significance and spatial distribution of clastic sediments infilling karst cavities. ERT proved to be a practical and useful method for differentiating mesoscale (>2.5 m^2) stratigraphic heterogeneity. Resistivity contrasts allowed the identification of sedimentary thickness variations, interbedded breccias, and cave floor. Results showed that the siliciclastic sediment thickness varied from 25 m to >45 m, occupying a minimum of 69-95 % of the available accommodation space.

Finally, a novel interactive tool for evaluating cavern stability and forward model collapse and infill processes was developed. The tool employs conventional cave survey data, field measurements and geomechanical data of the host rock to simulate potential post-collapse morphologies and generate spatial output data suitable for geocellular modelling. Collapse propagation, and eventually the volume affected by the collapse, is controlled by user-defined paleokarst facies proportions and associated average porosities following a “mass-balance-principle” (i.e., porosity is final and only redistributed over a larger volume). Three different collapse scenarios were modelled using the Agios Georgios cave system in northern Greece as an analogue. The results show that it is feasible to use cave surveys to simulate collapse and infill processes and estimate the final paleokarst reservoir architecture. The morphology, volume and relative facies-proportions rendered in the reservoir models are comparable to those calculated in the forward collapse modelling tool, indicating that the geocellular model echoes the simulation. The results also show that the vertical continuity and target volume of a reservoir increases significantly with increasing bedding dip. This suggests that improved forecasting of the final reservoir architecture may optimise well positioning, production planning and eventually improve recovery prediction.

Contents

Part I

Background and Synthesis

This part introduces the scientific problems addressed in this PhD research and outlines the motivation for developing robust concept-driven workflows for paleokarst reservoir modelling. The results are discussed in full length within the individual papers presented in *Part II*, but an overview of the main results is presented and synthesised within a broader framework.

1. Introduction and motivation

This dissertation is linked to the relatively recent hydrocarbon discoveries in paleokarst reservoirs located in the Barents Sea, Norway. Although a well-known reservoir type (e.g., Soudet et al., 1994; Lomando et al., 1993; Kaiser and Pulsipher, 2007; Yan, 2002; Trice, 2005; Zempolich and Cook, 2002; Craig, 1988; White et al., 1995; Coogan et al., 1972; Blickwede and Rosenfeld, 2010), the discoveries of the Gotha field in 2013, and Alta field in 2014, introduced a relatively new reservoir type on the Norwegian continental shelf (NCS). These discoveries ultimately resulted in a demand for new expertise and productions strategies on the NCS. Almost concurrent with the discoveries, the Paris agreement to lower the global emission of greenhouse gases was signed (2015). The world was now determined transitioning into renewable sources of energy (low carbon) to mitigate global warming and reach specific climate goals, and the petroleum industry´s future dimmed. Still, to meet the future global energy consumption, the world is reliant on a broad mixture of energy sources, also including oil and gas. Petroleum and other fossil sources of energy may thus still be in the energy mix for many more years to come. An independent report by Schalk (2019) shows that, even though declining, oil, gas and coal are anticipated to still account for about half of the world's primary energy consumption in 2050 (Fig. 1).

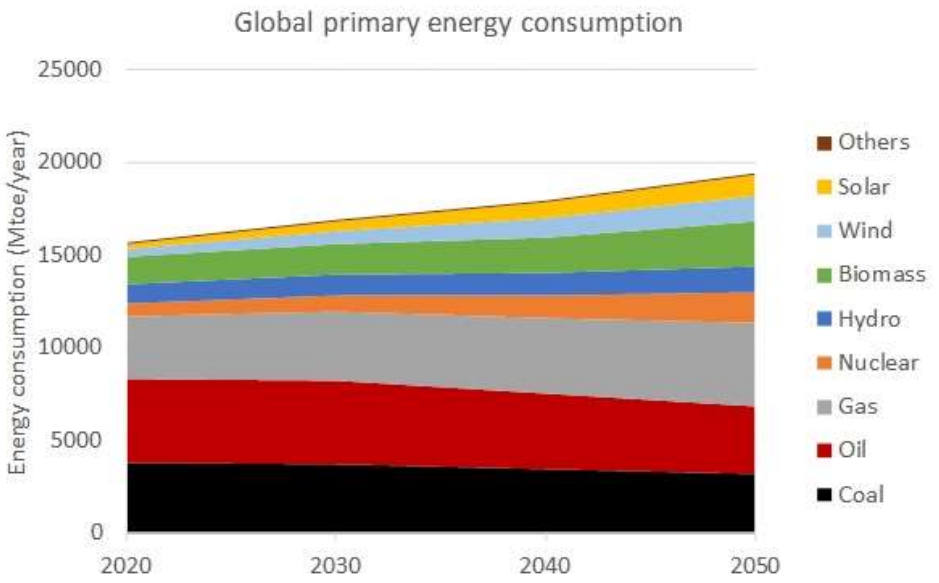

Fig. 1: Predicted global energy consumption by Schalk Cloete (https://energypost.eu/an-independent-global-energy-forecast-to-2050-to-compare-with-the-ieas-weo-2018/)

Even though the initial motivation for the thesis was related to petroleum production, new motivational factors emerged as I became aware of other potential areas where accurate modelling of paleokarsts may be useful. In the search for alternative energy sources and sites to store captured greenhouse gases, paleokarst reservoirs can provide excellent repositories for hydrogen and CO_2. Also, karst aquifers supply more than 15% of the global population with drinking water, and in many regions and countries, these reservoirs are the only available sources of freshwater (Parise et al., 2018). This equal ~1.2 Billion people (2020 world population - www.worldometers.info) being dependant on safe and sustainable water exploitation from this reservoir type. Whether it is for petroleum- and water production or for CO2 and hydrogen storage, paleokarst forms an important type of reservoir the world will be dependent on for years to come. Forecasting of architecture, seismic characteristics, and flow behaviour of paleokarst reservoirs may thus be essential to reach some of the goals for sustainable development set by the UN.

Robust conceptual models, using industry-standard reservoir modelling techniques, may improve our understanding of how to best manage these heterogeneous-, and often

morphologically complex, reservoirs. Combined with seismic modelling (e.g., Jensen et al., 2021) and fluid flow analysis (e.g., Balyesiima, 2020), conceptual models may potentially be used to improve subsurface detectability and production- or storage strategies. In turn, this may result in enhanced recovery/storage and lowering of exploration- and production-related emissions. Yet, most methods for modelling paleokarst used by the industry are proprietary or only exist in the literature as abstracts and MSc theses.

In this PhD thesis, I address some of the issues related to paleokarst reservoir modelling using industry-standard reservoir modelling tools. The work includes developing new methods and tools for mapping clastic sediments within caves, geocellular rendering- and forward collapse simulation of cave systems. I believe that an open cross-disciplinary approach is the best solution for advancing our knowledge of paleokarst reservoirs. The proposed methods and tools are, therefore, designed to be accessible (based on free- or common software suites), transparent (equations are visible) and only dependant on readily available input data.

In the following section, the aim and objectives of the dissertation are presented, followed by a short introduction to the interlinkage between the manuscripts reproduced in Part II. Finally, essential terms and abbreviations are summarised.

1.1 Hypothesis, aims and objectives

This PhD dissertation has a clear hypothesis to be tested:

"Cave surveys can be used to generate conceptual models of paleokarst reservoirs using industry-standard reservoir modelling tools."

To test this hypothesis, pre-established concept-driven methods were evaluated to identify potential weaknesses and pinpoint areas of improvement. This study primarily aims to develop new and improved methods for generating conceptual paleokarst reservoir model analogues using cave surveys as input. The work emphasises on accurate volumetric and geometric rendering, and grid cell coherency. Three papers dealing with various scientific grey boxes of current paleokarst reservoir modelling

techniques constitute the academic contribution of this thesis. The papers address the following topics and associated questions:

- Geocellular rendering of geometrically complex geobodies
  - How can conventional cave survey data be used for geocellular rendering of karst systems?
  - What is the volumetric and geometric accuracy of our proposed method compared to similar pre-established methods?
  - Can grid cell coherency be secured?
- Clastic sediments in karst systems.
  - How does the presence of cave-fill impact the volume and morphology rendered by a cave survey?
  - What is the volumetric importance of clastic sediments in paleokarst reservoirs?
  - Can electrical resistivity tomography (ERT) be used to map clastic sediment thickness distributions and sub-sediment cave floor morphologies within a cave system?
- Forward collapse modelling of karst systems
  - Which parameters control cavern stability?
  - Do all karst corridors collapse during burial?
  - Can we predict cavern stability and forward model the post-collapse morphology and associated facies distribution?
  - What is the impact of bedding dip on cavern stability, post-collapse morphology and reservoir compartmentalisation?
  - What are the uncertainties of the proposed forward collapse modelling tool?

The basic idea behind the thesis is that by developing and sharing relatively simple workflows and tools, we can encourage other researchers to use and hopefully advance our work. I believe that our understanding of paleokarst reservoirs may improve significantly by an open, collective, and cross-disciplinary approach. Thus, the main aim is to develop workflows and tools for generating paleokarst reservoir model analogues

that are accessible for everyone. The generated models should be ready for subsequent petrophysical modelling, fluid flow analyses and seismic modelling .

1.2 Sequence of papers

The manuscripts included in this dissertation are ordered in a “step-by-step” approach leading to a complete workflow for conceptual modelling of paleokarst reservoirs (from outcrop to reservoir model). The sequence of papers is illustrated in Fig. 2.

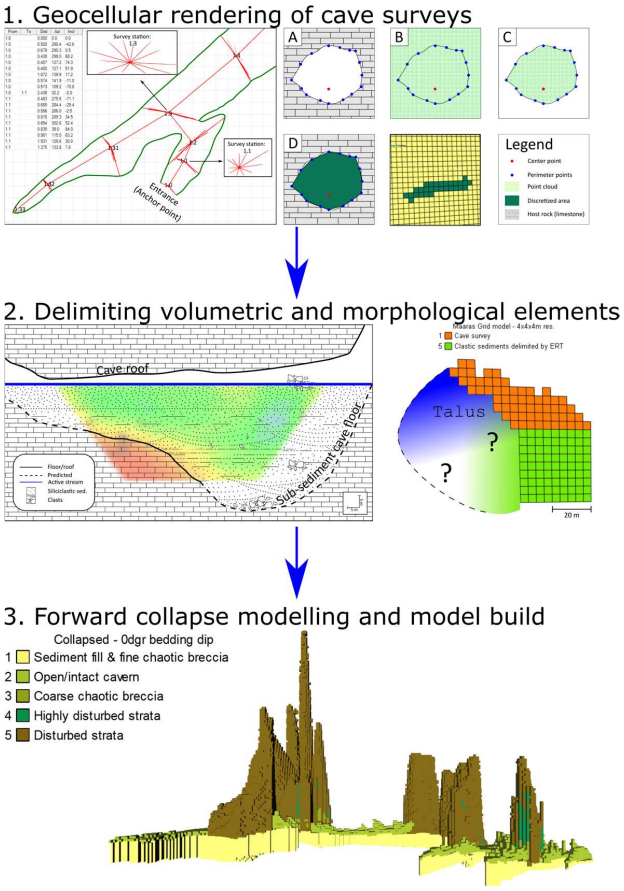

Fig. 2. The sequence of papers. The first paper presents a novel methodology for geocellular rendering of paleokarst reservoirs and benchmark the proposed method against pre-established methods and associated cave survey. The second paper evaluates karst elements that potentially result in inaccurate morphological and volumetric rendering while using cave surveys for grid modelling and demonstrate how these elements can be delimited in a grid model. The third paper presents a new tool for simulating karst collapse processes given various input parameters. This paper utilizes the findings of the previous papers to provide a comprehensive workflow for generating paleokarst reservoir model analogues using recent karst systems as analogues.

The first paper proposes a new method improving geocellular rendering of cave surveys. The geometric and volumetric accuracy of the method is benchmarked against the associated cave survey and the pre-established methods. The second paper evaluates the volumetric significance of clastic sediments in the Maaras cave system in northern Greece and investigates how the presence of clastic sediments may impact the depicted morphology of a cave survey. The final paper includes a newly developed interactive forward collapse modelling tool and associated workflow for geocellular facies discretization. In combination with results from the previous papers, Paper III presents a comprehensive workflow for all steps required to generate a paleokarst reservoir model from cave survey data (from outcrop to reservoir model).

1.3 Terminology and definitions

Centreline	A polygon representing the Euclidean distance between cave survey stations. Note that the term centreline might be misleading as the line is not in a conduit centred position but arranged according to the survey station.
DOI	Depth of investigation. The distance a logging tool can measure.
HC	Hydrocarbon
LRUD	Left, Right, Up and Down. Describing the direction of perimeter measurement of simple cave surveys.
NCS	Norwegian continental shelf
Polje	Large flat-floored, enclosed depression within a karst terrain
Reservoir	A volumetrically defined rock body that function as a repository for fluids and gasses. The fluid/gas composition and -saturation may vary locally within and between reservoirs.

Reservoir model	A mathematical representation of the physical space of a reservoir represented as an array of discrete cells delineated by a grid that can be regular or irregular. A reservoir model is typically constructed to predict subsurface fluid migration, estimate reserves and production planning.
RF	Recovery factor – The percentage of hydrocarbons in place that may be produced by primary, secondary and tertiary recovery methods.
Skeleton line	A set of polygons, connecting all individual cave survey stations, representing a cave system.
Talus	A pile or accumulation of allochthonous or autochthonous unconsolidated rock fragments/clasts. Here, talus is used to describe accumulations of unconsolidated angular clasts since breccia *sensu stricto* implies clasts are held together by either cement or fine-grained matrix. Talus is considered the predecessor to breccia.

2 Background and current state-of-the-art

This PhD thesis includes topics from multiple disciplines, and thus an introduction and summary on various relevant topics is appropriate. In the first section, I give a short theoretical introduction to karst and factors controlling karstification. A brief introduction to karst collapse processes and factors impacting cavern stability is provided to link recent karst systems to sub-surface paleokarst reservoirs. I then introduce paleokarst reservoirs, implications often associated to this reservoir type and how these are currently modelled and handled. Although outside the scope of this thesis, a short summary of other valuable resources commonly associated with karst is added to highlight potential areas where our work may also be applied. Finally, the study areas are described.

2.1 Karst

It is estimated that ~20% of the Earth´s ice-free continental surface is occupied by karst landscapes (Ford and Williams, 2013). Karst is commonly used to describe surface and subsurface landscape features developed on or within especially soluble rocks, such as limestone, marble and gypsum (Ford and Williams, 1989), whereas karstification relates to the dissolution processes eventually forming karst. Karstification can be classified into two main groups, epigene- and hypogene karstification (Palmer, 1991; Loucks, 1999; Gunn, 2004; Klimchouk, 2009; Klimchouk, 2012; Sendra et al., 2014; Audra et al., 2016). Epigene karst is formed by the dissolution of carbonate rocks imposed by CO_2-enriched waters originating from the surface, whereas hypogene karst is formed by chemically aggressive connate water originating from deep-seated sources or by the rejuvenation of epigenetic water by deep-seated processes. The relative abundance between the two karst types is, however, somewhat uncertain in the literature. While Palmer (1991) suggest that epigene karst systems are by far more extensive than hypogene, accounting for approximately 90% of all studied cave systems, Klimchouk (2009) suggest that hypogene are the most common type. The apparent low abundance of hypogene caves suggested by Palmer (1991) could however be a result of the inherent

lack of accessibility to hypogene caves from the surface, and may thus be considered an exploration bias (Sendra et al., 2014).

Note that in this thesis, I primarily focus on epigene karst systems due to data accessibility and thus hypogene karst will not be extensively elaborated. However, the proposed methods, workflows and tools may also be suitable for hypogene karst systems.

2.1.1 Epigene karst

The epigene karst profile can be separated into two main zones based on the water saturation: the vadose and the phreatic (Fig. 3). The vadose zone constitutes karst profiles comprising drained or partly drained pores, fractures, and fissures, whereas in the phreatic zone, these are completely water saturated. The epigene karst profile can be further subdivided into the upper and lower vadose-, shallow and deep phreatic-, and mixing zone (Fig. 3).

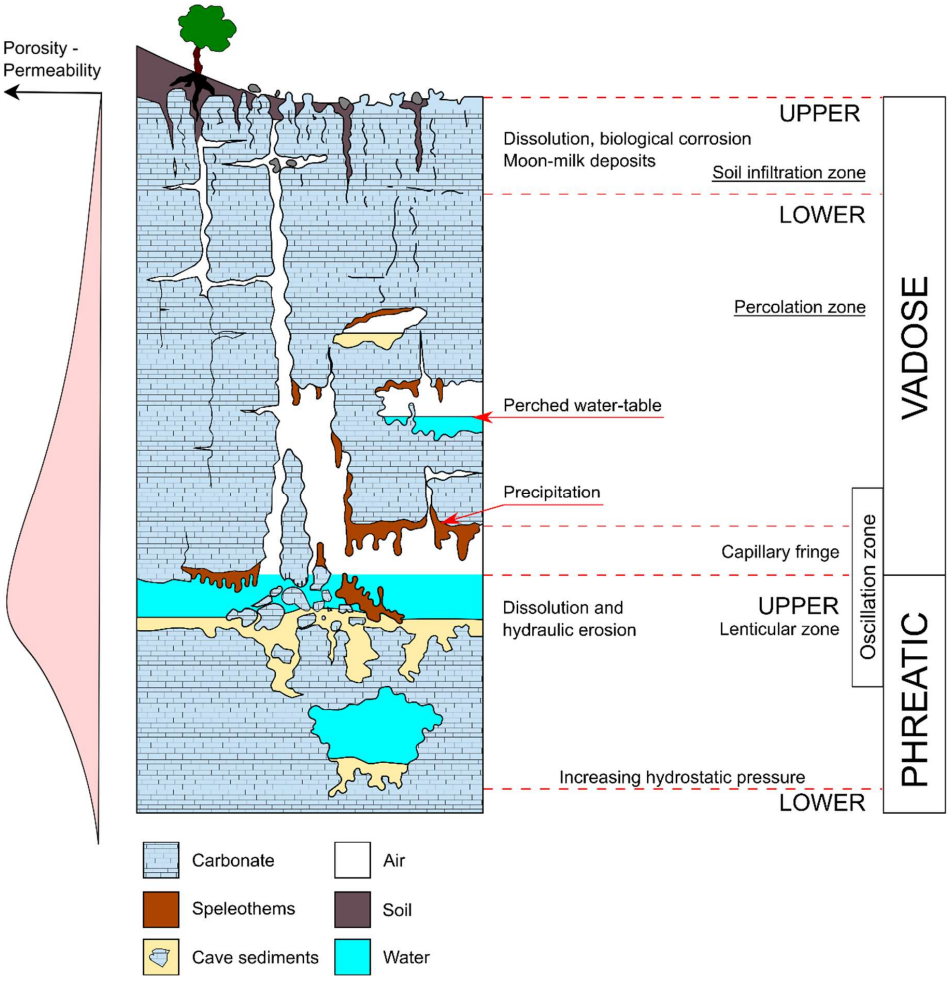

Fig. 3: Idealised mature epigene karst profile showing the transition from vadose to phreatic zone and associated relative relationship to porosity and permeability (note increasing porosity-permeability from exposure surface to the upper phreatic zone). Modified from Esteban and Klappa (1983); Esteban and Wilson (1993a)

Upper vadose zone (Soil infiltration zone)

The upper vadose zone (Fig. 3), also called the epikarst, comprises regolith and penetrating root systems (Ford and Williams, 1989). Depending on climatic conditions, meteoric water is generally abundant and active. Meteoric water may either dissolve or precipitate calcium carbonate ($CaCO_3$), depending on the partial CO_2 pressure (P_{CO2}). An increase in P_{CO2}, either by hydration of atmospheric CO_2 or by biological CO_2

upsurge in the soil cover, can increase dissolution (Bögli, 1964; Plummer, 1975; Wigley and Plummer, 1976; Esteban and Wilson, 1993a), whereas degassing and plant uptake of CO_2 may result in precipitation. Epikarst can develop immediately below the soil cover and often results in vertical to sub-vertical shafts that may be filled, to various degree, with sand, silt, clay, and collapse breccia. This collapse breccia can be tens of meters thick in many karst profiles (Esteban and Klappa, 1983). However, the porosity potential is generally low as porosity tends to be reduced under unconformities (Esteban and Wilson, 1993b; Flügel, 2010).

Lower vadose zone (Percolation zone)

In the lower vadose zone (Fig. 3), meteoric water moves vertically through pre-solutional openings and typically forms vertical to sub-vertical shafts. Horizontal passages or conduits in this zone are often relict features from deeper zones (such as phreatic tubes) or related to perched aquifers (local saturation zones) (Esteban and Wilson, 1993a; Ford and Williams, 2013). Dissolution is generally low (Esteban and Klappa, 1983) and vertical passages commonly show intense sedimentation, cementation or collapse (Esteban and Wilson, 1993a). Sediments in both the upper and lower vadose zones are usually reddish in colour (Esteban and Wilson, 1993a), indicating oxidising conditions. Increased dissolution is generally concentrated to localised areas of vadose flow, i.e., typically below sinkholes, thick soil covers or open fractures (Esteban and Klappa, 1983). Proximal to the capillary fringe zone (above the water table), cementation and speleothem formation is generally more abundant and varied than elsewhere in the karst profile (Esteban and Klappa, 1983). Lost mud circulation and drill-bit drops are very common while drilling this zone, but generally involve small pore volumes (Esteban and Wilson, 1993a).

Oscillation- (epiphreatic) and shallow phreatic zone

The oscillation- (vadose – phreatic) and shallow phreatic zones are quite difficult to distinguish in paleokarst. Both zones are characterised by predominantly horizontal to

sub-horizontal passages and erosional features, with locally well-developed bedding-plane control formed by mixing corrosion and elevated hydrostatic pressures (Esteban and Klappa, 1983; Esteban and Wilson, 1993a). Cavern porosity is predominantly formed in this zone, particularly just below the water table (Thrailkill, 1968; Esteban and Klappa, 1983). Loss of mud circulation and drill-bit drops in this zone are generally rare, but when it occurs, it usually involves large pore volumes. In cases of cave-in, an extension of the caliper tool in combination with a kick on the gamma ray and a decrease in sonic velocity may suggest penetration of the oscillation- and shallow phreatic zone (Esteban and Wilson, 1993a).

Lower (Deep) phreatic zone

The lower phreatic zone is very important for the early stage of karst porosity formation (Longman, 1980). Dissolution in this zone is predominantly related to mixing corrosion (meteoric/marine, hot/cold or differential P_{CO2}) and increasing hydrostatic pressures (Esteban and Klappa, 1983; Esteban and Wilson, 1993a). The dissolution decreases while cementation increases downward, grading into unaffected formation (Esteban and Wilson, 1993a). Phreatic passages can form at great depths, up to several hundreds of meters (Ford and Williams (2013) and, below the water table. The depths at which these can form are largely dependent on fracture orientation and density, strata dip (Loucks, 1999; Ford and Williams, 2013) and hydrostatic pressure (Esteban and Klappa, 1983). The four-state model of Ford (1971) explains the relationship between density, penetrability and linkage of fractures and bedding planes, and the hydraulic gradient orientation in unconfined systems (Ford and Ewers, 1978; Ford and Williams, 2013). According to this model, increasing fracture density results in higher abundance and shallower formation depths (closer to the piezometric surface) of phreatic passages (Ford and Williams, 2013).

Mixing zone

Mixing corrosion can occur where mechanical mixing of waters from substantially different sources take place, even when both waters are completely saturated with calcite and individual waters alone are incapable of further dissolution (Thrailkill, 1968; Bögli, 1980; Ford and Williams, 2013). Identical effects also apply for H_2S-rich waters derived from miscellaneous sources (Ford and Williams, 2013). The most prominent mixing zone solution occurs in coastal carbonates with high primary porosity. Solution is greatest at the interface between infiltrating CO_2-rich waters and phreatic waters with lower-CO_2 concentrations (e.g., at the top of the freshwater lens), or where fresh meteoric water mixes with saline seawater. Mixing of meteoric water with calcite-saturated marine waters results in an undersaturation of the mixed solution and subsequent dissolution of the surrounding rock (Plummer, 1975; Sanford and Konikow, 1989; Romanov and Dreybrodt, 2006; Ford and Williams, 2013; Lu et al., 2013). The thickness of a mixing zone in a steady-state homogenous rock, which can range from a few meters to kilometers, are basically only dependent on local dispersion (Lu et al., 2013)

2.1.2 Karst controlling factors

The formation of karst is controlled by several different variables and subaerial exposure alone does not necessarily create karst. Karstification is predominantly controlled by interrelated factors such as (1) climate, (2) reactive potential of groundwaters, (3) mineralogy, (4) duration, (5) existing pore networks, (6) depositional facies and stratigraphy, (7) hydrologic system, (8) size and topography of the exposed area, (9) base level and (10) tectonic setting (Saller et al., 1994; Budd et al., 1995; Mylroie and Carew, 1995):

1) The climate, in particular rainfall, controls the intensity of dissolution in the meteoric system. A positive water budget (annual precipitation > evapotranspiration) results in significantly increased dissolution (Mylroie and Carew, 1995; Palmer, 1995; Wagner et al., 1995; Ford and Williams, 2013). Thus, dissolution tends to be high in humid climates whereas meteoric

cementation may dominate in arid climates. In areas with high permeability and excessive amounts of water, dissolved materials are commonly transported out of the system, resulting in abundant secondary porosity and increased permeability (Wagner et al., 1995). Contrary to a humid climate, little porosity forms in very arid conditions and cementation prevails in the uppermost part of the vadose zone (Wagner et al., 1995). Thus, a slight increase in the water budget can shift cementation stratigraphically downwards into the underlying meteoric phreatic interval (Wagner et al., 1995).

2) The reactive potential of groundwater controls diagenetic alteration. Groundwater can become extra corrosive when two fluids in different equilibrium conditions are mixed (e.g., freshwater – seawater), or additional CO_2 is dissolved (Mylroie and Carew, 1988; Esteban and Wilson, 1993a; Matsuda et al., 1995; Mylroie and Carew, 1995; Palmer, 1995). In confined aquifers, ambient waters commonly have low reactive potential due to low recharge, and thus little diagenetic alteration occurs (Budd et al., 1993; Palmer, 1995).

3) The mineralogical composition of the bedrock influences the style and impact of freshwater diagenesis during subaerial exposure (Mylroie and Carew, 1995; Palmer, 1995; Wagner et al., 1995). Grains comprising more stable minerals (e.g., calcite) can retain their primary depositional pore geometries during exposure to freshwater diagenesis (Wendte and Muir, 1995), whereas grains of less stable mineralogical composition (e.g., aragonite) may be easily dissolved and produce secondary moldic porosity (James and Choquette, 1983; Moore, 1989; Budd et al., 1995; Lønøy, 2006; Flügel, 2010; Moore and Wade, 2013). Strata with a heterogeneous mixture of calcite/dolomite, dolomite/evaporites or calcite/evaporite may thus experience the preferential dissolution of less stable mineralogies during subaerial exposure (Budd et al., 1995), forming a wide variety of pore types: intercrystalline (Hurley et al., 1995), vuggy (Vahrenkamp, 1995) and cavern (Lucia, 1995).

4) The duration of exposure is essential for karstification and pore type distribution. Studies from Dickson and Saller (1995) and Mutti (1995) suggest that short periods of subaerial exposure (10 000 - 40 000 years) may favour matrix porosity development. Conversely, protracted subaerial exposure (1 - 40 m.y.) may reduce matrix porosity and increase fissure and cavernous porosity (Lucia, 1995; Tinker et al., 1995). Permeability is less altered than porosity during prolonged subaerial exposure, as high-permeability karst-related conduits can form relatively rapidly and persist for millions of years (Budd et al., 1995).

5) The existing pore networks guide the initial fluid flow and are contributory to the freshwater distribution, hence the location of dissolution and cementation (Lucia, 1995). In aquifers with conduit flow, diagenesis predominantly occurs in the host rock immediately adjacent to the conduit boundary. Thus, meteoric alteration, even in very porous rock, only affects a short interval proximal to the walls of the conduit (Cander, 1995; Palmer, 1995).

6) The depositional facies and stratigraphy have substantial control on permeability pathways (fractures, fissures and bed-plane partings) where the most pronounced karstification occurs (Ford and Williams, 2013). Grainstones commonly have high porosities and permeabilities, whereas mud-supported limestones are often tighter (Dickson and Saller, 1995; Hurley et al., 1995; Lucia, 1995; Mutti, 1995; Wagner et al., 1995; Wendte and Muir, 1995; Flügel, 2010).

7) The nature, size and configuration of a hydrologic system often determine how and where karst is generated (Beach, 1995; Mylroie and Carew, 1995; Ford and Williams, 2013; Ren and Jones, 2016). Especially, the spatial distribution of the meteoric phreatic- and mixing zone is of importance for where karstification occurs. Karstification is commonly most intense where discharge is high and the hydrologic system configuration allows for short flow distances (Palmer, 1995).

8) The size and topography of an exposed massif controls what type of hydrologic system that is formed and the amount of rock volume subjected to karstification

(Ford and Ewers, 1978; Palmer, 1991; Mylroie and Carew, 1995; Palmer, 1995). The freshwater flux increases with the size of the system, and in large systems, groundwater predominantly flows through conduits like fissures, fractures and caves (Budd et al., 1995).

9) Changes in base level (usually sea-level) will influence water-table configuration and when and where subaerial exposure will occur. Caves and conduits may often be observed at different levels and their spatial distribution often relate to the spatiotemporal sea level (Mylroie and Carew, 1988; Beach, 1995; Mylroie and Carew, 1995). High-amplitude sea-level fluctuations will cause certain areas to be subaerially exposed periodically. Lowering or rising of the base level consequently shifts the water-table position (represented by the oscillation zone in Fig. 3) and associated meteoric diagenesis down or up, respectively.

10) Karstification and tectonic setting have a parallel history (Quinif and Vandycke, 2001). Tectonics induce mechanical limits for karst expansion and control the main direction of karst systems (Quinif and Vandycke, 2001; Shanov and Kostov, 2014). In principle, the most convenient path for subsurface fluid flow in karst massifs are fractures oriented perpendicular to the minimum principal stress (Shanov and Kostov, 2014). The tectonic setting and associated stress field will therefore largely influence the formation, density and orientation of subsurface permeable pathways allowing karstification.

2.1.3 Cavern stability and breakdown

Karstification may expand permeable pathways into larger cavities, ultimately developing extensive cave systems (Bosák, 1989; Esteban and Wilson, 1993a; Ford and Williams, 2013; Kaufmann et al., 2019). These cave systems can have lengths of tens of kilometers and comprise conduits and cavities exhibiting diameters up to hundreds of meters. These cavities can be preserved in paleokarst but may also experience collapse during burial. Modern understanding of cave collapse mechanisms and subsurface

cavern stability mostly originates from the rock mechanics of mining (White, 2012). Yet, there is a significant difference between karst systems and mines. Karst systems form over thousands of years by the slow dissolution of soluble by aggressive fluids (White, 1988; Ford and Williams, 2002; Parise et al., 2018), whereas mines are constructed over relatively short time spans (tens of years). The long formation process of karst allows sufficient time for horizontal strains to anneal out and ambient stress fields to equilibrate (White, 2012; Benson and Yuhr, 2016b). Most natural caves are located at depths under sufficient rock cover for stable compressional arches to form and therefore open caverns and conduits can survive to great burial depths. However, at shallow depths, breaching of the encompassing stress dome by surface erosion or other geological processes can destabilize karst cavities and result in breakdown (Waltham and Fookes, 2003; White, 2012). Breakdown can be initiated by several processes that affect the encompassing stress dome and ceiling beds:

- Dissolution in the phreatic zone is a continuous process, and unless a karst system is drained, passage enlargement continues until the cavity becomes mechanically unstable. If the conduit growth surpasses a critical unsupported size, mechanical rupturing and collapse may occur (Jameson, 1991; White, 2012; Benson and Yuhr, 2016b). Further, as adjacent passages or chambers grow in size, they may intersect each other and eventually form larger and larger caverns (Travis, 2014). Conduit enlargement also increases the roof span and causes a redistribution of the surrounding tension field, subsequently resulting in a predominantly vertical expansion of the stress dome (White and Culver, 2011; Benson and Yuhr, 2016b).

- Conduit drainage removes buoyant support from the cave roof and walls. The Archimedes principle (Heath, 1897) states that a liquid-filled cavity is buoyed upward by the density difference between the liquid and the confining solid (host rock/matrix). Water drainage in a limestone cavity with a typical matrix density of 2.65 g/cm^3 will normally lower the buoyant support by 35-42% (White and White, 1969a; White, 2012) and subsequently reduce the cavern stability. In addition, buoyant support may, in a phreatic setting, be significantly reduced by hydrocarbons displacing connate brines (Travis, 2014). Hypogene- and flank

margin caves are formed in phreatic conditions decoupled from any surface hydrology and are thus expected to have a lower breakdown potential due to the conduit drainage. On the contrary, epigenic caves are formed in near-surface conditions often subjected to seasonal fluctuations in recharge and thus have a higher potential for removal of buoyant support. In addition, epigene karst may experience base level back flooding. Cave passages exposed to the floodwater zone can be subjected to rises and falls in the local base level, resulting in repeated flooding and drainage. This may lead to flexing of the ceiling and additional dissolution along ceiling joints, potentially turning fixed beams into cantilever beams, possibly resulting in rock fatigue (White and White, 1969a; Ford and Williams, 2002; White, 2012; Travis, 2014).

- Surface erosion (e.g., vadose incision or glacial abrasion) causes removal of overlying strata and reduction of the rock cover thickness, subsequently shortening the distance between the surface and the stress dome. Once the stress dome breaches the surface, the gravitational load is no longer evenly distributed onto the cave walls, and the cavern may become unstable and collapse (White and White, 1969a).

- Undersaturated vadose waters can transform the roof beam configuration from a fixed beam into a cantilever beam by ceiling beds being cut during the formation of solution enlarged fractures, chimneys, and vertical shafts, subsequently lowering the cavern stability (Osborne, 2002; White, 2012).

- Weathering of pyrite can promote breakdown in two ways. The weathering itself may release strong acids that can dissolve the carbonate rock. If not quickly washed away, the reaction products may result in the growth of gypsum crystals and subsequently give rise to crystal wedging (Osborne, 2002).

- Crystal-wedging occurs because of the volumetric expansion of replacement minerals. The replacement of calcite by gypsum or other sulphate minerals may

create enough expansion force subsequently resulting in bedrock fracturing (White and White, 1969a; Jameson, 1991; White and White, 2003; White, 2012).

- Ice-wedging can occur in cold climates because of cold airflow inside the cave system. Inherent pore- and fracture fluids may go through cyclic freeze and thaw processes, which expand joints and bed-plane partings and disintegrate the cave roof and walls, subsequently converting the ceiling beam configuration (White and White, 1969a; White and Culver, 2011; Benson and Yuhr, 2016b).

Cave systems may experience multiple cycles of deposition, degradation, burial, uplift, and karst rejuvenation before forming sub-surface reservoirs and may thus be considered polyphase and polygenetic. The features and properties originating from this succession of interacting processes are commonly labelled "paleokarst" and is widely related to unconformities represented by all scales, from brief episodes of local subaerial exposure to long-lasting regional events.

2.1.4 Cave surveying

Cave surveys are commonly used to capture and render the morphology of a karst system and to map associated karst features. Although high-tech high-resolution equipment exists, geospatial data from caves are usually gathered using simple digital equipment such as laser rangefinders (e.g., Leica™ Disto X310) and handheld computers (e.g., a personal digital assistant - PDA). A cave survey comprises consecutive line-of-sight measurements between the survey stations, in addition to multiple cross-sectional cave wall/roof measurements (Fig. 4). The laser rangefinder records the distance, azimuth and inclination, and automatically transfers and stores it to a PDA. The PDA displays the data numerically and graphically, allowing the addition of sketches directly on the screen. The data are anchored to a geo-referenced point (usually the cave entrance), and cave surveying software (e.g., Therion) is used for loop closure, generating 2D maps and 3D models of the cave system. Cave maps and -models render the spatial distribution and shape of open caverns and cave corridors accessible to the surveyor and only provide a snapshot of the cave systems evolution. The

morphology and clastic sediment-fill of a cave system may be altered through time, especially while karstic processes are still active. Ongoing processes such as sediment deposition/flushing, dissolution, cave roof/wall break down etc., can largely affect the morphology and volume. Thus, cave surveys lack crucial information for modelling cave systems related to the distribution, volume, and preservation of infills.

Readers are referred to Heeb (2008, 2009, 2010, 2014) and Trimmis (2018) for common "paperless" cave surveying techniques, and Budaj and Mudrák (2008); Budaj and Stacho (2019) give information about the Therion cave-surveying software.

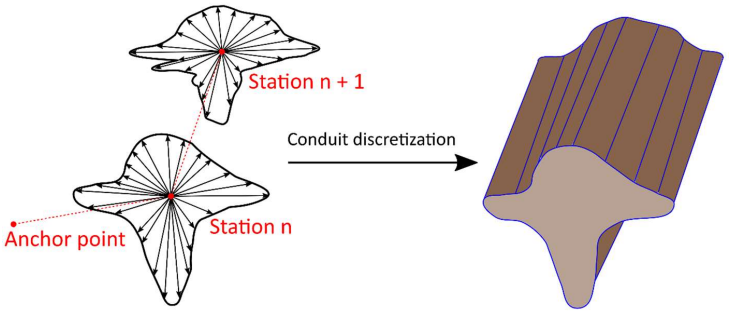

Fig. 4: Conceptual illustration of conventional cave surveying and conduit discretization. Red dashed lines indicate measurements between survey stations (red dot) and black arrows perimeter measurements. Illustration from Paper III.

2.2 Paleokarst reservoirs

Worldwide, approximately 60% of hydrocarbons are found in carbonate reservoirs (Schlumberger, 2007; Burchette, 2012; Agada et al., 2014), where 20-30% of all recoverable hydrocarbons are, to some extent, related to unconformities and surface-related karst (Fritz et al., 1993; Mazzullo and Chilingarian, 1996; Flügel, 2010; Zou, 2013). Paleokarst can provide excellent petroleum reservoirs, as evidenced by numerous major paleokarst hydrocarbon fields worldwide, e.g., the Yates field (Craig, 1988; White et al., 1995) and Ellenburger group (Kerans, 1988; Kerans, 1990, 1993) of West Texas; the Golden Lane fields in Mexico (Coogan et al., 1972; Blickwede and Rosenfeld, 2010); the Rospo Mare field in Adriatic Sea (Soudet et al., 1994); the Casablanca field

in offshore Spain (Lomando et al., 1993); the Kharyaga field in the Russian Arctic (Zempolich and Cook, 2002); the Kashagan field in Kazakhstan (Kaiser and Pulsipher, 2007); the Kirkuk field in Iraq (Trice, 2005), and the Tahe field of the Tarim Basin in China (Yan, 2002).

Although a well-known reservoir type (Choquette and James, 1988; Fritz et al., 1993; Lucia, 2007), boasting some of the most productive hydrocarbon wells in the history (Viniegra and Castillo-Tejero, 1970), paleokarst reservoirs can often be challenging to detect and characterise, have poor recovery factors (Sun and Sloan, 2003; Montaron, 2008; Agada et al., 2014; Montaron et al., 2014), and are commonly considered high-risk plays. The factors often considered as "stubbornly difficult to deal with" in carbonate reservoir characterization (e.g., Roehl and Choquette, 2012) are further compounded in paleokarst reservoirs by heterogeneities linked to large-scale, focused dissolution features and collapses, infills, and cementation associated with these. The difficulties linked to characterising and forecasting property distributions in paleokarst fields express themselves in unexpected water breakthroughs, unpredictable sweep patterns, erratic pressure behaviour (Agar and Hampson, 2014) and by circulation loss (La Ode Ahdyar et al., 2019). All these factors adversely affect costs and production forecasting, as well as posing a significant challenge to well positioning and safe drilling. Moreover, the complex formation history, pronounced spatial complexity and unpredictable heterogeneity of paleokarst reservoirs often result in explorationists tending to overlook (La Ode Ahdyar et al., 2019) or deny that they are dealing with this reservoir type (Trice, 2005).

A well-known challenge in improving reserve estimates from paleokarst reservoirs relates to volumetric determination and estimation of cave-size statistical distributions, cave geometries, geomorphology and oil recovery factors (Montaron et al., 2014). When compared to conventional carbonate- and organic build-up reservoirs, the recovery factor (RF) from karst-related reservoirs is generally very low (Fig. 5) (Sun and Sloan, 2003; Montaron, 2008; Montaron et al., 2014). Unlike conventional sandstone and carbonate reservoirs, oil recovery in paleokarst reservoirs is commonly not impaired by

capillary forces, and gravity forces predominantly govern the recovery. Once the pore size equals or exceeds the oil-water capillary length, capillary forces will no longer affect the recovery. Carbonate reservoirs commonly range in wettability from neutral to strongly oil-wet (Treiber and Owens, 1972; Chilingar and Yen, 1983; Tiab and Donaldson, 2015). Thus, even with optimal recovery, a thin film of residual oil is expected where oil is in immediate contact with the rock surface (Montaron et al., 2014).

A study involving production simulations of 512 synthetic caves suggests that recovery is very sensitive to the initial water level, cave- slope, and morphology (Montaron et al., 2014). Simulations showed that recovery deteriorates rapidly with increasing initial water content and increased abundance of localised oil traps along the cave roof. Furthermore, the slope angle of the karst system has a significant effect on the RF. With producing wells located at one end, the RF_{mean} of completely oil-saturated horizontal caves was 48%. Conversely, running similar simulations with a slight change in the slope angle of the cave causes the recovery to decrease to 24% (-2° slope angle) or increase to 61% (+2° slope angle) (Montaron et al., 2014). This indicates that the recovery is very sensitive to the slope angle of the cave and the overall reservoir morphology. The low recovery factor often associated with paleokarst could, therefore, relate to that current modelling techniques generate reservoir models which are not representative in terms of morphology and spatial distribution, which in turn may affect recovery estimations.

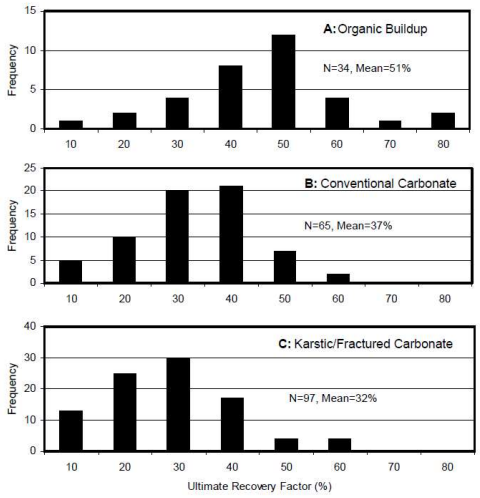

Fig. 5: Medium and light oil recovery factors for three different types of carbonate reservoir. A total of 197 reservoirs were subdived into A) Organic buildup-, B) Conventional carbonate- and C) Karstic/fractured carbonate reservoir. Note that when compared to A) and B), karstic/fractured carbonate reservoirs are associated with significantly lower mean recovery factors. Graphs from Sun and Sloan (2003).

Paleokarst reservoirs are currently predominantly modelled by employing adapted or modified versions of conventional reservoir modelling workflows used for siliciclastic and carbonate reservoirs (e.g., Ringrose and Bentley, 2015). These models are typically generated by data-driven approaches which include the use of Object-Based Modelling (OBM) (e.g., Henrion et al., 2008; Rongier et al., 2014; Fernandez-Ibanez et al., 2019); Sequential Gaussian Simulation (SGS) (e.g., Henrion et al., 2008; Frantz et al., 2021); Multi-Point Statistics (MPS) (e.g., Strebelle, 2002); fast marching approach (e.g., Borghi et al., 2010; Borghi et al., 2011; Erzeybek Balan, 2012; Rongier et al., 2014), or discrete fracture network (DFN) (e.g., Fernandez-Ibanez et al., 2019) conditioned on seismic and well data to populate model domains. Genetic approaches for rendering karst aquifers (e.g., Borghi et al., 2010; Borghi et al., 2012) and conceptual reservoir modelling of flank margin caves have been employed too (Labourdette et al., 2007). Moreover, attempts to generate analogues for paleokarst reservoirs have been carried out by geocellular rendering of cave surveys (e.g., Furnée, 2015; Ledsaak, 2016).

It should be noted that available publications on geo-modelling of paleokarst reservoirs using industry-standard reservoir modelling tools are relatively limited, with the bulk consisting of conference abstracts and student theses. However, it can only be assumed that several unpublished proprietary methods and workflows exist as paleokarst reservoirs are quite common in several oil provinces all over the world.

2.3 Other areas of application

Paleokarst is not only important for exploration and production of hydrocarbons but also excellent localities for ground water and economically valuable mineral deposits. Although not elaborated in this paper, it should be noted that paleokarst is often associated with bauxite, phosphate, lead, zinc, copper, fluorite, marcasite, galena, barite, sphalerite, pyrite, antimony, mercury, uranium, vanadium, uranium, nickel, manganese, clay and coal (Kyle, 1983; Sangster, 1988; Böcker and Vizy, 1989; Bosák, 1989; Dżułyński and Sass-Gustkiewicz, 1989; Fuchs, 1989; Zötl, 1989; Mazzullo and Chilingarian, 1996; Ford and Williams, 2002; Gunn, 2004; Bárdossy, 2013; Ford and Williams, 2013; Benson and Yuhr, 2016b). In addition, due to the complex morphology of karst, significant economic concentrations of alluvial gold, diamonds, cassiterite, rare earth elements (REE), and other precious stones may be trapped in karst surfaces (Gunn, 2004; Benson and Yuhr, 2016a). Even though this thesis primarily focuses on reservoir modelling of paleokarst for oil and gas production, other industries dealing with paleokarst may benefit from the methods developed and proposed here.

2.4 Study Areas

In this thesis, the overall aim was to develop robust methods and workflows for process-driven paleokarst reservoir modelling using cave-survey data as input. Two epigene karst systems were chosen as analogues, i.e., the Maaras (MA)- and Agios Georgios (AG) cave system. The caves are located in the prefecture of Eastern Macedonia in northern Greece, within the mountains bordering the Aggitis river basin, (Fig. 6). The latter basin constitutes a well-defined Neogene tectonic graben controlled by two NW-

SE trending normal faults (Vavliakis et al., 1986) and is bounded by the mountains of Falakro to the north, Ori Lekanis to south-southeast, Paggeon to the south, and Menikion to the east-northeast. The surrounding mountains source alluvial sediments that cover the central part of the basin, whereas the margins are characterized by complex alluvial fans (Pennos et al., 2011). The mountains primarily consist of pre-Neogene metamorphic rocks (marbles, gneisses, and schists) with minor plutonic intrusions (Christanis et al., 1998). The western part of the basin contains Miocene lacustrine clastic sediments deposited during a period of raised sea level (Papaphilippou-Pennou, 2004), whereas the lowlands in the eastern part comprise recent deltaic deposits from the Xiropotamos-Doxato stream (Pennos et al., 2016b).

The MA cave (red cave in Fig. 6) is a near 12-km long cave system which developed parallel to the north-western margin of the Aggitis basin, within the marbles of the Rhodope massif. The cave system hosts an active fluvial system that drains the Kato Nevrokopi polje in the northwest. Meteoric water is fed through localized inlets near the village of Ochiro (Novel et al., 2007) at approximately 545 m.a.s.l. and exits the subsurface through a spring near the village of Aggitis at 123 m.a.s.l. The cave comprises two shorter tributary passages that join to form a more extended master conduit to the spring and exhibits a cave pattern resembling the typical branchwork type classified by Palmer (1991). The cave floor is mostly flat and covered by thick deposits of allochthonous sandy clastic sediments (local sediment thicknesses exceeding 45 m - Paper II) and localized accumulations of talus.

The AG cave (orange cave in Fig. 6) is an approximately 600-m long cave system located at the southern margin of the Aggitis river basin, within pre-Palaeozoic marbles. The AG cave system is currently dry and exhibits cave corridors with a predominant NE-SW orientation. The corridors orientation coincides with the strike of surface-lineaments and fractures suggesting that the cave may have formed by structurally controlled speleogenesis. The cave floor is relatively flat and predominantly comprises fine-grained clastic sediments with a locally high abundance of guano. Proximal to the cave entrance, the fine-grained sediments are overlain by a layer of angular clasts. Local

accumulations of angular clasts and slabs also appear within a relatively long cave corridor at the centre of the cave system, and the innermost part of the cave.

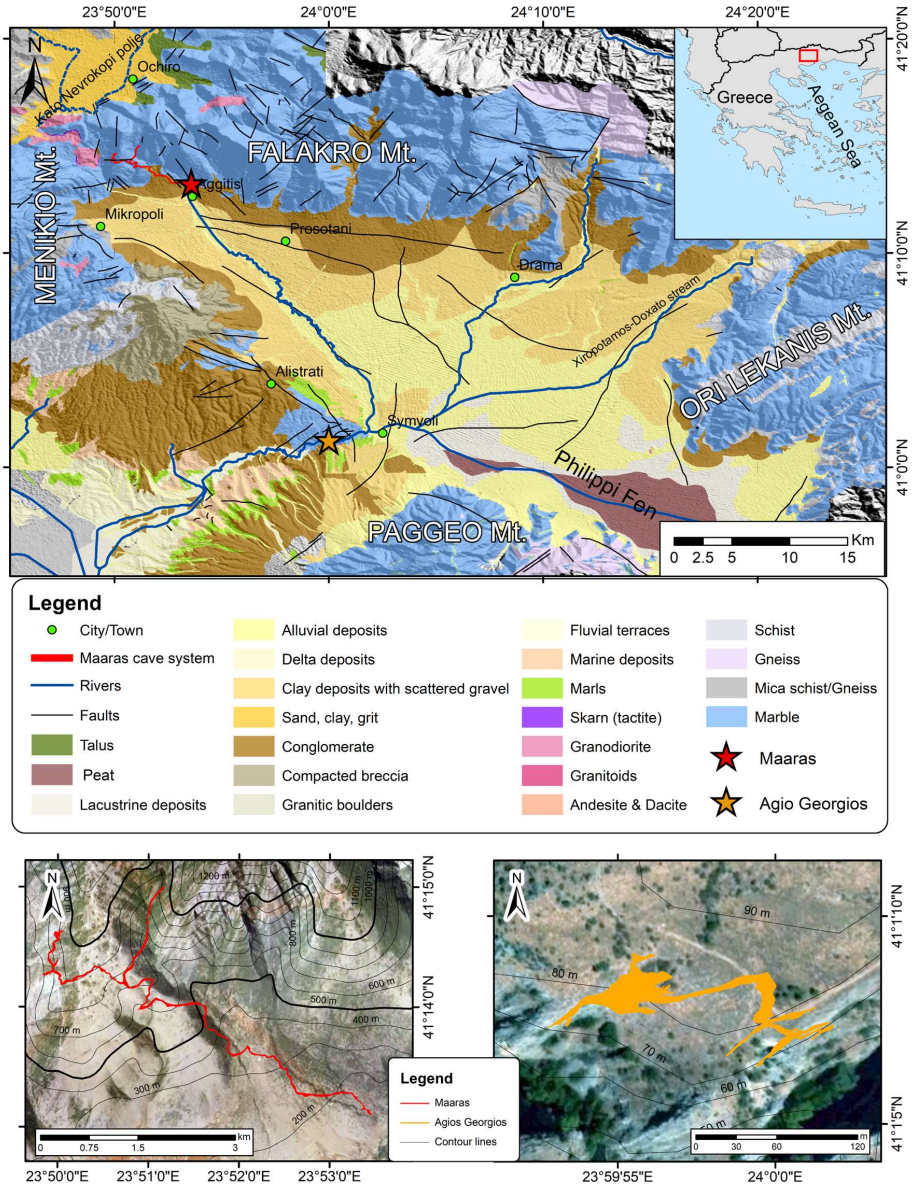

Fig. 6. Overview map of the Aggitis river basin, surrounding study area and location of the cave systems used as analogues in this research. Upper: Geological map modified from Pennos et al. (2016b) and Papapetros (1982) and superimposed on a Digital Elevation Model (NASA/METI/AIST/Japan Spacesystems, 2019). Lower left: Cave survey of the Maaras cave system (Pennos et al. 2016) superimposed on an orthophotography (www.ktimatologio.gr). Lower right: Cave survey of the Maaras cave system (Pennos et al. 2016) superimposed on an orthophotography (World Imagery by Esri).

3 Methods

This PhD study integrates a broad range of methods. These are described in detail in the relevant manuscripts and only summarised here.

Dr. Christos Pennos generously donated the two cave surveys used in this thesis. These include survey data from the MA- and AG cave systems (Pennos et al., 2016; Pennos et al., 2018, respectively). The surveyors that surveyed both the cave systems used conventional surveying techniques, including multiple perimeter measurements for each survey station.

This study is the first to use electrical resistivity tomography (ERT) inside active karst systems for large-scale mapping of clastic sediment infill. Therefore, reconnaissance was carried out inside the MA and AG caves before ERT mapping. Electrode spacing and survey line positioning were evaluated on-site to optimize depth of investigation (DOI) given the available cable length. The ERT survey was carried out using a 10-channel resistivity meter (IRIS INSTRUMENTS) with a 48-cable multiplexing ability. ERT was carried out in two dimensions (2D) and performed with dipole-dipole and gradient configurations. In total, 597 m of cave length was surveyed using ERT, i.e., 414 m in MA and 183 m in AG.

In MA, all distinct outcropping taluses were mapped throughout the master conduit. Within the same conduit, a representative sediment terrace was logged and sampled. The logged section was sampled for grain size analysis to supplement the findings of Pennos et al. (2016a). A laser diffraction particle analyser (Mastersizer 3000) at the EARTHLAB facilities, University of Bergen, was used to measure the grain size distribution. The orientation of surficial fractures, joints, and lineaments were mapped above, around and within the AG cave system.

In addition to the conventional methods applied and summarized above, new methodologies were developed and tested. The various methods are described in detail in the manuscripts reproduced in Part II. The developed methods include:

- a new method for geocellular rendering of cave surveys,

- a new approach to large-scale mapping of clastic sediments in active karst systems, and
- an interactive tool for forward modelling of collapse- and infill processes.

4 Main results

In this section, the main results for each paper are outlined. A significant amount of the workload was invested in developing the methods used in this dissertation and the methods themselves are therefore regarded as a result of the work. Thus, the developed methodologies are shortly summarized here.

4.1 Paper I

This initial paper focuses on developing a new method for geocellular rendering of cave surveys in paleokarst reservoir models. Industry-standard reservoir modelling software suites usually do not have established workflows or dedicated add-ins for handling the complex geometries and property distribution often characterizing paleokarst reservoirs. Previous efforts of rendering cave surveys in geocellular frameworks are, to our knowledge, limited to two MSc theses (Furnée, 2015; Ledsaak, 2016). Here, Method 1 refers to the method proposed by Furnée (2015), whereas Method 2 refers to that of Ledsaak (2016). Although the pre-established methods laid the foundation for- and improved geocellular rendering of cave surveys, geometries are either rendered oversimplified when transferred to a geocellular framework (Method 1) or require substantial and time-consuming editing to match observations (Method 2) (Lønøy et al., 2019; Lønøy et al., 2020).

In Paper I, focus was given to develop a novel methodology for geocelluar rendering of caves with improved geometric and volumetric accuracy. Dr. Christos Pennos coded a MATLAB™ algorithm that generates dense, equally-spaced point clouds (representing the cave system) from conventional cave-survey data. The point clouds can be imported into industry-standard reservoir modelling software such as RMS 11TM and used for subsequent geometrical modelling and discretization of cave systems. The various methods were used to generate three different grid models of the MA cave survey. The volumetric and geometric accuracy of the methods was then evaluated and benchmarked against that of the cave survey.

The results demonstrate that all the methods capture the orientation and connectivity of the conduits and secure grid cell coherency. However, our proposed method (Method 3) offers improved geometric and volumetric accuracy when compared to the pre-established methods. The total rendered volume using Method 3 was 1.55 Mm3, which is similar, within 2%, to the estimated value from the original cave survey (1.58 Mm^3). In contrast, the two other methods significantly under- or overestimated the total cave volume. Method 1 underestimated the cave volume by 0.45 Mm^3 (relative difference of 33%), whereas Method 2 overestimated the volume by 1.08 Mm^3 (relative difference of 51%). The applied global grid cell resolution may have significance on the rendered morphology and volume, and cell-to-cell interlinkage. This issue especially applies to Method 1 and 2 (for further details, see Paper I). For Method 3, the volumetric accuracy is mostly dependent on the filter cut-off value applied during geometrical modelling, and there is a clear polynomial trend between the employed filter cut-off value and rendered volume. Thus, if the surveyed volume and desired global grid resolution are known, an optimal filter cut-off value can be determined, allowing accurate volumetric rendering.

4.2 Paper II

In Paper II, the focus is to delimit karst elements that impact the volumetric and geometric rendering of cave surveys, with emphasis on fluvial sediment-fill and breakdown material. Previous research has shown that karst systems can act as traps and conveyors for clastic sediments (Bosch and White, 2004; White, 2007; Bosch and White, 2018; Bella et al., 2020). Once the system is detached from processes active on the surface, the latter are typically shielded from erosive forces and can be preserved in the rock record and fill in substantial parts of pre-existing karst voids. Active karst caverns and conduits can be partially- or completely occluded by clastic sediments and breakdown material and thus conceal the actual cave morphology and dimension. Unless being excavated or removed by erosion, the spatial distribution and volumetric significance of clastic sediments in karst systems remain unknown and widely underestimated (Farrant and Smart, 2011). In addition, there are, to our knowledge, no

known non-destructive methods for mapping their actual thickness. A pilot study for mapping sedimentary thickness variations and cave floor morphologies was carried out inside the MA cave system in northern Greece using a combination of pre-established methods. This multi-methodological approach includes ERT, stratigraphic logging, grain-size analysis, and talus mapping. The ERT data were used to discretize the clastic sediment-fill in the grid model from Paper I. Two identical cave-floor horizons (sediment top) were generated, and one of these was depth shifted according to the interpreted sub-sediment cave floor (from the ERT). The clastic-sediment fill was then discretized by geometrical modelling using the "assign values between horizons"-function.

In MA, thick sediment accumulations are pervasive and cover the cave floor. The results show that pseudo-3D inverted ERT data can be used for identification of macro-scale (>1.5m^2) lithological contrasts, sub-sediment cave-floor morphology along the passages and used to estimate sedimentary thicknesses. A correlation between the spatial distribution and magnitude of resistivity in the processed survey stations, and field observations of sediment infill, resulted in the classification of four different electrical resistivity facies (RF): porous- and highly porous siliciclastic sediments, autochthonous breccias (marble), and host-rock (marble). The sediment thickness in MA varied from approximately 20 m to >45 m, indicating that clastic sediments occupy more than 69-95% of the actual cavern cavity. However, the relative proportion of clastic sediments to open-cavern cavity declines to 67-79% when discretized in the grid model. The stratigraphic log and grain-size analysis combined with relevant publications show that the sediment-fill in MA is predominantly comprised of siliciclastic sand interbedded with coarser silts. The sedimentary structures, grain-size distributions, sorting, etc., match that of "channel facies" described by Bosch and White (2004) and are thought to make up the bulk of sediment-fill in MA. The talus mapping indicates that these are locally confined to the inner bend of conduits or conduit widenings and comprise angular marble clasts that vary in size (few centimeters to several meters) between localities, but also locally within the same accumulation. Several of the accumulations are covered by thick speleothems, making it difficult to map clast-size distribution and their true extent.

4.3 Paper III

Paper III focuses on developing methods for simulating collapse and infill processes of karst systems by using cave surveys and conventional field data as input. The paper proposes a novel interactive tool for predicting and simulating cavern collapse. This tool can be utilized to generate output data suitable for a subsequent discretization of post-collapse morphologies and associated paleokarst facies. Although paleokarst reservoirs are relatively common in many oil provinces, methods, or workflows for modelling this reservoir type are relatively sparse in the literature, and especially when it comes to using cave-survey data as input to industrial reservoir modelling tools. It can only be presumed that here are several unpublished proprietary methods and workflows used by the industry, but few or none of these are openly accessible. The proposed tool and associated workflow are therefore intended to be transparent, easily customizable, and available to most users.

The forward collapse simulation tool is designed for two purposes: (1) to distinguish stable (intact) from unstable (collapsed) cave sections, and (2) to generate output data suitable for generating point clouds. The post-collapse morphology is simulated and rendered for each paleokarst facies over the entire cave system (i.e., total collapse) before cavern stability is evaluated and output data cropped accordingly (stable vs. unstable). The workflow is summarized below:

Cave-survey raw data are imported into the forward collapse modelling tool and transformed into a cartesian coordinate system so that each survey measurement is represented by a vector. The user then inserts the desired relative paleokarst facies proportions and associated average porosities to calculate a “target porosity” for each facies. The “target porosity” is further used to simulate the post-collapse morphology for the entire cave system (i.e., total collapse) and generate output data suitable for generating point clouds (workflow described in Paper I). This process is carried out for each defined paleokarst facies. Once the point clouds are generated, these can be cropped according to the simulated cavern stability of each survey station. Finally, the various paleokarst facies are discretized in a specific order (elaborated in Paper III) using

conventional reservoir modelling tools and following the workflow presented in Paper I and II.

The results show that the forward collapse modelling tool and proposed workflow provides satisfactory rendering of post-collapse volumes and -morphologies. The accuracy of the simulation is evaluated by comparing the input- and expected output values with those simulated in the tool and rendered in the grid model (Table 1). As an example, a collapse simulation of the AG cave system with a given target porosity of 10% shows that the simulated post-collapse porosity varies among the survey stations, ranging from 6.9 to 11.4% (9.3 ±0.7 mean ±SD)[1]. Although porosity deviates locally, this evens out over the entire system. The facies proportion and associated volumes discretized in the grid model are comparable to those defined in- and calculated by the forward collapse modelling tool, indicating that the reservoir model reflects the simulation.

Table 1. Volumetric accuracy of collapse simulation and associated workflow for each facies rendered. Simulated collapse (predicted) vs. rendered volume (gridded). PKF-3 refer to the coarse chaotic breccia-, PKF-4 to the highly disturbed strata-, and PKF-5 to the disturbed strata facies (see Paper III for description). Note that the presented volumes represent a completely collapsed cave system.

Facies	Proportion - input (%)	Complete collapse				
		Predicted volume (m^3)	Gridded volume (m^3)	Deviation (%)	Parameter filter cut-off	Gridded proportion – output (%)
PKF-3	20	16 660	16 656	0.0	0.59	19.9
PKF-4	30	24 989	25 598	-2.4	0.50	30.5
PKF-5	50	41 649	41 579	0.2	1.55	49.6
Total	100	83 298	83 833	-0.6	-	100

The results indicate that some cave sections may remain open and intact during burial, and cavern porosity can be preserved at depth under certain conditions. This implies that paleokarst reservoirs may be compartmentalized due to the differential breakdown of the karst systems. In turn, this may result in the formation of localized bypass zones,

[1] One outlier removed (see discussion in Paper III)

i.e., “permeable highways”, and a potential decrease in target exploration volume because restricted sections are unaffected by collapse and infill processes. The findings confirm what has already been widely known in the industry and evidenced by numerous drill-bit drops worldwide (indicating penetration into open cavities). However, this shows that accurate modelling of the paleokarst reservoir architecture is crucial to improve the well-planning and forecasting of production behaviour and mitigate drilling hazards. The proposed concept-driven approach for generating paleokarst reservoir model analogues (Paper III) offers high-resolution geocellular models that can improve fluid-flow analyses and seismic modelling. In turn, this could potentially expand our understanding of managing this reservoir type.

5 Synthesis

This PhD thesis addresses reservoir modelling of paleokarst reservoirs targeted for hydrocarbon production. The research focuses on developing methods for process-driven conceptual reservoir modelling using conventional cave-survey data.

But what are the drawbacks of conventional paleokarst reservoir modelling methods? As mentioned in chapter 2.2, the available modelling approaches are based on adapted or modified workflows used for siliciclastic and carbonate reservoirs, and are often conditioned on subsurface well- and seismic data. Paleokarst reservoirs generally have morphological complexities where reservoir units may crosscut several different stratigraphic intervals. High seismic velocities within carbonates, combined with the complex spatial distribution of petrophysical properties often associated with these reservoirs (Trice, 2005), make reservoir modelling solely based on data collected by conventional methods (e.g., seismic and coring) a challenge due to significant resolution issues. Consequently, with data-driven approaches, there is a significant gap between the scales at which features are resolved and rendered (Fig. 7). Thus, these modelling methods often fail to incorporate the spatial distribution, morphology, volume and, crucially, connectivity of paleokarst features in a realistic manner, or employ non-gridded models that are not optimal for fluid flow analyses and production forecasting.

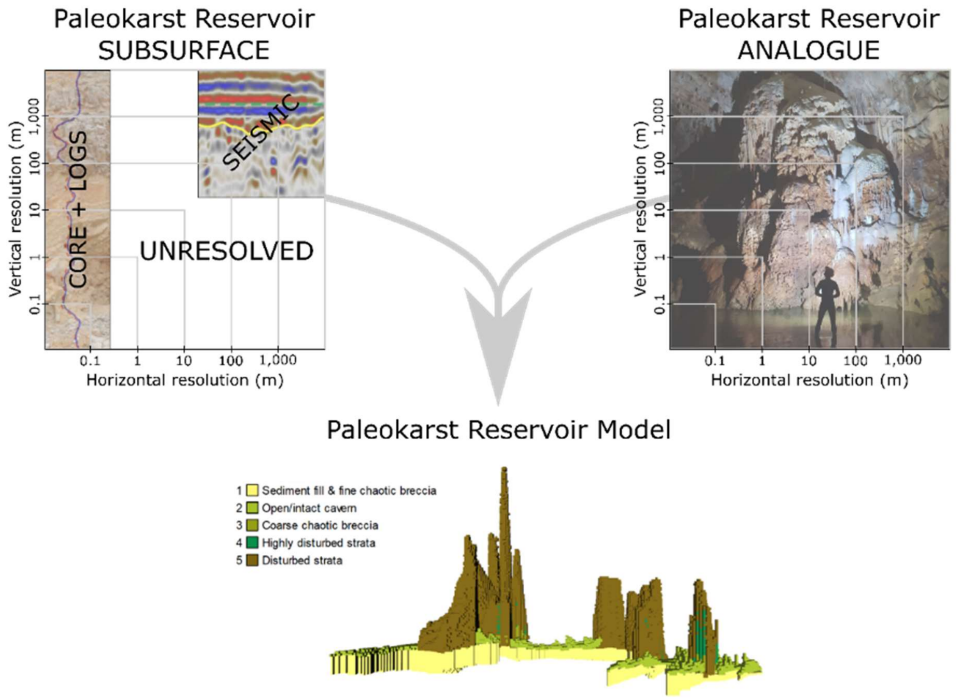

Fig. 7. Conceptual illustration of attainable data resolution from subsurface paleokarst reservoirs and paleokarst analogues. Upper left: Although cores and well-logs can provide excellent vertical resolution, the horizontal resolution is commonly limited to the diameter of the drill bit and depth of investigation of the logging tool applied. On the contrary, seismic data may provide excellent resolution of large-scale features, but often have insufficient resolution to capture morphology at scales typical for paleokarst reservoirs. Upper right: In parallel, many recent karst systems are often well-studied and cave surveys are ubiquitous, allowing features to be studied at all scales and used for forecasting paleokarst reservoir architectures. Note that actual vertical- and horizontal resolutions may vary depending on employed logging tool, reservoir depth, seismic impedance contrasts etc.

Concept-driven (rather than data-driven) approaches, incorporating karst formation and associated and subsequent degradation, infill and diagenesis, may offer important insights and provide improved constraints for model-rendering of paleokarst reservoirs (Trice, 2005; Tveranger, 2019). Conceptual modelling of karst aquifers (e.g., Borghi et al., 2010; Borghi et al., 2012) and flank-margin caves (Labourdette et al., 2007) have proven to provide cave patterns that mimic anticipated initial karst morphologies. However, as the rendered morphology of the karst systems are based on simulations, there may be significant uncertainties tied to how representative the overall morphology and spatial facies distribution are. These models also often represent open cave systems (e.g., Borghi et al., 2010; Borghi et al., 2012) or do not differentiate between collapsed

and intact sections (e.g., Labourdette et al., 2007) and may thus not provide models that are representative of a paleokarst reservoir setting.

The tectono-stratigraphic history of different karst systems is, in most cases, well known, and cave-survey data are ubiquitous. Concept-driven approaches using survey data from recent cave systems as analogues to paleokarst reservoir modelling could ensure representation of actual large-scale cave geometries. However, accurate and efficient modelling of complex reservoir morphologies is challenging (Branets et al., 2009; Mallison et al., 2014) as industry-standard reservoir modelling software such as RMS and Petrel currently have no established workflows or dedicated add-ins for capturing the geometries and property distributions characterizing paleokarst reservoirs. Workarounds for geocellular rendering of cave surveys have been suggested (e.g., Furnée, 2015; Ledsaak, 2016), but geometries are often rendered oversimplified or require substantial and time-consuming editing to match observations. Also, forward modelling of infill and collapse processes are not included in these methods.

Clearly, if cave surveys are to be used as analogues to paleokarst reservoir modelling, new workarounds, methods and tools must be developed. In this PhD research, three themes related to concept-driven paleokarst reservoir modelling based on cave-survey data were addressed in detail: (1) geocellular rendering of cave-survey data, (2) delimiting karst elements affecting the morphological and volumetric accuracy of cave surveys, and, (3) forward modelling of collapse and infill processes. The themes are introduced in the three manuscripts: Paper I, Paper II and Paper III, respectively.

When we evaluated the pre-established methods for geocellular rendering of cave surveys (i.e., Furnée, 2015; Ledsaak, 2016), it quickly became evident that accurate geometric and volumetric geocellular rendering is not as “straight-forward” as expected. As stated earlier, because industry standard reservoir modelling software suites have no established workflows or dedicated add-ins handling the complex geometries often associated with karst/paleokarst, developing workarounds demanded a lot of “trial and error” before a robust method was established. MATLAB^{TM} was used to make an algorithm that employs cave-survey data to generate a dense, equally-spaced point cloud

representing the cave system (Paper I). The point cloud can then be imported into any standard reservoir modelling software and used to discretize the cave system in a geocellular framework by geometric modelling. This approach provides a significantly improved geometric and volumetric rendering of the cave system (Paper I) when compared to the two pre-established methods (i.e., Furnée, 2015; Ledsaak, 2016). A volumetric and morphological deviation is, however, expected when "forcing" an irregular geometry to conform to a gridded framework. This is because grid cells will either extrude beyond the periphery (volume overestimated) or fail to precisely fill in the detailed shape of the actual body (volume underestimated). The morphology and volume rendered by our novel methodology are comparable to that of the cave survey (Paper I), but accuracy is largely dependent on fine-tuning of the parameter filter cut-off value and applied grid-cell resolution, which in turn is dependent on available CPU power. Results showed that, as anticipated, morphologic and volumetric accuracy increases with finer grid-cell resolution. Although the accuracy is largely constrained by available CPU power, the details rendered by our method (Paper I) and current computational power are beyond anything achievable using seismic and well data.

Geocellular rendering of cave surveys can be carried out with excellent volumetric and geometric precision, as evidenced in Paper I. However, the accuracy of the morphology rendered by a cave survey is highly uncertain as it is derived from a compilation of consecutive cross-sectional line-of-sight measurements representing the distance to the closest obstacle. Cave systems, and especially epigene, can act as conveyors and traps for clastic sediments (Bosch and White, 2004; White, 2007) while conventional methods for cave surveying commonly do not include instruments for mapping sediment thicknesses. Consequently, the sediment top is often treated as the cave floor. Mapping of clastic sediment infill is usually only carried out on a local scale (e.g., Kadlec et al., 2008; Martini, 2011; Bella et al., 2020) and, although recent studies (e.g. Tian et al., 2017; Li et al., 2018) suggest that there is a growing interest in quantification and qualification of the role sediments play as part of paleokarst reservoirs, this is still a rather unexplored topic. Unless being excavated or removed by erosion, there are no known non-destructive methods for knowing the true extent and significance of clastic sedimentary infill in caves (Farrant and Smart, 2011). Sediment deposits may fill in

substantial parts of pre-existing karst cavities, possibly altering petrophysical properties that control local reservoir porosity and permeability. In addition, the sediment infill may induce lithostatic pressure on cave walls and floor, providing physical support, and constrain, redirect, or dampen fluid flow in karstic systems, subsequently affecting cavity breakdown processes and the development of drainage paths. These processes will, in turn, affect reservoir properties of paleokarst reservoirs originating from them. This implies that there is significant uncertainty related to the shape and volume of cave surveys as the actual cave morphology may in fact be concealed by cave-fill such as sand, silt, clays, breakdown-derived clasts, speleothems etc. (Paper II and III). Failing to recognize and discretize clastic sediments may thus have a significant impact on prospect evaluations as pre-burial infill is expected to comprise contrasting petrophysical properties to infill related to cavern breakdown during burial (cf., Loucks and Mescher, 2002). This brings us back to conceptual modelling methods using, e.g., object-based-modelling to generate synthetic cave networks. Modelling based on geostatistical data from cave surveys should be handled with care when employed for paleokarst reservoirs. Statistics concerning a cave system's shape and volume may be inaccurate and pre-burial infill rendered erroneous if overlooked.

Although Paper II proposes that pre-burial infill can, to some extent, be mapped using electrical resistivity tomography (ERT) and conventional mapping techniques, cave surveys only provide a “snapshot” of the karst evolution and do not depict the final paleokarst reservoir morphology. Thus, the forward modelling of collapse and infill processes is essential for rendering representative subsurface reservoir morphologies and facies distributions. Forward collapse modelling has previously been carried out with great success on object-based models (Boolean simulations) of flank-margin caves by Labourdette et al. (2007). However, this modelling approach has some shortcomings:

(1) The cave network is generated by object-based modelling. This implies that the geostatistical input data determine the morphology and spatial distribution of the conduits. For flank-margin caves, this may be a valid approach as they are expected to have a low abundance of sediment influx and thus the shape

and volume derived from a cave survey may be representative. However, if the cave system is filled by large volumes of clastic sediments, associated geostatistical data may be inaccurate and not suitable for object-based modelling.

(2) The modelling approach by Labourdette et al. (2007) assumes that the entire cave system collapses during burial. This implies that the collapse and infill simulation does not differentiate between intact (i.e., preserved cavern porosity) and collapsed sections. Open active-karst systems have been documented down to 2200 m (Klimchouk et al., 2009; White and Culver, 2011), suggesting that, under certain conditions, cavern porosity may be preserved to at least this depth. Meter-scale drill bit drops, indicating penetration into open cavities, have also been reported down to an incredible 6353-m depth (e.g., Lu et al., 2017), indicating cavern porosity can be preserved or formed at great depths. Failing to adequately evaluate cavern stability and forward model collapse processes may thus result in inaccurate rendering of the final reservoir architecture and facies distribution.

(3) Forward collapse modelling of synthetic cave networks may prove difficult as the morphology is simulated based on geostatistical data. Cavern stability is determined by the critical beam thickness needed to support a given cavity (White, 2012). This thickness can be calculated if the host rock density (g/cm3), passage width/roof span (m), the flexural strength of the ceiling beam (MPa), and bedding dip (°) are known. This implies that, although cavern stability can be evaluated based on a simulated morphology, there is significant uncertainty related to the spatial distribution of collapsed/intact sections as the shape and consequently the passage width may be erroneous.

These shortcomings may be overcome by employing realistic cave geometries derived from cave surveys. Cave surveys can be used to enable model rendering of reservoir morphologies that more closely echoes the actual collapse and infill processes (Paper

III). Cavern collapse can result in enhanced vertical reservoir continuity, and areas subjected to collapse are anticipated to comprise larger exploration targets (Loucks, 1999; Travis, 2014). Forecasting the spatial distribution of intact and collapsed sections are thus crucial because these sections have contrasting petrophysical properties and vertical extent. Localized collapse does not alter the overall bulk porosity of the cave system but may compartmentalize a reservoir and form zones comprising elevated permeabilities. In turn, these "permeable highways" may significantly impact fluid flow by forming by-pass zones or result in early water breakthrough. The forward collapse modelling tool proposed in Paper III uses morphological data from cave surveys to evaluate cavern stability for each survey station and simulates probabilistic collapse and infill processes accordingly. Depending on the stability of a cave system, this approach results in models that are segmented into intact or collapsed sections, eventually providing more realistic paleokarst reservoir architectures than a uniform collapse. According to Montaron et al. (2014), oil in paleokarst reservoirs is commonly not capillary bound, and only gravity traps prevent oil from being produced. This will, however, not be the case for clastic sediment-infill. The proposed novel conceptual paleokarst reservoir modelling approach may thus improve forecasting the presence, spatial distribution, and morphology of sedimentary infill and gravity traps, and ultimately lead to enhanced oil recoveries.

If diagenetic overprinting is kept aside, a paleokarst reservoir may simplistically be subdivided into three conceptual endmembers based on the organisation and composition of facies (Fig. 8A-C). All endmembers are not necessarily present in every paleokarst reservoir setting, and transitional types should be expected (e.g., Fig. 8D, E). In the lower part of Fig. 8, the paleocave facies classification of Loucks and Mescher (2002) is used to describe the internal facies distribution of the endmembers.

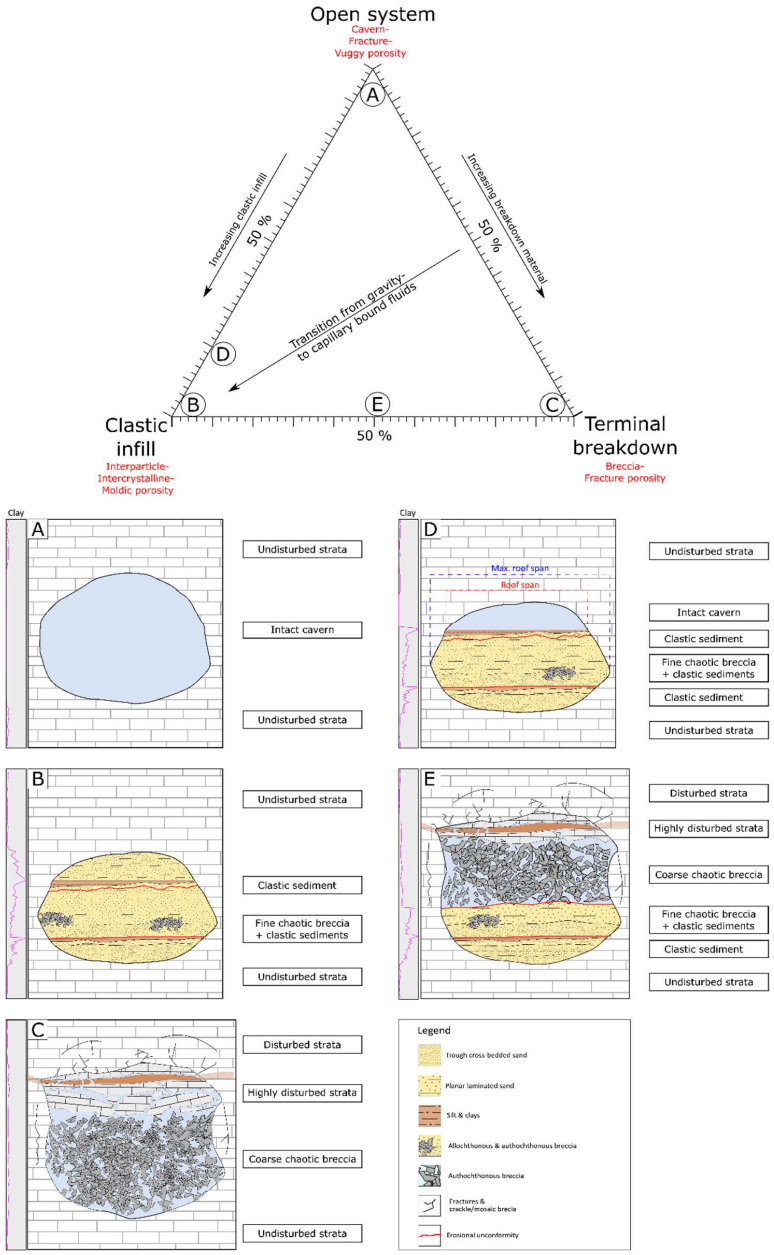

Fig. 8: Ternary plot of proposed paleokarst reservoir endmembers. Conceptual models of various paleokarst settings (A-E) and associated, facies distribution and relative clay abundance. A) Endmember A: Karst system subaerially exposed and flushed of sediments prior to burial, or cavern porosity formed at depth. Minor to no clay content present., B) Endmember B: Karst system subaerially exposed and completely infilled with allochthonous clastic sediments before burial. A high abundance of allochthonous clay may be present., C) Endmember C: Karst system subaerially exposed and flushed of sediments or cavern porosity formed at depth. Terminal breakdown of the conduit at depth. Conduit sections comprise coarse chaotic breccia and disturbed and highly disturbed host

rock facies., D) Transitional type D: Karst system subaerially exposed and partly infilled with allochthonous clastic sediments before burial. Conduit section remains intact during burial and cavern porosity is preserved. High clay abundance constrained to sediment-fill. Clay content is expected to be absent in the preserved cavity. Note that the roof span decreases as the sedimentary infill exceeds the maximum diameter, eventually enhancing cavern stability. Cavern stability may be further enhanced by pore-filling fluids, E) Transitional type E: Karst system subaerially exposed and partly infilled with allochthonous clastic sediments followed by a terminal breakdown. High clay content is constrained to sediment-fill. Note that clay abundance is relative and that the host rock is generally very pure, clay content <5% (Bögli, 1980). Also note that the cross-sectional shape in the conceptual models are for illustrative purposes and that different conduit morphologies (e.g., vadose incision/"keyhole morphology" or paragenetic half tubes) may be present. The paleocave facies classification by Loucks and Mescher (2002) is used to describe the internal facies organisation of the conceptual models.

Endmember A represents intact-conduit sections lacking infill (Fig. 8A). Clastic sediments are thus either flushed out of the system pre-burial (e.g., epigene karst), or cavern porosity is formed in a phreatic setting (e.g., hypogene karst and flank-margin caves). Epigene karst is commonly formed at relatively shallow depths and consists of open-conduit systems comprising one or more inlets and springs. Thus, large volumes of clastic sediments may be flushed in, through and out of a karst system during periods of elevated discharge. If cavern stability is sufficient, drained cavities may thus remain intact during burial and open at depth. Conversely, closed systems formed under phreatic conditions, at depths and pressure regimes significantly different to those typical for epigene karst, are expected to comprise low or no abundance of clastic sediments as these cave systems are detached from surficial processes. The Archimedes principle states that a liquid-filled cavity is buoyant upward by a force proportional to the density difference between the fluid and the confining solid (host rock/matrix) (Heath, 1897; White, 2012). The presence of connate fluids can thus provide buoyant support to the ceiling beds (White and White, 1969b; Osborne, 2002; White, 2012; Ford and Williams, 2013; Travis, 2014) and increase the preservation potential of cavern porosity. Thus, cavern porosity can in a phreatic setting, as opposed to a vadose or epiphreatic one, has an elevated preservation potential.

Endmember B represents intact-conduit sections that are filled with clastic sediments (Fig. 8B). The infill predominantly consists of allochthonous poorly- to well-sorted clay- to cobble-sized material, interbedded with various amounts of fine chaotic breccias (transported during floods). The preservation of these deposits is closely linked to the

system's morphology, scale, changes in base level and local hydrology, but in a manner less straightforward than is the case for clastic depositional systems on the surface. Lowering of base level can, for example, cause sediments to be partly or entirely removed locally. It can also alter drainage patterns, causing bypass and preservation of sediment-filled passages (Bosch and White, 2004). Bypass and sediment presevation can also occur as the karst system evolves under stable base level conditions. Depositional systems in caves differ from their surface counterparts as the accommodation space is constrained by the shape and dimensions of the conduits they inhabit. Thus, sediment distribution patterns in caves are inherently complex and commonly discontinuous. In intact and filled caverns, the lithostatic pressure from clastic sediments may impede or prevent wall spalling and roof breakdown. If a cavern remains intact, the encompassing stress field caused by the overburden is evenly distributed along the cave walls, and cave deposits may thus be shielded from compaction. The reservoir quality of paleocave sediment infill is mainly dependent on texture and mineralogy. According to Loucks and Mescher (2002), clay- and quartz-rich sediments tend to have low porosity and permeability, whereas carbonate sediments may be porous and permeable. Contrary, breccia can have porosities exceeding 20% and permeabilities in the Darcys (Loucks and Mescher, 2002). Although the reservoir quality of siliciclastic sediments in paleokarst reservoirs is expected to be poor (Loucks and Mescher, 2002), the sediment infill may retain high porosities inside intact cavities unless cemented or compacted under a subsequently collapsing roof. Endmember B is expected to comprise interparticle, intercrystalline and moldic pore-systems predominantly, and capillary forces may impair oil recovery.

Endmember C represents collapsed-conduit sections comprising no pre-collapse infill (Fig. 8C). Terminal breakdown causes a redistribution of the initial cavern porosity. The cavity is filled in by coarse chaotic breccia; underlying sediments are compacted, and encompassing strata are fractured and brecciated (highly disturbed- and disturbed strata facies) because of the collapse. The overall porosity post-collapse will thus remain the same (unless altered by diagenetic processes) but will be redistributed beyond the rock

volume affected by karstification. The endmember is anticipated to comprise breccias and disturbed host rock predominantly. The size, shape, lithology, and pore-network of the breccia clasts will result from the associated bed thickness, fracture density/orientation and lithology of the encompassing host rock. The presence of clastic sediments is thus expected to be very low or absent. Endmember C predominantly comprises pore systems related to inter-, intra-breccia and fracture porosity, and gravity is expected to control oil recovery, while capillary forces do not impair recovery.

Transitional type D represents conduit sections comprising undisturbed strata, clastic sediment infill, fine chaotic breccia and intact cavern sections (Fig. 8D). Facies proportions may vary. This transitional type represents karst cavities that have not collapsed during burial and have a varying abundance of clastic sediment infill. A high degree of infill provides lithostatic pressure on cave walls and may, depending on the shape of the cave roof, narrow the roof span (Fig. 8D), ultimately increasing cavern stability (Jameson, 1991). Caverns not affected by mechanical breakdown processes remain intact during burial, eventually resulting in cavern porosity being preserved and clastic sediments shielded from compactional processes. The transitional type D comprises pore networks associated with the sediment infill and preserved cavern porosity.

Transitional type E represents cave sections that may have a similar depositional history as transitional type D (Fig. 8D), but cavern instability results in a terminal breakdown of the cavity (Fig. 8E). Consequently, the paleokarst volume increases. The volumetric expansion will largely be controlled by the pre-collapse cavern porosity and pore-space reduction of underlying sediments by compaction.

The presence and spatial distribution of the endmembers can, to some extent, be forecasted by delimiting the pre-burial clastic sediment infill (Paper II) and simulating subsequent collapse- and infill processes (Paper III). The endmembers can then be

discretized in a geocellular framework using industry-standard reservoir modelling software suites (Paper I and III). However, applied grid-cell resolution may largely control the representativity of these models. Upscaling of paleokarst reservoir models has a significant impact on the preservation of petrophysical contrasts and morphologic resolution, as evident from the petrophysical models presented in Fig. 9. The contrasts and morphological detail evident at 1 m x 1 m x 1 m grid-cell resolution diminish rapidly as the reservoir model is upscaled (Fig. 9). The graphs in Fig. 10 show that preservation of petrophysical contrasts during upscaling, however, largely depends on the upscaling approach. Although outside the scope of this thesis and not elaborated here, it is important to highlight that the applied grid-cell resolution can have a major impact on the accuracy and outcome of fluid-flow analyses and associated prospect evaluations (e.g., Balyesiima, 2020; Balyesiima et al., in review).

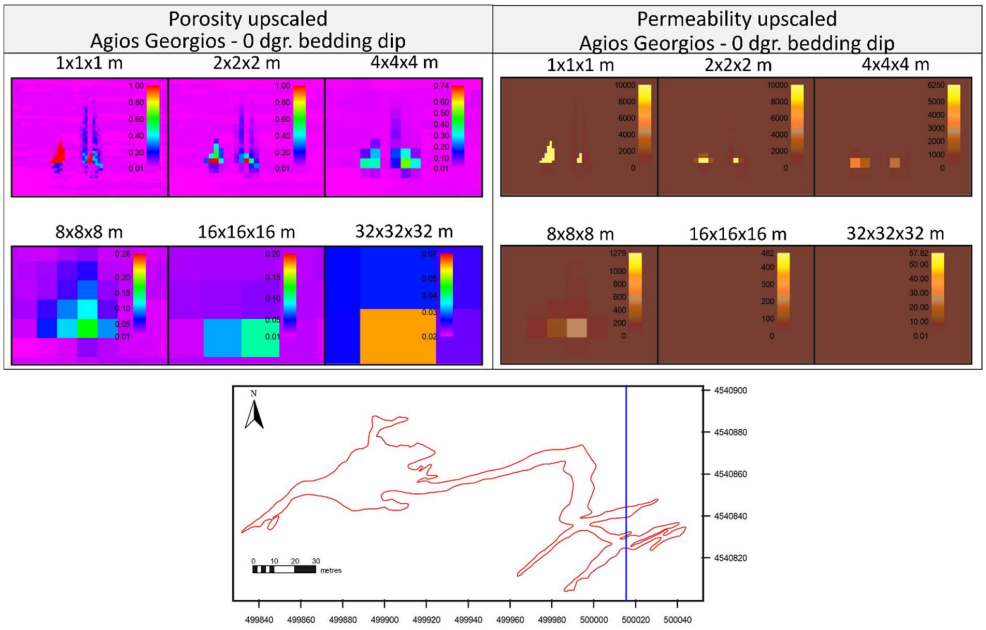

Fig. 9: Grid cell resolution sensitivity on petrophysical properties. Conceptual paleokarst reservoir model of the Agios Georgios cave system in horizontally bedded stratigraphy (Paper III). Petrophysical modelling is carried out using the porosity and permeability ranges presented in Paper III. The methods for upscaling are arithmetic for porosity and harmonic-arithmetic for permeability. Note that permeability contrasts diminish rapidly as grid cell size increases. This upscaling effect will have a significant impact in Areas comprising preserved cavern porosity as "permeable highways" will average out (smoothing).

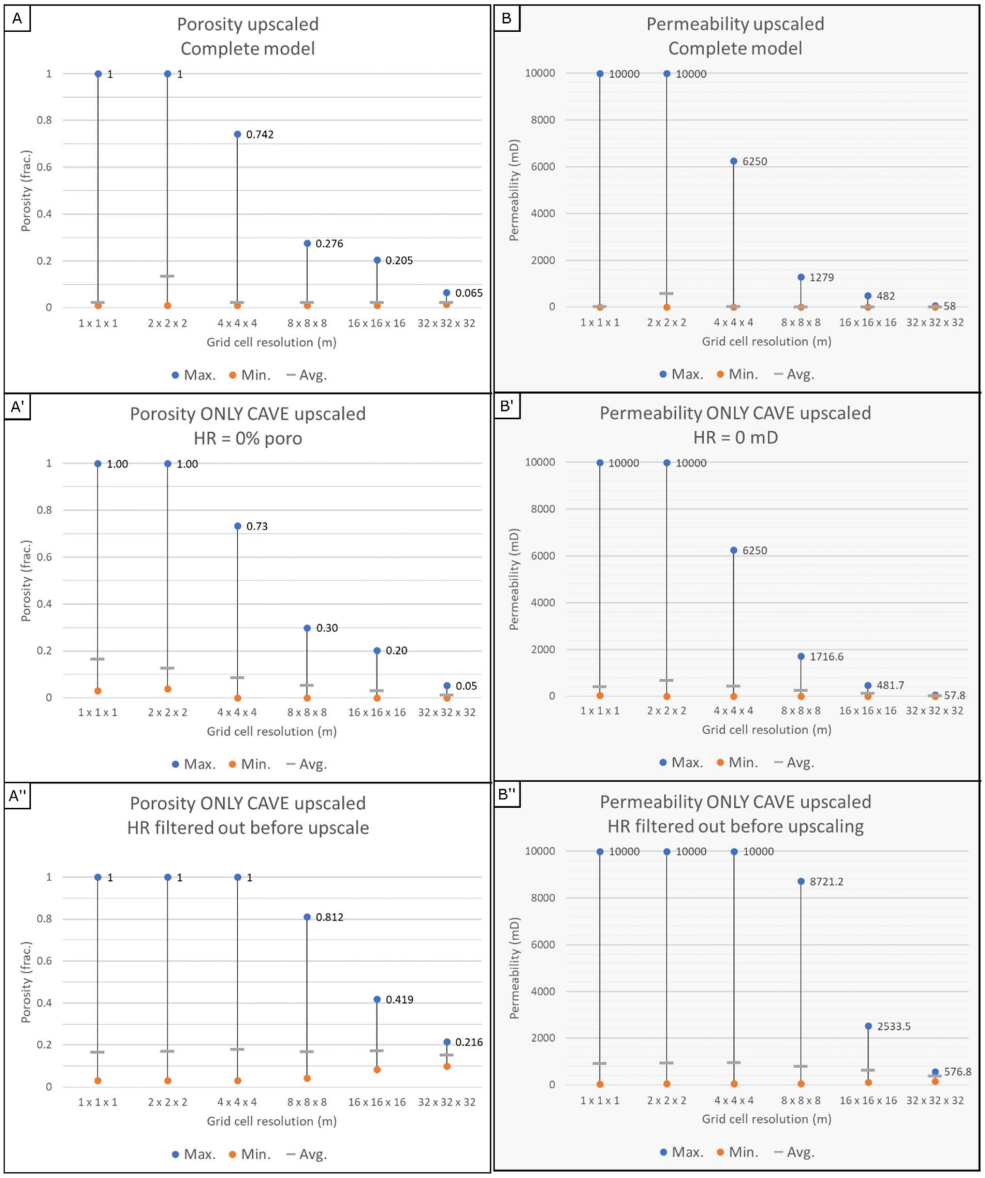

Fig. 10: Petrophysical property distribution during upscaling. The graphs show the maximum, minimum and average porosity (A) and permeability (B) following different upscaling approaches. A & B) The complete grid model (host rock and paleokarst) is populated with petrophysical properties and upscaled. Note that the petrophysical contrasts diminish as the model is upscaled and maximum values lowered. A' & B') The host rock's petrophysical properties are set to 0, whereas the paleokarst volume is populated according to the ranges proposed by Labourdette et al. (2007) (see Paper III for values). Note that petrophysical contrasts still diminish during upscaling as the maximum values decrease. A'' & B'') The host rock is filtered out and only the paleokarst volume is upscaled. The paleokarst volume is populated with petrophysical properties according to the ranges proposed by Labourdette et al. (2007). Note the enhanced preservation of petrophysical contrasts and average values.

To summarize, publicly available paleokarst reservoir modelling approaches often fail to incorporate the spatial distribution, morphology, volume, and, crucially, connectivity of paleokarst features in a realistic manner. Accurate and efficient modelling of complex morphologies is challenging but geocellular rendering of cave surveys can be carried out using industry-standard reservoir modelling software suites (Paper I). Point clouds can be used to discretize a cave system in a geocellular framework by geometric modelling, ensuring grid-cell coherency and high volumetric and geometric accuracy. To our knowledge, there are no previously known non-destructive methods for large-scale mapping the true extent and spatial distribution of sediment infill and associated sub-sediment cave floor morphology. The results from Paper II and III emphasize the importance of delimiting volumetric and geometric elements in caves and highlight some of the uncertainties associated with using cave surveys as analogues to paleokarst reservoir modelling. The volumetric extent of pre-burial clastic sediments can be delimited by using conventional geophysical methods (e.g., ERT) and common field mapping (Paper II). Although ERT has its limitations, it may be a good starting point for improving our understanding of the spatial distribution and volumetric significance of clastic sediment infill in active karst systems, and eventually the preservation potential during burial.

To synthesize, all these papers build on each other to form a robust and complete workflow for processes-driven conceptual modelling of paleokarst reservoirs. The proposed approach allows resolving geological heterogeneities on both relatively small scale (e.g., stratigraphic alterations of clastic sediment infill) and large scale (e.g., cave morphology). The work presented in this thesis can be combined with current data-driven modelling techniques and surficial geophysical mapping to account for unidentified cave volumes not rendered by cave surveys. This approach can provide realistic paleokarst reservoir analogues as karst features can be studied and rendered at most scales. The learnings from this PhD study and the developed methods are expected to be applicable for any karst system. Conceptual models of paleokarst may improve our understanding of how to best manage this reservoir type and ultimately enhance

recovery. Moreover, the methods and tools developed and presented here may prove beneficial for geocellular rendering of other geometrically complex geobodies.

6 Conclusions

To conclude, first let us look back at the overall hypothesis of this research:

“Cave surveys can be used to generate conceptual models of paleokarst reservoirs using industry-standard reservoir modelling tools.”

As indicated by the conceptual models in Paper III, the short answer to this hypothesis is "most likely”. The proposed modelling approach seems to offer an improved and coherent rendering of the heterogeneous morphology and facies distribution commonly associated with paleokarst reservoirs. However, more research is required to evaluate how accurate the reservoir-model analogues reflect actual subsurface reservoir conditions to give a definitive yes. The conclusion to specific problems and assumptions for using cave surveys as a framework for process-driven conceptual modelling of paleokarst reservoirs is listed in the individual manuscripts but, in a broader sense, the following conclusions can be inferred from this work:

- Geocellular discretization of cave surveys can be carried out using industry-standard reservoir modelling software suites.
  - Volumetric over- or underestimation is expected when irregular shapes are “forced” to conform to a geocellular framework.
  - Similar pre-established methods systematically and significantly either overestimate- or underestimate the actual cave volume.
  - Cave systems represented by dense equally-spaced point clouds can be used for geometrical modelling and subsequent geocellular discretization.
  - Our novel methodology provides significantly improved volumetric and geometric rendering compared to previous methods. Precision is limited by the cave-survey quality, grid-cell resolution and applied parameter filter cut-off.

- An optimal parameter filter cut-off value can be estimated if the "actual" cave volume and desired grid-cell resolution is determined.

- Delimiting elements infilling and concealing the true cave morphology can significantly improve the geometric and volumetric accuracy of cave surveys.
  - Significant volumes of clastic sediments can accumulate in active karst systems and potentially be preserved during burial.
  - Volumes derived from cave surveys may be significantly underestimated if clastic sediments are present.
  - Elements ("cave interior") obstructing clear line-of-sight measurements during cave surveying can alter the rendered morphology significantly.
  - Electrical resistivity tomography (ERT) can be used for identification and differentiation of macro-scale resistivity contrasts in sediment-filled conduits.
  - ERT can be used to map the sub-sediment longitudinal cave floor morphology.
  - ERT can be used to map large-scale sedimentary thickness variations and obtain more accurate data on cave dimensions.
  - In-field mapping of the spatial distribution and extent of taluses (breakdown material) in caves can improve volumetric and morphological accuracy of cave surveys.
  - A high degree of pre-burial infill will result in less accommodation space available for subsequent breakdown-derived material and eventually affect the architecture of coalesced cave collapses.
  - Sediments can provide lithostatic pressure to the cave walls and impede or prevent wall spalling.
  - Sediments in paleokarst reservoirs may retain great porosities and permeabilities if caverns remain intact during burial while the

deposits are shielded from compactional processes. This implies that porosity and permeability in sediment-filled cavities may be high despite deep burial.

- The spatial distribution and extent of sediment infill in paleokarst reservoir models will largely impact subsequent fluid-flow analyses. Consequently, this will affect the resource estimates, recovery factors, and eventually associated prospect evaluations carried out on these models.
- Geostatistical analyses derived from cave surveys should be critically evaluated when applied for modelling purposes.

- Probabilistic modelling of paleokarst reservoir architectures can be carried out using cave surveys.
  - Cavern stability can be inferred from the caverns roof span and bed thickness, stratigraphic dip and flexural strength of the host rock.
  - The roof span along the cave can be estimated from spatial data derived from cave surveys.
  - Collapsed sections can be differentiated from intact sections (preserved cavern porosity) by evaluating the stability of different cave sections.
  - Forward modelling of collapse and infill processes can be carried out following a mass-balance principle (total porosity is final and only redistributed).
  - Cave sections in steeply bedded host rock, as opposed to horizontal, are more unstable and likely to collapse.
  - The cave morphology pre-collapse and associated stratigraphic- and mechanical properties of the host rock govern the final paleokarst reservoir architecture.
  - Cave corridors with long roof spans (wide and low cross-sectional shape) are more unstable and prone to collapse than those with narrow roof spans (narrow and tall cross-sectional shape).

- Preserved cavern porosity (intact sections) can compartmentalize the reservoir and form bypass zones and “permeable highways” for fluids and gases.
- Open caverns pose potential drilling hazards and may result in drill-bit drop, mud loss, erratic reservoir pressure and, worst-case scenario, uncontrolled blowout.
- Cavern collapse enhances the vertical continuity of a reservoir and target volume.
- Conceptual process-driven modelling approaches allow the rendering of karst features commonly undetectable in seismic and cores.
- Reservoir models derived from cave surveys can provide analogues to paleokarst formed in different tectonic, climatic, hydrological, and lithological settings.

6.1 Outlook

As expected with all research, new questions and challenges arise and limitations are discovered as the work unfolds. The research related to this PhD thesis is no exception. The use of cave surveys for conceptual modelling of paleokarst reservoirs is at an early stage and there are still several scientific grey boxes that must be addressed, but the outlook is promising.

Accurate volumetric and geometric rendering of paleokarst reservoirs is crucial to optimize cost- and production forecasting, well positioning and drilling. The conceptual process-driven approach proposed in this thesis may improve rendering of paleokarst reservoirs and ultimately how we manage these reservoirs. Still, geometric and volumetric accuracy is limited by current technology, computational power, and methods for data collection.

Most cave surveys are carried out using handheld laser rangefinders that provide manually acquired single measurements along cross-sections and in between survey stations. The cave morphology between survey stations is usually rendered by infield 2D sketching of the wall boundary. This implies that the rendered shape and volume of a cave are constrained to a relatively sparse set of measurements and that geometric resolution is largely dependent on the density of measurements and survey stations. Acquisition of high-resolution spatial data can be achieved by using relatively new and semi-automated instruments such as LIDAR scanners. In recent years, the LIDAR scanner technology has evolved and improved drastically, and specialized tools are being made for a wide range of different surveying purposes and environments (e.g., close/long-range, surface/subsurface, handheld/stationary/vehicle-mounted, high/low resolution, etc.). As these scanners have entered the consumer market (e.g., smartphones, cars, vacuum cleaners, etc.), the price has plummeted. Although LIDAR scanning is currently not widely used for cave mapping, I predict that this instrument will be a standard tool for cave surveying as the price becomes more reasonable. Thus, the geometric resolution rendered by cave surveys are probably going to improve drastically in a relatively short time.

In this thesis, we introduce the use of conventional geophysical methods (e.g., ERT) in caves for large-scale mapping of clastic sediments. Future optimization of electrode spacing and survey array configurations may significantly improve ERT use in caves. However, our work has barely scratched the surface on the potential of using pre-established geophysical methods within karst systems. Methods initially intended for other tasks may also prove suitable in caves and could provide enhanced depth of investigation and resolution. As recent studies suggest that there is a growing interest in quantification and qualification of the role sediments play in paleokarst reservoir settings (e.g., Tian et al., 2017; Li et al., 2018), new mapping techniques are expected to emerge. I believe robust methods securing accurate forecasting of the spatial distribution, volumetric significance, and composition of clastic sediments in caves will soon be established. In turn, better pre-burial infill constraints will result in more accurate modelling of paleokarst reservoirs and consequently improve production planning. Moreover, delimiting morphological and volumetric elements in karst systems can yield more accurate statistical data on cave size distribution.

In general, CPU power is often the Achilles heel of many reservoir models. CPU power limits the achievable grid-cell resolution and, in turn, the volumetric and geometric accuracy. In homogenous reservoirs, high grid resolution may not be necessary to build models appropriate to conduct reasonable prospect evaluations. However, for morphologically complex reservoirs with heterogeneous facies distributions (e.g., paleokarst reservoirs), grid-cell resolution, and in turn, volumetric and geometric accuracy, can be the difference between success and failure. In our study, we were able to apply a global grid cell resolution of 1 m x 1 m x 1 m on a commercial reservoir scale. Although fluid flow analyses will probably not be achievable at this scale, the grid resolution allows differentiating contrasting petrophysical properties before upscaling. This shows that currently available computational power may be sufficient for rendering the complex morphology often associated with paleokarst reservoirs. Still, fluid-flow analyses on these reservoir models may be inaccurate because localized contrasts in petrophysical properties are lost during upscaling. The empirical Moore´s law projects that the number of transistors in a dense integrated circuit almost doubles every two years. Although there are debates whether this law is still valid or not, it implies that

CPU power increase significantly year by year. This indicates that computational power sufficient for handling fluid-flow analyses on high-resolution grid models may soon be available, potentially improving our understanding of fluid behaviour in paleokarst reservoirs.

The methods proposed in this thesis are designed to circumvent the limitations and shortcomings of recent industry-standard reservoir modelling software. Consequently, the workarounds require manual work that can be time-consuming, and approximations must be made for evaluating cavern stability. However, all workflow steps can be automated by developing appropriate software add-ins to current reservoir modelling tools. Moreover, current approximations used in the forward modelling of the collapse and infill process may become more accurate as computational power and surveying techniques evolve. Therefore, I highly encourage other researchers to build on our work and aid constraining the remaining uncertainties. Furthermore, programmers are encouraged to automate our workflow and generate built-in tools suitable for common reservoir modelling software.

With a cross-disciplinary approach and application of new methods for rendering paleokarst heterogeneity, the outlook of enhancing our understanding of these reservoirs is bright.

References

Agada, S., Chen, F., Geiger, S., Toigulova, G., Agar, S., Shekhar, R., Benson, G., Hehmeyer, O., Amour, F., Mutti, M., Christ, N., and Immenhauser, A., 2014, Numerical simulation of fluid-flow processes in a 3D high-resolution carbonate reservoir analogue: Petroleum Geoscience, v. 20, no. 1, p. 125-142.

Agar, S. M., and Hampson, G. J., 2014, Fundamental controls on flow in carbonates: an introduction: Petroleum Geoscience, v. 20, no. 1, p. 3-5.

Audra, P., Bigot, J.-Y., and Mocochain, L., 2016, Hypogenic Caves in Provence (France): Acta carsologica, v. 31, no. 3.

Balyesiima, M., 2020, Flow Simulation and Sensitivity Analysis of Paleokarst Carbonate Reservoirs [MSc: The University of Bergen.

Balyesiima, M., Pettersen, Ø., Tveranger, J., and Lecomte, I., in review, Flow in complex generic paleokarst reservoirs: A simulation approach: Petroleum science and engineering.

Bárdossy, G., 2013, Karst bauxites, Elsevier.

Beach, D. K., 1995, Controls and effects of subaerial exposure on cementation and development of secondary porosity in the subsurface of Great Bahama Bank.

Bella, P., Gradziński, M., Hercman, H., Leszczyński, S., and Nemec, W., 2020, Sedimentary anatomy and hydrological record of relic fluvial deposits in a karst cave conduit: Sedimentology.

Benson, R. C., and Yuhr, L. B., 2016a, The Development of a Landfill over an Abandoned Limestone Mine, Site Characterization in Karst and Pseudokarst Terraines: Dordrecht, Springer Netherlands, p. 333-363.

Benson, R. C., and Yuhr, L. B., 2016b, Site Characterization in Karst and Pseudokarst Terraines: Practical Strategies and Technology for Practicing Engineers, Hydrologists and Geologists, Springer.

Blickwede, J., and Rosenfeld, J., 2010, The Greatest Oil Well in History? The Story of Cerro Azul# 4.

Böcker, T., and Vizy, B., 1989, Hydrogeological Problems of Hungarian Bauxite and Coal Depostis, Developments in Earth Surface Processes, Volume 1, Elsevier, p. 533-548.

Bögli, A., 1964, Mischungskorrosion—Ein beitrag zum verkarstungsproblem: Erdkunde, p. 83-92.

-, 1980, Karst hydrology and physical speleology: Springer-Verlag, Berlin, p. 284.

Borghi, A., Renard, P., and Jenni, S., 2010, How to Model Realistic 3D Karst Reservoirs Using a Pseudo-Genetic Methodology–Example of Two Case Studies: Advances in Research in Karst Media, p. 251-255.

Borghi, A., Renard, P., and Jenni, S., 2011, A pseudo-genetic stochastic model to generate karstic networks: Journal of hydrology, v. 414, p. 516-529.

Borghi, A., Renard, P., and Jenni, S., 2012, A pseudo-genetic stochastic model to generate karstic networks: Journal of Hydrology, v. 414, p. 516-529.

Bosák, P., 1989, Clays and sands in paleokarst, Developments in Earth Surface Processes, Volume 1, Elsevier, p. 431-442.

Bosch, R. F., and White, W. B., 2004, Lithofacies and transport of clastic sediments in karstic aquifers, Studies of cave sediments, Springer, p. 1-22.

-, 2018, Lithofacies and Transport for Clastic Sediments in Karst Conduits, Karst Groundwater Contamination and Public Health, Springer, p. 277-281.

Budaj, M., and Mudrák, S., Therion–digital cave maps therion–cartographie souterraine digitale, *in* Proceedings Presented on the 4th European Speleological Congress, Banska Bystrica, Slovakia2008.

Budaj, M., and Stacho, M., 2019, Therion.

Budd, D. A., Hammes, U., and Vacher, H. L., 1993, Calcite cementation in the upper Floridan aquifer: A modern example for confined-aquifer cementation models?: Geology, v. 21, no. 1, p. 33-36.

Budd, D. A., Saller, A. H., and Harris, P. M., 1995, Unconformities and Porosity in Carbonate Strata, American Association of Petroleum Geologists, v. v. 63.
Burchette, T. P., 2012, Carbonate rocks and petroleum reservoirs: a geological perspective from the industry: Geological Society, London, Special Publications, v. 370, no. 1, p. 17-37.
Cander, H., 1995, Interplay of water-rock interaction efficiency, unconformities, and fluid flow in a carbonate aquifer: Floridan aquifer system.
Chilingar, G. V., and Yen, T., 1983, Some notes on wettability and relative permeabilities of carbonate reservoir rocks, II: Energy Sources, v. 7, no. 1, p. 67-75.
Choquette, P. W., and James, N. P., 1988, Paleokarst, Springer-Verlag.
Christanis, K., Georgakopoulos, A., Fernandez-Turiel, J. L., and Bouzinos, A., 1998, Geological factors influencing the concentration of trace elements in the Philippi peatland, eastern Macedonia, Greece: International Journal of Coal Geology, v. 36, no. 3-4, p. 295-313.
Coogan, A. H., Maggio, C., and Bebout, D. G., 1972, Depositional Environments and Geologic History of Golden Lane and Poza Rica Trend, Mexico, an Alternative View: American Association of Petroleum Geologists Bulletin, v. 56, no. 8, p. 1419-&.
Craig, D. H., 1988, Caves and other features of Permian karst in San Andres dolomite, Yates field reservoir, west Texas, Paleokarst, Springer, p. 342-363.
Dickson, J., and Saller, A. H., 1995, Identification of subaerial exposure surfaces and porosity preservation in Pennsylvanian and Lower Permian shelf limestones, eastern Central Basin platform, Texas.
Dżułyński, S., and Sass-Gustkiewicz, M., 1989, Pb-Zn ores, Paleokarst. A Systematic and Regional Review, Volume 1, Elsevier, p. 377-397.
Erzeybek Balan, S., 2012, Characterization and modeling of paleokarst reservoirs using multiple-point statistics on a non-gridded basis: Ph.D. Dissertation, The University of Texas at Austin, p. 1-307.
Esteban, M., and Klappa, C. F., 1983, Subaerial exposure environment: Carbonate Depositional Environments: American Association of Petroleum Geologists, Memoir, v. 33, p. 1-54.
Esteban, M., and Wilson, J. L., 1993a, Introduction to karst systems and paleokarst reservoirs: Special publications of SEPM, p. 1-9.
-, 1993b, Introduction to karst systems and paleokarst reservoirs.
Farrant, A. R., and Smart, P. L., 2011, Role of sediment in speleogenesis; sedimentation and paragenesis: Geomorphology, v. 134, no. 1-2, p. 79-93.
Fernandez-Ibanez, F., DeGraff, J. M., Moore, P. J., Ahdyar, L., and Nolting, A., 2019, Characterization of non-matrix type and flow potential using lost circulation information: Journal of Petroleum Science and Engineering, v. 180, p. 89-95.
Flügel, E., 2010, Microfacies of Carbonate Rocks, Berlin, Heidelberg, Springer Berlin Heidelberg, Analysis, Interpretation and Application.
Ford, D., and Williams, P. D., 2013, Karst hydrogeology and geomorphology, John Wiley & Sons.
Ford, D. C., 1971, Geologic structure and a new explanation of limestone cavern genesis: Transactions of the Cave Research Group of Great Britain, v. 13, no. 2, p. 81-94.
Ford, D. C., and Ewers, R. O., 1978, The development of limestone cave systems in the dimensions of length and depth: Canadian Journal of Earth Sciences, v. 15, no. 11, p. 1783-1798.
Ford, D. C., and Williams, P. W., 1989, Karst geomorphology and hydrology, Unwin Hyman London.
-, 2002, Karst geomorphology and hydrology, Unwin Hyman London.
Frantz, Y., Collon, P., Renard, P., and Viseur, S., 2021, Analysis and stochastic simulation of geometrical properties of conduits in karstic networks: Geomorphology, v. 377, p. 107480.
Fritz, R. D., Wilson, J. L., and Yurewicz, D. A., 1993, Paleokarst related hydrocarbon reservoirs, SEPM, v. 18.
Fuchs, Y., 1989, Paleokarst-related uranium deposits, Paleokarst. A Systematic and Regional Review, Volume 1, Elsevier, p. 473-480.
Furnée, J. P. B., 2015, Geo-modeling and fluid flow simulation in paleokarst reservoirs: The University of Bergen.

Gunn, J., 2004, Encyclopedia of caves and karst science, Taylor & Francis.
Heath, T. L., 1897, The works of Archimedes, Cambridge, University Press.
Heeb, B., 2008, Paperless Caving-An Electronic Cave Surveying System La topo sans papier-un système électronique de topographie, IV th European speleological congress: Isére - France.
-, 2009, An all-in-one electronic cave surveying device: Cave Radio & Electronics Group Journal, v. 72, p. 8-10.
-, 2010, PocketTopo.
-, 2014, The next generation of the DistoX cave surveying instrument: CREG Journal, v. 88, p. 5-8.
Henrion, V., Pellerin, J., and Caumon, G., A stochastic methodology for 3D cave systems modeling2008.
Hurley, N. F., Tanner, H. C., and Barcat, C., 1995, Unconformity-Related Porosity Development in the Quintuco Formation (Lower Cretaceous), Neuquén Basin, Argentina.
James, N. P., and Choquette, P. W., 1983, Diagenesis .5. Limestones - Introduction: Geoscience Canada, v. 10, no. 4, p. 159-161.
Jameson, R., 1991, Concept and classification of cave breakdown: An analysis of patterns of collapse in Friars Hole Cave System, West Virginia: Appalachian Karst. National Speleological Society, p. 35-44.
Jensen, K., Johansen, M. K., Lecomte, I., Janson, X., Tveranger, J., and Kaschwich, T., 2021, Paleokarst reservoirs: Efficient and flexible characterization using point-spread function-based convolution modeling: Interpretation, v. 9, no. 2, p. 1-65.
Kadlec, J., Chadima, M., Lisa, L., Hercman, H., Osintsev, A., and Oberhaensli, H., 2008, Clastic cave deposits in Botovskaya cave (Eastern Siberia, Russian federation): Journal of Cave and Karst Studies, v. 70, no. 3, p. 142-155.
Kaiser, M. J., and Pulsipher, A. G., 2007, A review of the oil and gas sector in Kazakhstan: Energy Policy, v. 35, no. 2, p. 1300-1314.
Kaufmann, G., Romanov, D., and Dreybrodt, W., 2019, Modeling the evolution of karst aquifers, Encyclopedia of Caves, Elsevier, p. 717-724.
Kerans, C., 1988, Karst-Controlled Reservoir Heterogeneity in Ellenburger Group Carbonates of West Texas: Aapg Bulletin-American Association of Petroleum Geologists, v. 72, no. 10, p. 1160-1183.
Kerans, C., 1990, Depositional systems and karst geology of the Ellenburger Group (Lower Ordovician), subsurface West Texas: University of Texas Bureau of Economic Geology.
-, 1993, Description and interpretation of karst-related breccia fabrics, Ellenburger Group, West Texas.
Klimchouk, A., 2009, Morphogenesis of hypogenic caves: Geomorphology, v. 106, no. 1-2, p. 100-117.
Klimchouk, A., 2012, Speleogenesis, hypogenic: Studies, v. 69, p. 114À134.
Klimchouk, A., Samokhin, G., and Kasian, Y., The deepest cave in the world in the Arabika massif (Western Caucasus) and its hydrogeological and paleogeographic significance, *in* Proceedings ICS Proceedings, 15th International Congress of Speleology, Kerrville2009, Volume 27, p. 898-905.
Kyle, J. R., 1983, Economic aspects of subaerial carbonates: Carbonate depositional Environments, p. 73-92.
La Ode Ahdyar, R. P. S., Mohammad, S. R., Fernandez-Ibanez, F., and Moore, P. J., 2019, Integrated Carbonate Non-Matrix Characterization in Banyu Urip Field.
Labourdette, R., Lascu, I., Mylroie, J., and Roth, M., 2007, Process-like modeling of flank-margin caves: From genesis to burial evolution: Journal of Sedimentary Research, v. 77, no. 11-12, p. 965-979.
Ledsaak, K., 2016, Geo-modelling of paleokarst reservoirs-from cave-survey to geocellular paleokarst model: The University of Bergen.
Li, Y. Q., Hou, J. G., Sun, J. F., Kang, Z. J., Liu, Y. M., Song, S. H., and Han, D., 2018, Paleokarst reservoir features and their influence on production in the Tahe Oilfield, Tarim basin, China: Carbonates and Evaporites, v. 33, no. 4, p. 705-716.

Lomando, A. J., Harris, P. M., and Orlopp, D. E., 1993, Casablanca field, Tarragona Basin, offshore Spain: a karsted carbonate reservoir: Special publications of SEPM.
Longman, M. W., 1980, Carbonate Diagenetic Textures from Nearsurface Diagenetic Environments: Aapg Bulletin-American Association of Petroleum Geologists, v. 64, no. 4, p. 461-487.
Lønøy, A., 2006, Making sense of carbonate pore systems: AAPG bulletin, v. 90, no. 9, p. 1381-1405.
Lønøy, B., Pennos, C., Tveranger, J., Lauritzen, S.-E., Furnée, J. P., and Ledsaak, K., 2019, Paleokarst reservoir modelling based on active cave system analogs - implementing cave survey data in geocellular reservoir models, Winter conference 2019: Bergen.
Lønøy, B., Tveranger, J., Pennos, C., Whitaker, F., and Lauritzen, S.-E., 2020, Geocellular rendering of cave surveys in paleokarst reservoir models: Marine and Petroleum Geology, p. 104652.
Loucks, R. G., 1999, Paleocave carbonate reservoirs: Origins, burial-depth modifications, spatial complexity, and reservoir implications: Aapg Bulletin-American Association of Petroleum Geologists, v. 83, no. 11, p. 1795-1834.
Loucks, R. G., and Mescher, P. K., 2002, Paleocave facies classification and associated pore types: American Association of Petroleum Geologists.
Lu, C. H., Chen, Y. M., Zhang, C., and Luo, J., 2013, Steady-state freshwater-seawater mixing zone in stratified coastal aquifers: Journal of Hydrology, v. 505, no. Supplement C, p. 24-34.
Lu, X. B., Wang, Y., Tian, F., Li, X. H., Yang, D. B., Li, T., Lv, Y. P., and He, X. M., 2017, New insights into the carbonate karstic fault system and reservoir formation in the Southern Tahe area of the Tarim Basin: Marine and Petroleum Geology, v. 86, p. 587-605.
Lucia, F. J., 1995, Lower Paleozoic cavern development, collapse, and dolomitization, Franklin Mountains, El Paso, Texas.
-, 2007, Carbonate reservoir characterization: an integrated approach, Springer Science & Business Media.
Martini, I., 2011, Cave clastic sediments and implications for speleogenesis: new insights from the Mugnano Cave (Montagnola Senese, Northern Apennines, Italy): Geomorphology, v. 134, no. 3-4, p. 452-460.
Matsuda, H., Tsuji, Y., Honda, N., and Saotome, J.-i., 1995, Early diagenesis of Pleistocene carbonates from a hydrogeochemical point of view, Irabu Island, Ryukyu Islands: Porosity changes related to early carbonate diagenesis.
Mazzullo, S., and Chilingarian, G., 1996, Hydrocarbon reservoirs in karsted carbonate rocks, Developments in Petroleum Science, Volume 44, Elsevier, p. 797-865.
Montaron, B., 2008, Carbonate evolution: Oil & Gas Middle East, p. 26-31.
Montaron, B. A., Xue, F. J., Tian, W., Han, R., and Ray, P., 2014, Cave Geomorphology and its Effects on Oil Recovery Factors in Tarim Karst Reservoirs, West China, International Petroleum Technology Conference: Kuala Lumpur, Malaysia, p. 13.
Moore, C. H., 1989, Carbonate diagenesis and porosity, Elsevier.
Moore, C. H., and Wade, W. J., 2013, Carbonate reservoirs: porosity and diagenesis in a sequence stratigraphic framework, Newnes.
Mutti, M., 1995, Porosity development and diagenesis in the Orfento Supersequence and its bounding unconformities (Upper Cretaceous, Montagna della Maiella, Italy).
Mylroie, J. E., and Carew, J. L., 1988, Solution Conduits as Indicators of Late Quaternary Sea-Level Position: Quaternary Science Reviews, v. 7, no. 1, p. 55-64.
Mylroie, J. E., and Carew, J. L., 1995, Karst development on carbonate islands.
NASA/METI/AIST/Japan Spacesystems, a. U. S. J. A. S. T., 2019, ASTER Global Digital Elevation Model V003, *in* DAAC, N. E. L. P., ed.
Novel, J. P., Dimadi, A., Zervopoulou, A., and Bakalowicz, M., 2007, The Aggitis karst system, Eastern Macedonia, Greece: Hydrologic functioning and development of the karst structure: Journal of Hydrology, v. 334, no. 3-4, p. 477-492.
Osborne, R., 2002, Cave breakdown by vadose weathering: International Journal of Speleology, v. 31, no. 1, p. 3.

Palmer, A. N., 1991, Origin and Morphology of Limestone Caves: Geological Society of America Bulletin, v. 103, no. 1, p. 1-21.
Palmer, A. N., 1995, Geochemical models for the origin of macroscopic solution porosity in carbonate rocks, Unconformities and Porosity in Carbonate Strata, Volume 63, American Association of Petroleum Geologists, p. 313.
Papapetros, P., 1982, Geological map of Greece, scale 1:50000.
Papaphilippou-Pennou, E., 2004, Dynamic evolution and recent exogenic processes of Strymon river network in Serres graben (North Greece) [Ph.D.: Aristotle University of Thessaloniki, 212 p.
Parise, M., Gabrovsek, F., Kaufmann, G., and Ravbar, N., 2018, Recent advances in karst research: from theory to fieldwork and applications: Geological Society, London, Special Publications, v. 466, no. 1, p. 1-24.
Pennos, C., Astaras, T., Vouvalidis, K., Papaphilippou-Pennou, E., and Pechlivanidou, S., 2011, Geomorphological and morphotectonic features of the alluvial fans of the nortern part of the Aggitis river: Bulletin of the Geological Society of Greece, v. 44, p. 29-36.
Pennos, C., Lauritzen, S. E., Pechlivanidou, S., Aidona, E., Haflidason, H., and Sotiriadis, Y., 2016a, Decoding clastic sediment sources from the Maaras Cave Northern Greece, 18th Joint Geomorphological Meeting: Chambery, France.
Pennos, C., Lauritzen, S. E., Pechlivanidou, S., and Sotiriadis, Y., 2016b, Geomorphic constrains on the evolution of the Aggitis river basin Northern Greece (a preliminary report): Bulletin of the Geological Society of Greece, v. 50.
Plummer, L., 1975, Mixing of sea water with calcium carbonate ground water: Geological Society of America Memoirs, v. 142, p. 219-236.
Quinif, Y., and Vandycke, S., 2001, "Karst and tectonic"-Preface: Geologica Belgica [En ligne], v. 4, no. number 3-4 Karst & Tectonics, p. 171-173.
Ren, M., and Jones, B., 2016, Diagenesis in limestone-dolostone successions after 1 million years of rapid sea-level fluctuations: A case study from Grand Cayman, British West Indies: Sedimentary Geology, v. 342, p. 15-30.
Ringrose, P., and Bentley, M., 2015, Reservoir model design - A practioner´s guide, Springer.
Roehl, P. O., and Choquette, P. W., 2012, Carbonate petroleum reservoirs, Springer Science & Business Media.
Romanov, D., and Dreybrodt, W., 2006, Evolution of porosity in the saltwater-freshwater mixing zone of coastal carbonate aquifers: An alternative modelling approach: Journal of Hydrology, v. 329, no. 3-4, p. 661-673.
Rongier, G., Collon-Drouaillet, P., and Filipponi, M., 2014, Simulation of 3D karst conduits with an object-distance based method integrating geological knowledge: Geomorphology, v. 217, p. 152-164.
Saller, A. H., Budd, D. A., and Harris, P. M., 1994, Unconformities and Porosity Development in Carbonate Strata - Ideas from a Hedberg Conference: Aapg Bulletin-American Association of Petroleum Geologists, v. 78, no. 6, p. 857-872.
Sanford, W. E., and Konikow, L. F., 1989, Porosity development in coastal carbonate aquifers: Geology, v. 17, no. 3, p. 249-252.
Sangster, D. F., 1988, Breccia-Hosted Lead—Zinc Deposits in Carbonate Rocks, Paleokarst, Springer, p. 102-116.
Schalk, C., 2019, An independent Global Energy Forecast to 2050, to compare with the IEA's WEO 2019.
Schlumberger, 2007, Carbonate Reservoirs - Meeting unique challenges to maximize recovery.
Sendra, A., Garay, P., Ortuno, V. M., Gilgado, J. D., Teruel, S., and Reboleira, A. S. P. S., 2014, Hypogenic versus epigenic subterranean ecosystem: lessons from eastern Iberian Peninsula: International Journal of Speleology, v. 43, no. 3, p. 253-264.
Shanov, S., and Kostov, K., 2014, Dynamic tectonics and karst, Springer.

Soudet, H. J., Sorriaux, P., and Rolando, J. P., 1994, Relationship between Fractures and Karstification - the Oil-Bearing Paleokarst of Rospo Mare (Italy): Bulletin Des Centres De Recherches Exploration-Production Elf Aquitaine, v. 18, no. 1, p. 257-297.

Strebelle, S., 2002, Conditional simulation of complex geological structures using multiple-point statistics: Mathematical geology, v. 34, no. 1, p. 1-21.

Sun, S. Q., and Sloan, R., 2003, Quantification of uncertainty in recovery efficiency predictions: lessons learned from 250 mature carbonate fields, SPE Annual Technical Conference and Exhibition: Denver, Colorado, Society of Petroleum Engineers, p. 15.

Thrailkill, J., 1968, Chemical and hydrologic factors in the excavation of limestone caves: Geological Society of America Bulletin, v. 79, no. 1, p. 19-46.

Tiab, D., and Donaldson, E. C., 2015, Petrophysics: theory and practice of measuring reservoir rock and fluid transport properties, Gulf professional publishing.

Tian, F., Lu, X. B., Zheng, S. Q., Zhang, H. F., Rong, Y. S., Yang, D. B., and Liu, N. G., 2017, Structure and Filling Characteristics of Paleokarst Reservoirs in the Northern Tarim Basin, Revealed by Outcrop, Core and Borehole Images: Open Geosciences, v. 9, no. 1, p. 266-280.

Tinker, S., Ehrets, J., and Brondos, M., 1995, Multiple karst events related to stratigraphic cyclicity: San Andres Formation, Yates field, west Texas.

Travis, R., 2014, Evaluation and quantification of modern karst features as proxies for paleokarst reservoirs [MSc: Mississippi State University, 114 p.

Treiber, L., and Owens, W., 1972, A laboratory evaluation of the wettability of fifty oil-producing reservoirs: Society of petroleum engineers journal, v. 12, no. 06, p. 531-540.

Trice, R., Challenges And Insights In Optimising Oil Production Form Middle Eastern Karst Reservoirs, *in* Proceedings SPE Middle East Oil and Gas Show and Conference2005, Society of Petroleum Engineers.

Trimmis, K. P., 2018, Paperless mapping and cave archaeology: A review on the application of DistoX survey method in archaeological cave sites: Journal of Archaeological Science-Reports, v. 18, p. 399-407.

Vahrenkamp, V. C., 1995, The Post-Rotliegend Reservoirs of Auk Field, British North Sea: Subaerial Exposure and Reservoir Creation.

Vavliakis, E., Psilovikos, A., and Sotiriadis, L., 1986, The epigenetic valley of the Aggitis river and its relation with the evolution of Drama and Serres basins: Geological and Geophysical studies (IGME), v. 6, p. 5-14.

Viniegra, F., and Castillo-Tejero, C., 1970, Golden Lane fields, Veracruz, Mexico.

Wagner, P., Tasker, D., and Wahlman, G., 1995, Reservoir degradation and compartmentalization below subaerial unconformities: limestone examples from west Texas, China, and Oman, Unconformities & Porosity in Carbonate Strata, Volume 63, American Association of Petroleum Geologists, p. 313.

Waltham, A. C., and Fookes, P. G., 2003, Engineering classification of karst ground conditions: Quarterly Journal of Engineering Geology and Hydrogeology, v. 36, no. 2, p. 101-118.

Wendte, J., and Muir, I., 1995, Recognition and significance of an intraformational unconformity in Late Devonian Swan Hills reef complexes, Alberta.

White, E. L., 2012, Breakdown, *in* White, W. B., and Culver, D. C., eds., Encyclopedia of Caves, Elsevier Science & Technology, p. 68-73.

White, E. L., and White, W., 1969a, Processes of cavern breakdown: National Speleological Society Bulletin, v. 31, no. 4, p. 83-96.

White, E. L., and White, W. B., 1969b, Processes of cavern breakdown: National Speleological Society Bulletin, v. 31, no. 4, p. 83-96.

White, W. B., 1988, Geomorphology and hydrology of karst terrains, v. 551.447 W4.

White, W. B., 2007, Cave sediments and paleoclimate: Journal of Cave and Karst Studies, v. 69, no. 1, p. 76-93.

White, W. B., and Culver, D. C., 2011, Encyclopedia of caves, Academic Press.

White, W. B., Culver, D. C., Herman, J. S., Kane, T. C., and Mylroie, J. E., 1995, Karst Lands: American Scientist, v. 83, no. 5, p. 450-459.

White, W. B., and White, E. L., 2003, Gypsum wedging and cavern breakdown: Studies in the Mammoth Cave System, Kentucky: Journal of Cave and Karst Studies, v. 65, no. 1, p. 43-52.

Wigley, T. M. L., and Plummer, L. N., 1976, Mixing of Carbonate Waters: Geochimica Et Cosmochimica Acta, v. 40, no. 9, p. 989-995.

Yan, X., 2002, Reservoir properties of Ordovician carbonate rocks in the Tahe Field, Tarim Basin, China: Shiyou Yu Tianranqi Dizh (Oil and Gas Geology), v. 23, p. 262-265.

Zempolich, W. G., and Cook, H. E., 2002, Paleozoic carbonates of the Commonwealth of Independent States (CIS): subsurface reservoirs and outcrop analogs, Paleozoic carbonates of the Commonwealth of Independent States (CIS): subsurface reservoirs and outcrop analogs, Volume 74: Special publications of SEPM, SEPM Society for Sedimentary Geology, p. 1-3.

Zötl, J., 1989, Paleokarst as an important hydrogeological factor, Paleokarst. A Systematic and Regional Review, Volume 1, Elsevier, p. 483-509.

Zou, C., 2013, Carbonate Fracture-Cavity Reservoir, Elsevier, 1-2 p.:

Part II

Paper 1

Geocellular rendering of cave surveys in paleokarst reservoir models

Marine and Petroleum Geology
Volume 122, December 2020, 104652

Marine and Petroleum Geology 122 (2020) 104652

Contents lists available at ScienceDirect

Marine and Petroleum Geology

journal homepage: www.elsevier.com/locate/marpetgeo

Research paper

Geocellular rendering of cave surveys in paleokarst reservoir models

Bjarte Lønøy [a,b,*], Jan Tveranger [a], Christos Pennos [b], Fiona Whitaker [c], Stein-Erik Lauritzen [b]

[a] NORCE – Norwegian Research Centre AS, Nygårdsgaten 112, 5008, Bergen, Norway
[b] University of Bergen, Department of Earth Science, Allégaten 41, 5020, Bergen, Norway
[c] University of Bristol, School of Earth Sciences, Queens Rd, Bristol BS8 1QE, United Kingdom

ARTICLE INFO

Keywords:
Paleokarst
Reservoir modelling
Cave survey data
Geocellular rendering
Karst morphology

ABSTRACT

Infilled and collapsed cave systems are an important component of many paleokarst reservoirs. Incorporating these features into industrial reservoir models commonly relies on geostatistical modelling methods that often fail to capture key aspects of connectivity, geometry and volume of the paleokarst features realistically. The present work investigates the implementation of realistic cave geometries in geocellular models using survey data from an active karst cave as a starting point. The proposed method utilizes cave survey data to generate a dense equally spaced point-cloud representing the cave system. The point-clouds are used for geometric modelling and subsequent geocellular discretization of the karst system. The volumetric and geometric accuracy of this novel reservoir modelling method is compared to that from two established methods by benchmarking against the cave survey data. Additionally, the interlinkage between grid cell resolution, applied filter cut-off and geocellular rendering are evaluated. This study demonstrates that our proposed novel methodology can provide an excellent geometric and volumetric geocellular rendering of karst systems using cave survey data as input. Employing a combination of cave network maps and forward modelling of collapse and infill may enable model rendering of these features that more closely echoes processes controlling cave and karst breccia formation and geometric characteristics. In turn, this could offer better constraints to forecast paleokarst reservoirs architecture and properties.

1. Introduction

Active epigene and hypogene karst systems are the precursors of paleokarst reservoirs and can be used as analogues for geometric configurations of paleokarst formed under given stratigraphic, tectonic and environmental constraints. The geometry and setting of existing caves can also form the starting point for forward modelling of collapse and infill processes. Thus, cave surveys form an important, and for reservoir modelling largely unused, source of data for generating paleokarst reservoir analogue models. A first step to facilitate the general use of this data to study subsurface flow behaviour in these systems is to provide workflows for rendering cave survey data in reservoir models using standard industrial software.

Karst systems, consisting of open and partially- or completely infilled conduits and cavities, can provide key insights into the numerous paleokarst reservoirs worldwide. Well-studied examples include the Yates field of West Texas (Craig, 1988; White et al., 1995), the Golden Lane fields in Mexico (Coogan et al., 1972; Blickwede and Rosenfeld, 2010), the Rospo Mare field in Adriatic Sea (Soudet et al., 1994), the Casablanca field in the offshore Spain (Lomando et al., 1993), the Kharyaga field in the Russian Arctic (Zempolich and Cook, 2002), the Kashagan field in Kazakhstan (Kaiser and Pulsipher, 2007), the Kirkuk field in Iraq (Trice, 2005), and the Tahe field of the Tarim Basin in China (Yan, 2002). Although boasting some of the most productive wells in oil history (Viniegra and Castillo-Tejero, 1970; Fournillon et al., 2012), the recovery factor (RF) from karst-related reservoirs is generally very low when compared to conventional carbonate- and organic build-up reservoirs (Sun and Sloan, 2003; Montaron, 2008; Montaron et al., 2014). Also, production from these reservoirs is often associated with issues such as rapid water breakthrough, bypass flow and drill-bit drops.

Some of the biggest challenges for improving paleokarst reserve estimations relate to volumetric determination and estimation of cave geometries and cave size statistical distributions, which directly impact on hydrocarbon recovery factors (Montaron et al., 2014). The spatial distribution and associated morphology of karst networks play a significant role in subsurface fluid flow behaviour (e.g. Chaojun et al., 2010; Tian et al., 2016), and has been recognized in many carbonate reservoirs (Rongier et al., 2014). Hence, robust reservoir models

* Corresponding author. NORCE – Norwegian Research Centre AS, Nygårdsgaten 112, 5008, Bergen, Norway.
E-mail address: bjarte.lonoy@norceresearch.no (B. Lønøy).

https://doi.org/10.1016/j.marpetgeo.2020.104652
Received 30 May 2020; Received in revised form 5 August 2020; Accepted 8 August 2020
Available online 15 August 2020

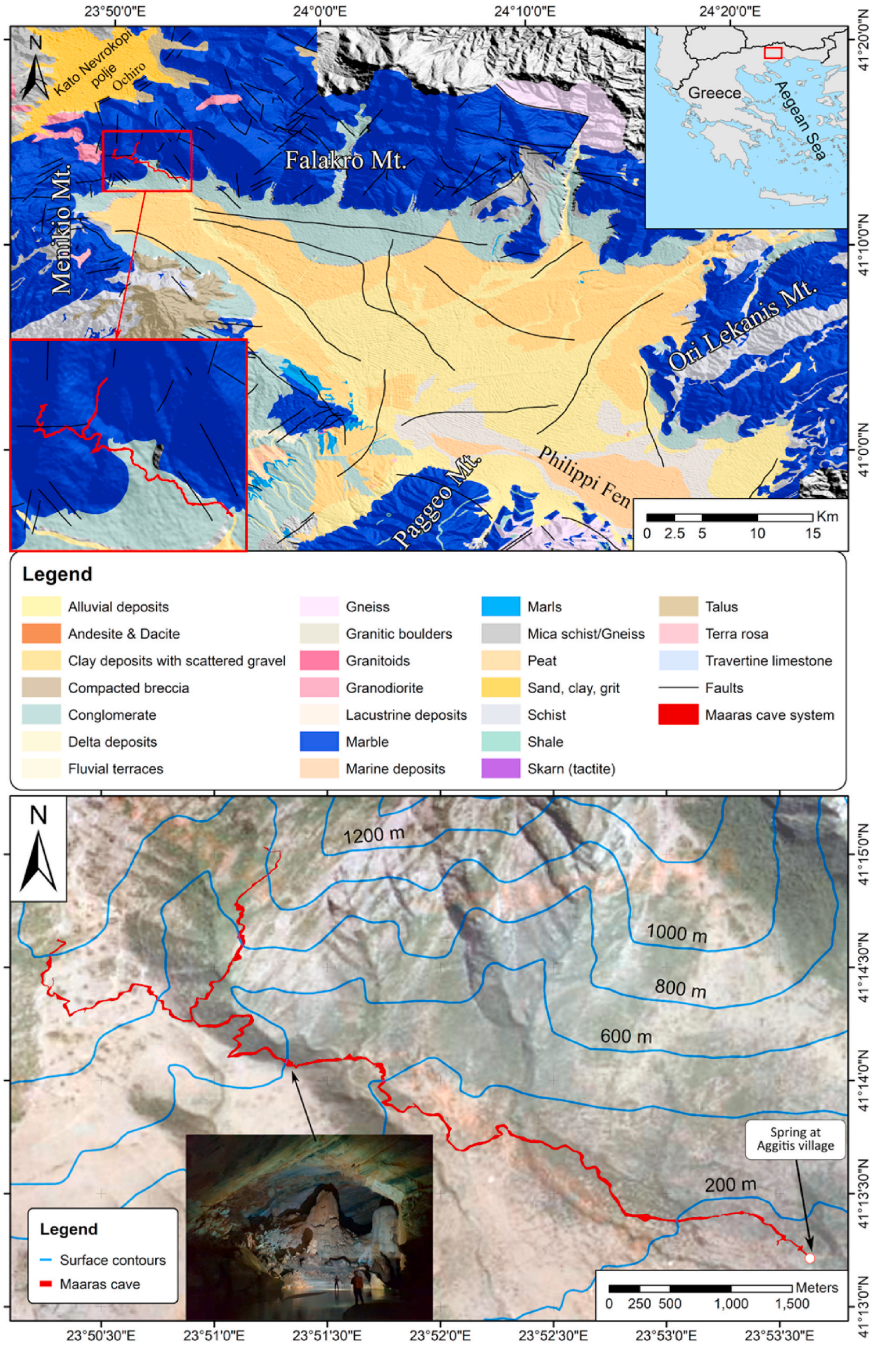

Fig. 1. An overview map of the modelled cave and surrounding area. Upper: Maaras cave (red) superimposed on a geological map modified from Pennos et al. (2016b) and a digital elevation model (ASTER GDEM). Insert: Close up of Maaras cave system. Lower: Outline of Maaras cave (from cave survey) with contour lines. Insert: picture to highlight cavern dimensions and interior. Note persons for scale. Orthophotographic map: www.ktimatologio.gr(For interpretation of the references to colour in this figure legend, the reader is referred to the Web version of this article.)

capturing the spatial distribution, morphology, and volume of paleokarst features are essential to improve resource estimates and facilitate low-risk well- and production planning.

Most current paleokarst reservoir models are based on stochastic simulations using various statistical methods such as "Object Based Modelling" (OBM), "Multiple Point Statistics" (MPS) or fast marching approach, which are conditioned on available well-data (e.g. Borghi et al., 2010; Erzeybek Balan, 2012; Rongier et al., 2014). However, this approach largely fails to adequately incorporate the geometry, volume and connectivity characteristics of karst features. Considering these difficulties, using a more concept-driven approach (rather than a data-driven) employing extant information about realistic karst cave systems as a starting point, seems to offer potential. As pointed out by Trice (2005), the use of use conceptual karst models is essential to understand the effect on karstification, and by extension, karst-degradation, infill and diagenesis of former karst systems on reservoir quality. In this context, recent cave systems are a natural starting point for generating analogues for geometries and infill features. Standard reservoir modelling software suites used by the petroleum industry currently have no established workflows or dedicated add-ins for handling the geometries and property distributions that characterize paleokarst reservoirs. Developing methods and workflows to handle this is a prerequisite for further work. Labourdette et al. (2007) address some of these issues from a non-epigenic viewpoint, and their results show that speleogenesis of flank-margin caves can be modelled with a close resemblance and coherence to field data using a combination of deterministic and stochastic methods. However, karst development on carbonate islands are typically controlled by the freshwater lens configuration (Mylroie and Carew, 1995), resulting in cave patterns different to those commonly associated with epigene karst systems (Palmer, 1991). Here, the primary focus is presenting a new methodology ("proof of concept") for geocullar rendering of epigenic karst system, but the proposed method may also be suitable for hypogenic- and flank margin karst systems.

The pioneering work of Furnée (2015) and Ledsaak (2016) produced two different approaches for incorporating geometrically complex karst systems into reservoir models by employing available tools. Their studies highlighted that although feasible to implement, geometries were either rendered oversimplified when transferred to geocellular grids, or required substantial and time-consuming editing to match observations (Lønøy et al., 2019b).

Building on these previous efforts, the present study outlines a quick and robust workflow for importing cave survey data into geocellular reservoir models in order to use these as starting points for forward modelling of collapse and infill, forward seismic modelling and fluid flow simulation. The study aims to evaluate the volumetric and geometric accuracy of the modelling methods as well as appraise the interlinkage between grid cell resolution, applied filter cut-off and geocellular rendering. The models in this study are based on a survey of the Maaras cave system, an active cave system in northern Greece (Pennos et al., 2016b).

2. Cave system analogue

2.1. Maaras cave

The Maaras cave is an almost 12 km long cave system which has developed parallel to the north-western margin of the Aggitis river basin in the prefecture of Eastern Macedonia in northern Greece (Fig. 1). The cave is developed within the marbles of the Rhodope massif, and four speleogenetic phases associated with changes in local base-level have been identified (Pennos et al. (2016b); and references within). Maaras cave hosts an active river system which exits the subsurface as a spring at 123 m.a.m.s.l. near the village of Aggitis. The mapped length of the cave is 10441 m, with the innermost mapped position located 71 m above the current level of the spring (Pennos et al., 2016a). The river slope varies

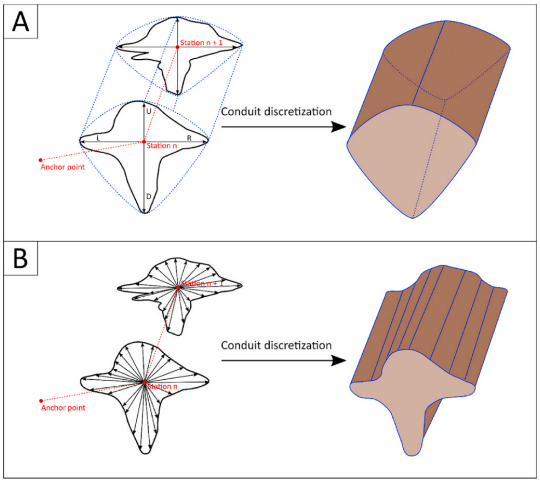

Fig. 2. Conceptual models of cave surveying techniques and conduit discretization. A) A simple cave survey method consisting of five measurements for each survey station: floor, roof, left, right wall and new survey station. B) Modern cave survey method consisting of multiple measurements from each survey station. Note that opposing measurements are not necessarily parallel and thus LRUD data derived from this method represent the maximum distance or a manually selected point for each direction. A higher density of shots increases the cross-sectional geometric resolution.

throughout the cave, from 3% to 67%, with steepest slopes occurring near the spring (Pennos et al., 2016b). The cave shows two shorter tributary passages; a western branch and an eastern branch that join to form a more extended master conduit to the spring (see Fig. 1). The cave system has no closed loops, but exhibits a pattern of lower-order passages joining tributaries to form higher-order passages; a cave morphology resembling the typical branchwork type as classified by Palmer (1991).

The cave is partly filled by thick accumulations of sandy clastic sediments, creating a relatively flat cave floor. Electric resistivity tomography (ERT) in some parts of the cave reveals that locally the sedimentary thickness exceeds 45m (Fikos et al., 2019; Lønøy et al., 2019a), filling 80–95% of the total karst cavity height. In contrast to the flat sediment floor, the cave roof has irregular morphology and cavity height varies from a few cm up to 60m; following a looping pattern.

3. Methodology

Methods and workflows for implementing traditional cave survey data into industry-standard reservoir modelling tools have previously been described by Furnée (2015) and Ledsaak (2016). The two workflows, hereafter labelled Method 1 and Method 2 respectively, are summarized below, and are used for comparison with the new method outlined in the present study (Method 3). The new workflow (Method 3), employs a combination of open source and commercial software used by the industry: PocketTopo (Heeb, 2010), Therion (Budaj and Stacho, 2019), MATLAB™ (MATLAB, 2010) and RMS™ (Roxar, 2018). The same results may be achieved using different software with similar functionalities. Terminology and functions mentioned in this article will refer to those presented and offered by the applied software.

If not stated otherwise, all grid models have a global grid resolution of 2 × 2 × 2m (X,Y,Z) and all mapped surfaces comprise a 2 × 2m (X,Y) grid resolution.

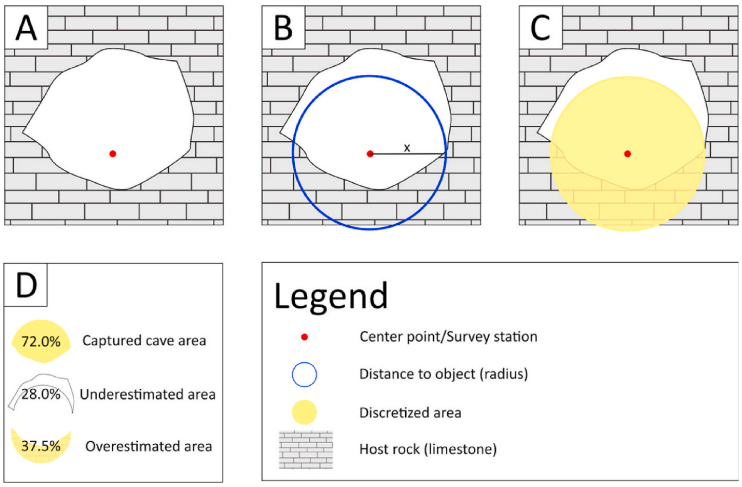

Fig. 3. Cross-sectional illustration of the workflow suggested by Furnée (2015) (Method 1). A) The centre points (red dot) is used as input for geometric modelling B) A cut-off value based on the "distance to object" calculation (blue circle) is set to delineate the estimated cave C) Final discretized cave area (yellow circle). D) Area coverage; area calculations based on image analysis from the illustration, show that for this example, 72.0% of the original cave area is discretized by this method. However, based on the illustration, the method fails to discretize 28.0% of the original cave area and overestimate the total area by 9.5%. Note that a smooth circular discretized area is used to illustrate the concept and that a geocellular representation would have a more "jagged" discretization, reflecting the grid cells. Also note that the over- or underestimation of the conduits cross-sectional area will largely depend on the spatial arrangement of the survey station (red dot) and applied filter (see Section 5). (For interpretation of the references to colour in this figure legend, the reader is referred to the Web version of this article.)

3.1. Cave surveying

Over the past decade, advanced terrestrial LiDAR instruments and photogrammetry have been introduced for cave mapping (e.g. Lerma et al. (2010); Gede et al. (2013); Gallay et al. (2015); Gallay et al. (2016), allowing high-resolution three-dimensional cave mapping. However, most modern cave surveys are still carried out using simple digital equipment such as laser rangefinders (e.g. Leica™ Disto X310) in combination with a handheld computer (e.g. a personal digital assistant - PDA) (http://paperless.bheeb.ch/). Conventional cave surveys consist of a series of consecutive line-of-sight measurements between survey-stations anchored to a geo-referenced point (often at the cave entrance). The stations can either be temporary or permanently marked locations and are chosen based on ease of access and line-of-sight to neighbouring stations. The rangefinder records distance, direction (azimuth) and inclination from horizontal (dip) between stations. The handheld computer display data numerically and graphically and can be used to store and manage measured data; allowing the addition of sketches directly on the screen. Moreover, the measurements between stations and the distance to the corridor walls (left, right, up, down – LRUD (Fig. 2A) or more points (Fig. 2B)) at a given station can be recorded to create a relatively high-resolution geometric representation of the cross-sectional shape of the conduits (Heeb, 2008, 2009, 2014).

The Maaras cave survey (Pennos et al., 2016b), applied here, was carried out using modern surveying techniques and includes multiple wall measurements for each survey station (e.g. Fig. 2B).

3.2. Method 1

The workflow for Method 1 (Furnée, 2015) comprises three steps (Fig. 3). The method assumes that the survey stations are centre points within the cave passage and generates a polygon ("skeleton line") by connecting the points. The skeleton line is then refined to generate additional, more densely spaced points along the line segments (between the survey stations). These points are used as input for geometric modelling. The geometric modelling function in RMS™, allows

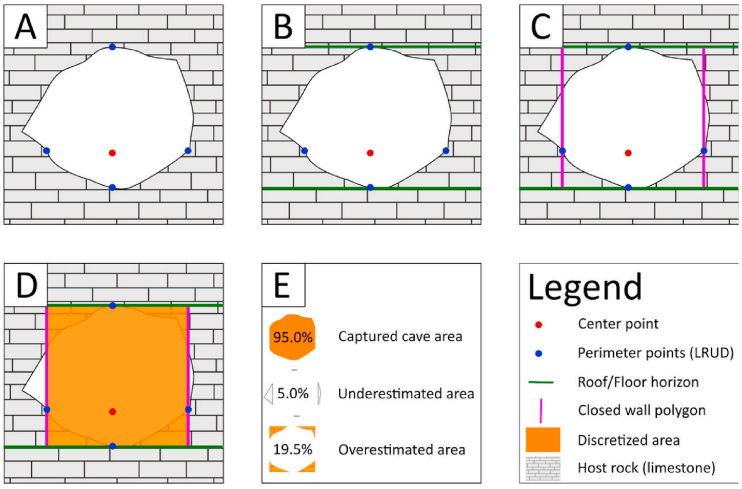

Fig. 4. Method 2 - Cross-sectional conceptual illustration of the workflow suggested by Ledsaak (2016). A) Cave survey data containing center-point (red dot) and LRUD (blue dots) is used as input to reservoir modelling software B) Roof- and floor horizons (green line) are constructed based on the up- and down points, respectively. The horizons constrain the vertical extent of the cave. C) Wall points (L and R) are used to generate a closed polygon (pink lines) used to constrain the lateral extent of the cave. D) The final discretized area representing the gridded cave (orange square). E) Area coverage: area calculations (image analysis from the illustration) show that for this example 95.0% of the original cave area is discretized by this method. However, based on the illustration, the method fails to discretize 5.0% of the original cave and overestimate the total area by 14.5%. (For interpretation of the references to colour in this figure legend, the reader is referred to the Web version of this article.)

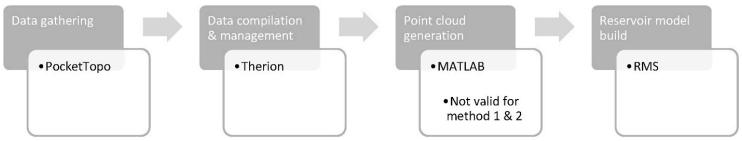

Fig. 5. Workflow steps (grey) and associated software (white) - from data collection to reservoir model build. The key aspect here is utilisation of a point cloud to discretize the cave network at higher resolution. In all cases alternative software could be employed to individual tasks.

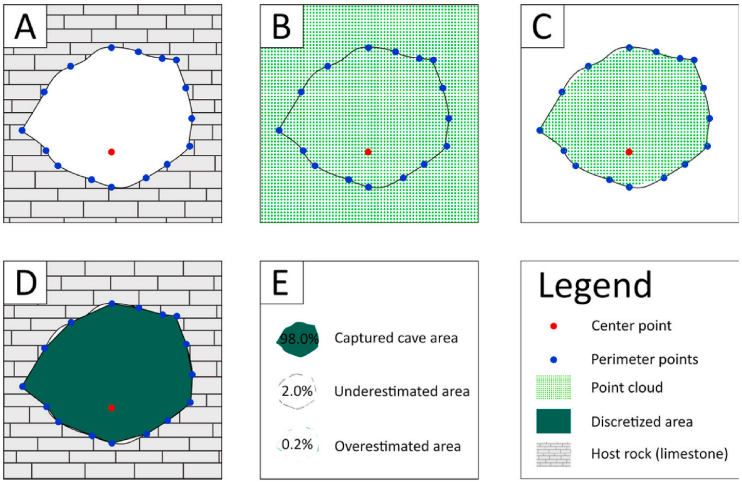

Fig. 6. Method 3 - Cross-sectional conceptual illustration of the workflow. A) Cave survey data containing centre-point (red dot) and wall shots (blue dots) is used as input into MATLAB. B) A defined volume of dense equally spaced points, representing the modelling domain, is generated in MATLAB. C) A predefined MATLAB code is used to discretize points inside the cave system, subsequently generating a *.csv file containing X, Y, Z -values for each point within the cave area. Note that the software discretizes the point cloud by drawing straight lines between the perimeter points. D) The dense point cloud representing the cave system is then imported into RMS and run through geometric modelling (calculating distance from object/point), subsequently filtering and discretizing the data. E) Area coverage: area calculations (image analysis from the illustration) show that for this example 98.0% of the original cave area is discretized by this method. However, based on the illustration, the method fails to discretize 2.0% of the original cave and underestimate the total area by 1.8%. However, volumetric over- or underestimation of the gridded volume should be expected when "forcing" a complex geometric shape into a gridded framework. The magnitude of which will be determined by a combination of the applied global grid cell resolution, point cloud density and applied filter cut-off. (For interpretation of the references to colour in this figure legend, the reader is referred to the Web version of this article.)

calculating "distance to object" parameter, the objects here being the points along the skeleton line segments. A filter function is then used to create a parameter rendering the "cave" as a string of cells with their centre-point at a given distance from the skeleton line (Fig. 3), defining a "filtered distance" hereafter referred to as cut-off or cut-off value. In this study, the estimated average conduit radius of 6 m (estimated mean roof height from the cave survey of the master conduit and two tributaries) is used as a cut-off. When employing a high grid resolution, Method 1 renders the cave passages as having a circular cross-section with a fixed and constant diameter (Fig. 3C). At lower grid resolutions, cross-sections will have a "blockier" appearance.

3.3. Method 2

Method 2 (Ledsaak, 2016) uses a four-step workflow (Fig. 4) and cave survey data in LRUD format (left-, right-, up- and down-points) in addition to the survey station positions employed in Method 1. The LRUD survey data is imported into RMS™ as points for each group; wall, roof and floor. For geometrically simple karst systems, such as single-tiered systems, the floor- and roof points are then used to generate bounding horizons, constraining the vertical extent of the cave. A new closed wall polygon is generated by manually tracing the wall points, which constrains the lateral extent of the cave. In the gridded model, the roof- and floor horizons and the closed wall polygon are then used to delimit the cave. In geometrically complex and multi-tiered cave systems, using this approach becomes a bit more demanding, as the horizons defining the roof and floor exist at multiple stratigraphic levels with overlapping XY positions which cannot be mapped as a single, continuous surface. As the software does not allow for stratigraphic zones crosscutting other zones, the surfaces and polygons must be grouped according to cave tier. In these cases, the wall polygons must be split into several segments for each cave tier, and subsequently merged into a single polygon. Horizon mapping must be carried out for each roof and floor polygon, and new surfaces generated. Finally, the cave must be gridded for each cave tier, constrained by the associated boundary surface and wall polygon, before merged into a single grid model.

3.4. Method 3

The new approach, Method 3, consists of a four-step workflow summarized in Figs. 5 and 6.

First, cave survey data, comprising spatial data of survey-station positions- and multiple wall points, is gathered using modern equipment and techniques (Fig. 6A). Collected data is imported into a cave survey data management software (Therion) to generate a 3D cave model and subsequently exported as X-, Y-, and Z-points. The entire modelling domain is then densely populated with equally spaced geo-referenced points in MATLAB (Fig. 6B), where an algorithm is used to discretize the cave volume and thus remove all points outside the cave boundary. This produces a dense point cloud representing the cave system (Fig. 6C). The MATLAB-generated geo-referenced points are then imported into RMS, and a new continuous parameter, representing the

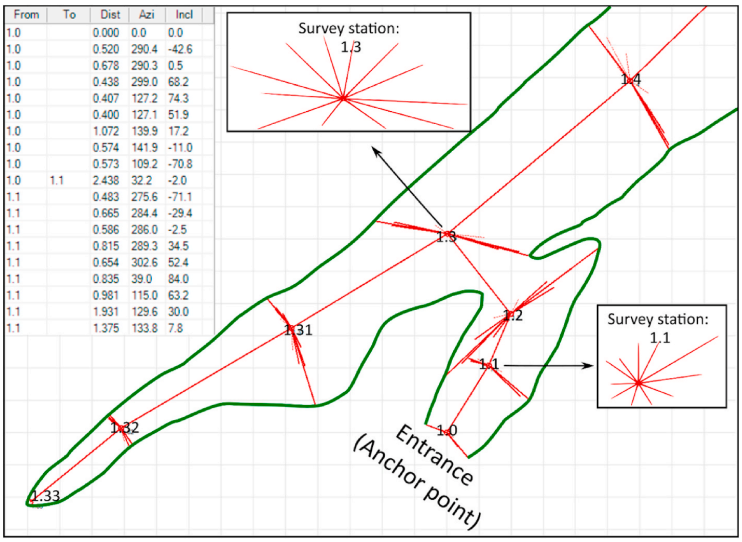

Fig. 7. Layout example of cave survey data in PocketTopo. Left: cave survey data showing station number (from and to), distance (m), azimuth (°) and inclination (°) of each shot. Right: Data visualization (red) in real-time allowing manual sketching (green line). Inserts show cross-section for survey station 1.1 and 1.3. (For interpretation of the references to colour in this figure legend, the reader is referred to the Web version of this article.)

distance to the points, is generated by geometric modelling; following the same workflow as Method 1. The cave system is then discretized by filtering the continuous parameter (Fig. 6D).

3.5. Software

PocketTopo is an application that receives and stores cave measurements (station number, distance, azimuth and inclination) directly from a laser rangefinder. The software allows managing survey data, reference points and trip information, and includes the possibility of freehand sketching between survey stations (e.g. green line in Fig. 7).

Therion is an open-source software for survey data processing. The software is used to compile cave surveys and for geo-referenced survey anchoring, loop-closure, map generation, 3D cave modelling and more (Budaj and Mudrák, 2008). In our proposed method, the survey data from PocketTopo (e.g. Fig. 7) is imported into Therion to generate a geo-referenced 3D model. The wall boundaries of the model are then exported as a *.txt file comprising X-, Y-, and Z-points.

In MATLAB, the modelling domain is densely populated with equally spaced, geo-referenced points. The wall periphery data, from Therion, are then imported and used to constrain the cave system by eliminating all points outside the cave. The remaining geo-referenced points now provide a point-cloud rendering of the cave system. These points can then be exported as a comma-delimited text file (*.csv). In this study, point clouds with two different point densities were constructed: 0.5m and 1m. Unless stated otherwise, all following models, graphs, and

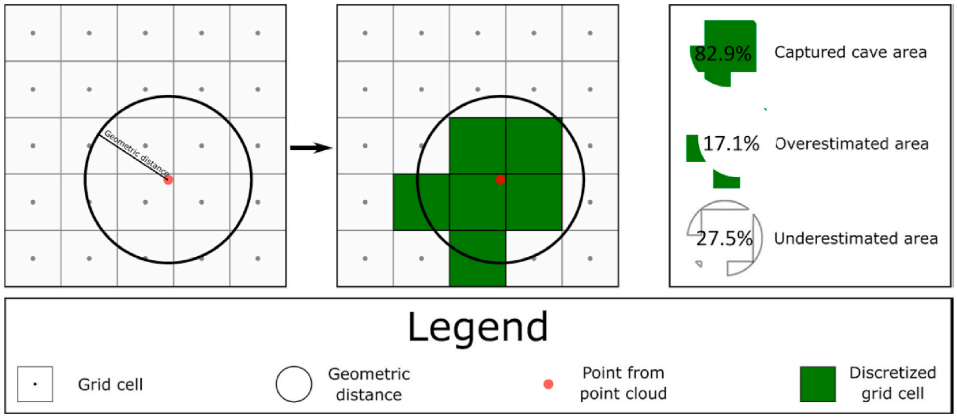

Fig. 8. 2D conceptual illustration of geometric modelling and associated geometric distance function. The built-in RMS™ function generates a continuous parameter with parameter values representing the geometric distance from an object, in this case, points. The parameter can be filtered, and a desired cut-off value can be applied to constrain a volume. Area coverage: area calculations (image analysis from the illustration) show that for this example 82.9% of the original cave area is discretized. Note that the illustration is in 2D, whereas the geometric distance is a 3D calculation.

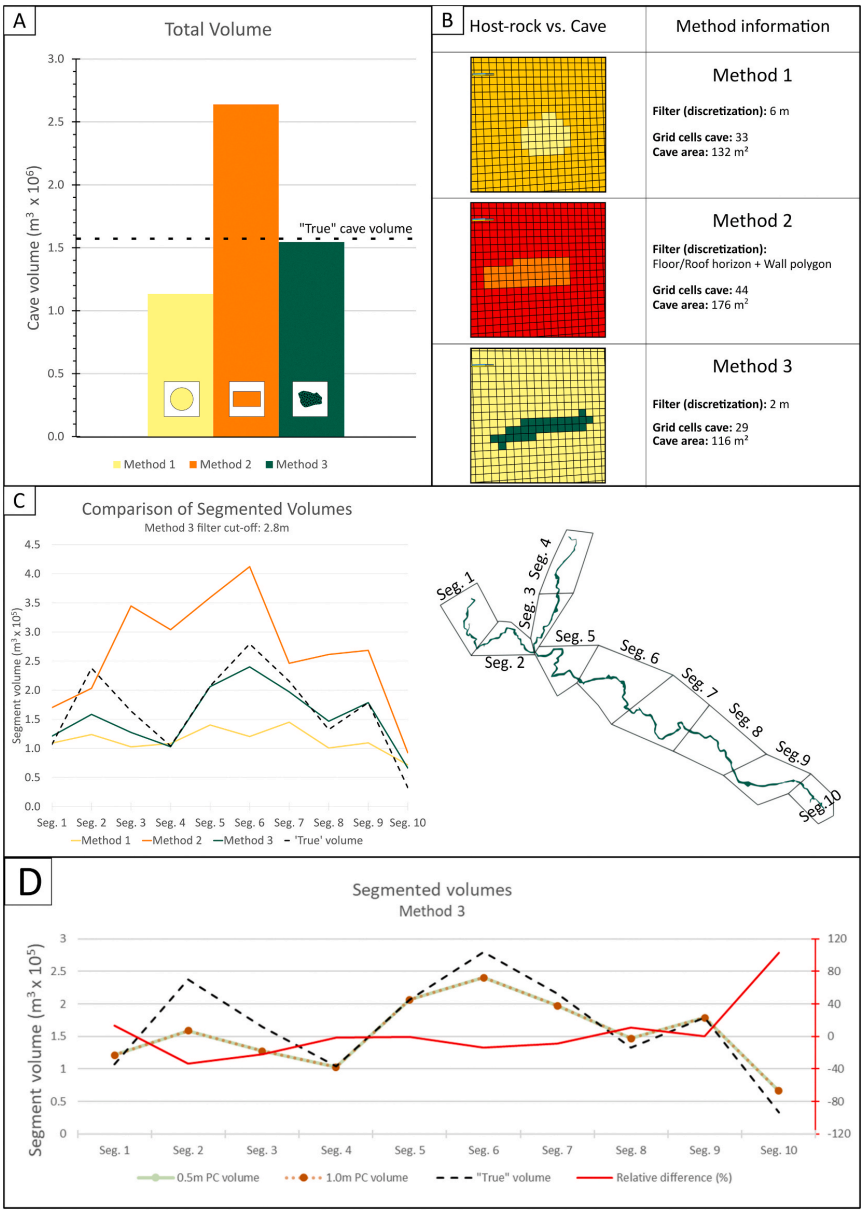

Fig. 9. A volumetric comparison of studied methods. All graphs represent a global grid resolution of 2 × 2 × 2m. A) Histogram showing the difference in total volumetric representation between the methods benchmarked against the "true" cave volume. B) Cross-sectional example of the gridded end-result of each method. Note that the angle of view and section are identical for all models. C) A volumetric comparison for 10 different segments (as marked on the cave plan) of the resulting grid models. D) The relative difference between Method 3 and the "true" cave volume. Segmented volumes rendered using two different point cloud densities (0.5 and 1-m spacing) show that the volumetric rendering is identical using different point cloud densities. Colour coding used for the different methods: Method 1 = Yellow, Method 2 = Orange, and Method 3 = Green are consistent with all following grids, charts, and graphs. (For interpretation of the references to colour in this figure legend, the reader is referred to the Web version of this article.)

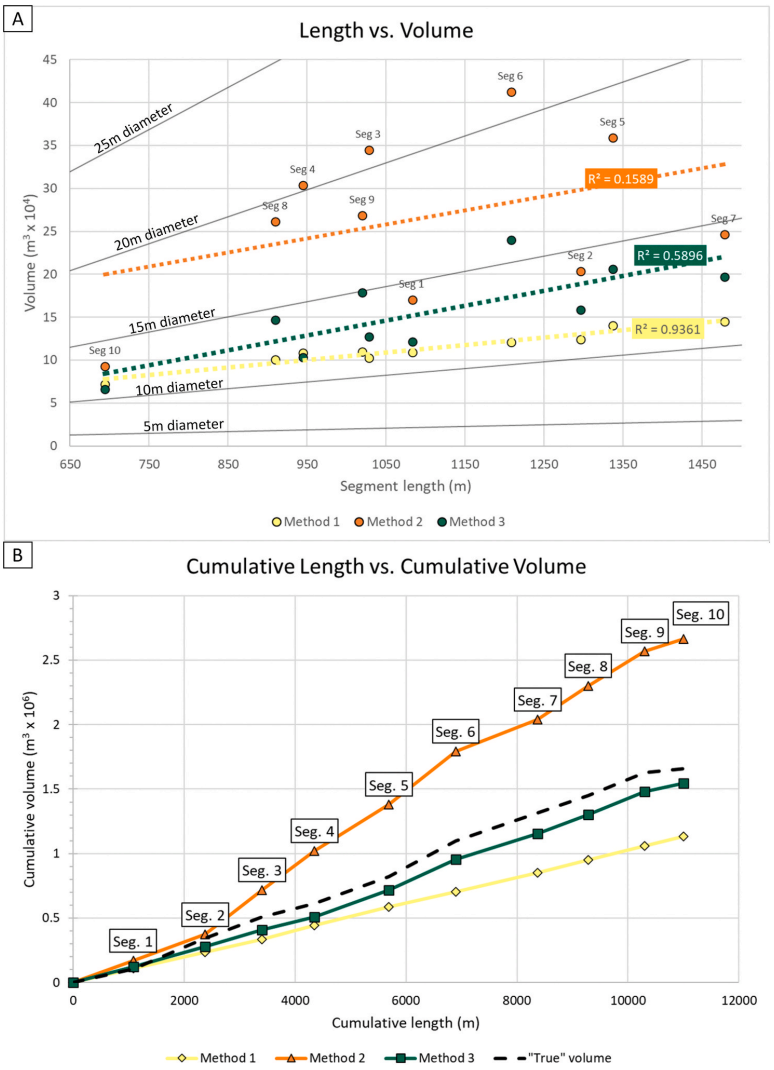

Fig. 10. Comparison of cave volume over passage length for different estimation methods for models using a global grid resolution of 2 × 2 × 2m. Method 1 is discretized by a filter cut-off of 6m, Method 2 by bounding horizons and a closed polygon, and Method 3 by a filter cut-off of 2.8m. A) Segment length vs volume. For comparison, grey contour lines show volume of cylinders with constant diameters. B) Cumulative length vs cumulative volume - Segments 1 to 10. Note the excellent correlation between the "true" volume and Method 3 in B) and that Method 1, as expected, results in a linear graph due to the uniform cylindrical rendering of the cave system.

illustrations refer to results from the 0.5m (X,Y,Z) point cloud.

The industry-standard reservoir modelling software RMS™ 11.0.1 is used to generate a gridded model of the cave system. Geo-referenced points (MATLAB generated *.csv file) representing the cave system are imported into RMS using the custom format function. In the custom settings, data headers are removed, and data treated as a single object with comma-separated columns. Note that it is important that the coordinate system used in previous steps is consistent with the one used in RMS. Even though correct global positioning is not required for a given study, significant decimal places vary between different coordinate systems (i.e. geographic coordinate system vs projected), which may cause import problems. The cave system now comprises a dense 3D point cloud. The point cloud can be used in pre-established gridded reservoir models or a new grid with appropriate grid parameters. The cave system is discretized using the built-in RMS parameter utility "*Geometric modelling*" and the associated "*Distance to objects*" function (Fig. 8). This function generates a continuous parameter with cell parameter values representing the distance from the objects, which in this case are the points within the cave. A new grid with discrete parameter values is then created to discretize the cave system. The cave system is discretized by using "*parameter utilities*" and the "*calculator*" function with the following equation (1):

IF "continuous geometric modelling parameter"⩽"cut − off value" THEN "new discrete parameter" = "desired parameter value" ENDIF (1)

In this study, the applied parameter names and cut-off values are used (2):

IF Geometric ≤ 2 *THEN CaveNoCave* = 1 *ENDIF* (2)

Here, an empirical cut-off value of 2m was applied to all models.

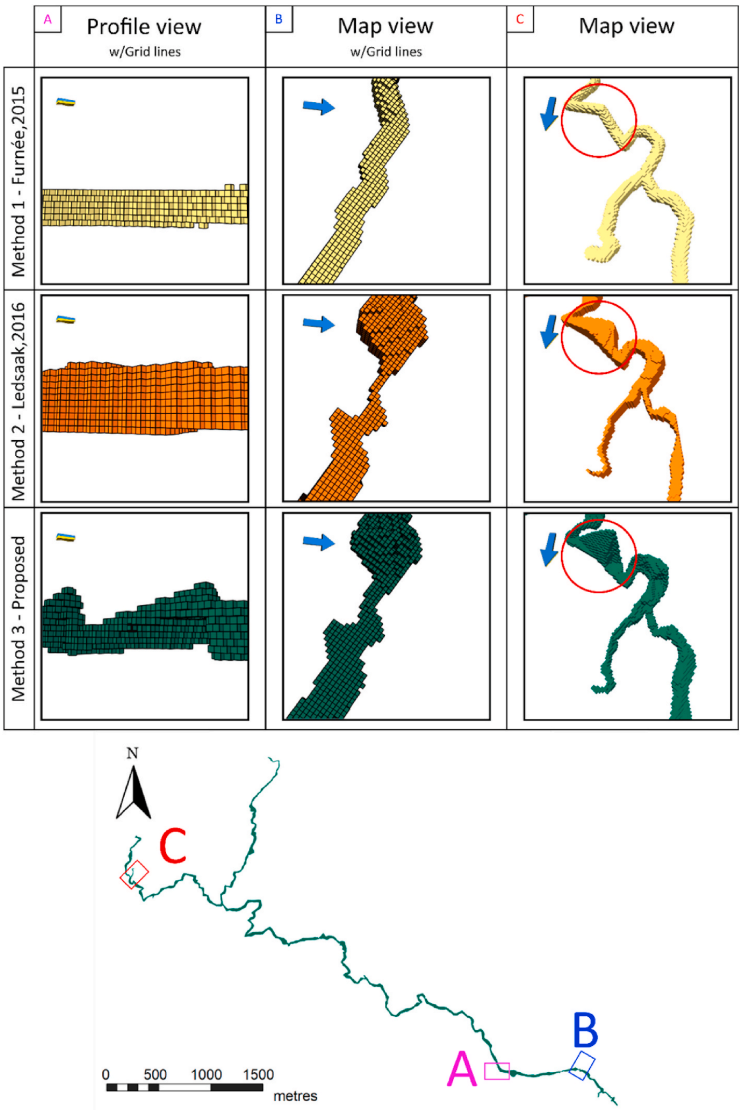

Fig. 11. Grid model comparison using various methods. All models in the same column show the same section, with an identical scale and angle of view. 3D close-up views show significant volumetric and geometric differences between the three methods. A) Profile view showing an apparent lack of geometric resolution in Method 1 and 2. Both methods fail to capture the looping morphology of the roof evident in Method 3. B) Map view showing, as expected, that Method 1 fails to capture abrupt conduit narrowing and widening, which are seen clearly in using both Method 2 and 3 that seem to provide good geometric representations of the cave system. However, in the narrow passage section Method 2 generates a lower volume compared to Method 3, with the difference likely relating to the input data used in Method 2. This method only utilizes only a single point for each wall to delineate the lateral extent of the cave and thus the modelling result is highly dependent on the spatial arrangement of the survey station or selected wall shots (e.g. as illustrated in Fig. 18). C) Map view of an area where a tributary joins between the western branch to the main conduit. All three methods ensure grid cell connectivity between the tributaries but result in significantly different geometric- and volumetric representations. The apparent looping conduit morphology in the southern part of model generated using Method 1 (red circle), clearly shows that this modelling approach may introduce morphological artifacts. It is clear from Methods 2 and 3 (red circles) that this is an area with elevated cave roof heights, and that the apparent looping morphology in Method 1 is a result of the spatial arrangement of the survey station. North direction in gridded models indicated by a blue arrow. (For interpretation of the references to colour in this figure legend, the reader is referred to the Web version of this article.)

Note that cut-off values used to discretize the cave system in the gridded model should be carefully selected and adjusted to fit grid- and point cloud resolution.

3.6. Volumetric estimation

In order to evaluate the volumetric accuracy of each method, grid volumes must be benchmarked against the best estimate of cave volume. In this study, an estimated cave volume is calculated by extrapolating the cross-sectional area between the survey stations. First, to calculate the area, the cave survey data must be transformed into vectors with coordinates (x_n, y_n) in a cartesian coordinate system. Then, the area can be calculated using equation (3) for planar non-self-intersecting polygons (Weisstein, 2020):

$$A = \frac{1}{2}\left(\begin{vmatrix} x_1 & x_2 \\ y_1 & y_2 \end{vmatrix} + \begin{vmatrix} x_2 & x_3 \\ y_2 & y_3 \end{vmatrix} + \ldots \begin{vmatrix} x_n & x_1 \\ y_n & y_1 \end{vmatrix}\right) \quad (3)$$

The cross-sectional area of each survey station is then multiplied by the distance to the consecutive station to get an estimated volume for each segment. Finally, all segments are summed to get an estimated total cave volume, hereafter referred to as the "true" cave volume. In order to ensure all cross-sections comprise non-self-intersecting polygons, a manual quality check was carried out for each survey station accompanied by data rearrangement.

4. Results

The Maaras cave survey was split into ten approximately equal

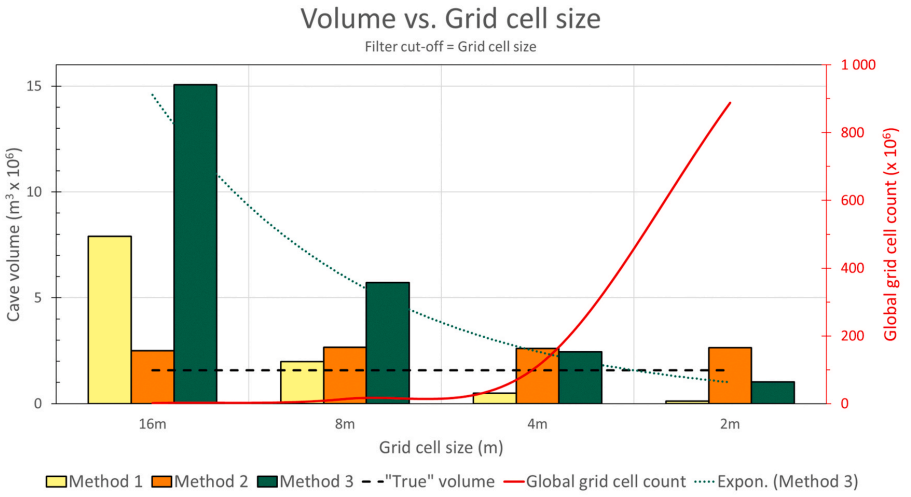

Grid cell resolution vs. filter cut-off

		Grid cell resolution 16m				Grid cell resolution 8m				Grid cell resolution 4m				Grid cell resolution 2m			
Filter cut-off (m)		2	4	8	16	2	4	8	16	2	4	8	16	2	4	8	16
Total volume (Mm^3)	Method 1	0.08	0.36	1.71	7.91	0.12	0.51	1.99	8.01	0.11	0.50	2.02	8.07	0.12	0.50	2.02	8.06
	Method 2	2.51				2.66				2.61				2.66			
	Method 3	0.84	2.04	5.24	15.07	1.10	2.39	5.72	15.34	1.11	2.45	5.84	15.55	1.03	2.38	5.73	15.40

Fig. 12. Variation in total volumetric representation by different methods, grid cell resolutions (X = Y = Z) and filter cut-off values. Tabulated total volumes are in most cases larger than the "true" cave volume of 1.58 Mm^3. Crossed-out cells in the table indicate geocellular rendering lacking complete cell interlinkage throughout the cave system. Note that Method 2 discretize the cave system by bounding horizons and closed polygons and thus the filter cut-off will not apply to this method.

segments, with main passage lengths of 1100m ± 220 (mean ± SD) (Figs. 9C and 10). Results are presented for three separate model versions of each segment generated using Methods 1, 2 and 3. Global grid resolution was kept identical for all models (2 × 2 × 2m) to allow comparison. If not specified otherwise in the graphs or illustrations, the cave system was discretized using a filter cut-off distance of 6 m in Method 1, a combination of bounding horizons and a closed wall polygon in Method 2, and a filter cut-off distance of 2.8 m for Method 3. At this grid resolution and associated boundary conditions, all three methods capture the orientation and connectivity of the cave conduits (Fig. 11), but geometric rendering differs significantly (e.g. Figs. 9B and 11). This is highlighted when comparing calculated cavity volumes from the three grid model versions with the "true" 3D volume from the survey data. The total volume yielded by Method 1 is 1.13 Mm^3 (assuming a mean conduit diameter of 12 m), which is less than half the total volume of 2.66 Mm^3 yielded by Method 2 (Fig. 9A). Both estimates are significantly different from the "true" cave volume of 1.58 Mm^3, with Method 1 resulting in an underestimate (relative difference of 33%) and Method 2 an overestimate (relative difference of 51%). The volumetric estimate yielded by Method 3 is 1.55 Mm^3 which is within 2% of the estimated "true" cave volume.

Considering individual segments, models generated using Method 2 consistently overestimate the cave volume (in all segments except in Segment 2) when compared to models built by using Method 1 and 3 (Fig. 9C). The latter two provide comparable volumes in some segments (notably the upper sections of both branches of the cave), but show a significant volumetric deviation in all but the last segment in the main passage downstream of the confluence of the western and eastern branches (segments 5, 6, 7, 8 and 9; Figs. 9C and 15).

In order to investigate the impact of grid cell resolution and applied filter cut-off values, a series of models were built using different grid cell dimensions and filter cut-off values equalling associated grid cell sizes: 16m, 8m, 4m, and 2m (Fig. 12). Due to CPU constraints, the highest practical grid resolution tested was 2 × 2 × 2m, which resulted in a global grid with ~9 × 10^8 grid cells.

For Method 3, the relationships between volumetric representation and applied cut-off values were plotted for different grid cell resolution, to identify potential interlinkage between model set-up and resulting volumetric rendering (Fig. 13A). Similarly, multiple segments (only two presented in this article) were appraised to confirm these trends (Fig. 13B and C). The full geocellular cave model and all segmented models show a clear polynomial trend (coefficient of determination R^2 of 1), for a given grid cell resolution, between the filter cut-off value and resulting volumetric rendering (Fig. 13).

A visual evaluation of cell-to-cell interlinkage (Fig. 12) show that Method 1 renders all grid models with a cut-off value less than the grid cell resolution incoherent. For Method 2, only a grid cell resolution of 2 × 2 × 2m provides interconnected cave grid cells, whereas all other grid cell resolutions result in disconnected cave grid cells. Method 3 provides the best grid cell coherency with most grid cells resolutions and filter

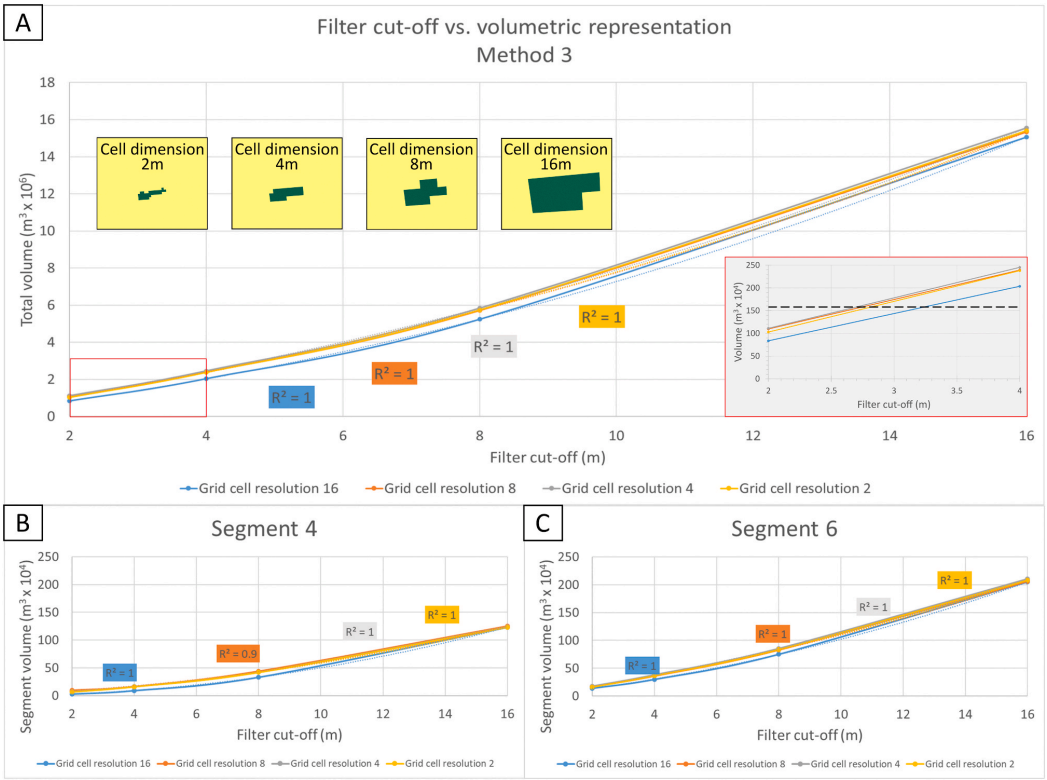

Fig. 13. Volumetric rendering at various grid cell resolutions and applied filter cut-off values. A) Volumetric rendering of the complete grid model. Insert: close-up (red square) of cut-off value ranges that give volumes close to the "true" cave volume (black line). Yellow boxes: Cross-sectional view of a cave corridor at different grid cell resolutions (X = Y = Z). The filter cut-off (2m) and angle of view is identical for all boxes. The trend lines show an evident polynomial trend (coefficient of determination (R^2) of 1) between volumetric rendering, grid cell resolution, and filter cut-off values. B) Volumetric rendering of segment 4 (Fig. 15). C) Volumetric rendering of Segment 6 (Fig. 15). Note the clear polynomial relationship between filter cut-off and resulting volumetric rendering in all graphs. Grid cell resolution has a minor impact on the volumetric rendering for values of 8 m^3 or lower, but at 16 m^3, the rendered volume is reduced by 19–25% using a filter cut-off of 2m. (For interpretation of the references to colour in this figure legend, the reader is referred to the Web version of this article.)

cut-off values resulting in coherent cave models. However, at coarser grid cell resolutions and low cut-off values, also Method 3 failed to render a continuous cave model (e.g. Figs. 12 and 14).

5. Discussion

The results show that although all methods are applied to the same cave survey data, the volumetric and geometric representations of the cave system in the geocellular model will differ depending on the algorithm used. Method 3, apparently provides a better geometric description of the cave system compared to the two other methods (Figs. 6 and 11). However, the modelled volume in all methods deviates from the benchmarked volume (1.13, 1.55 and 2.66 Mm^3 for Method 1, 3 and 2, respectively, compared to a "true" volume of 1.58 Mm^3). This could suggest that the volumetric representations of the grid models reflect a combination of the resolution and availability of input data, the modelling approach and the grid model set-up (grid resolution). Method 3, with optimal cut-off value, results in a volumetric rendering close to that of the "true" volume from the cave survey. Nevertheless, it is crucial to keep in mind that the "true" volume is most likely an underestimation, as the wall shots only represent the distance to the closest obstacle (e.g. Fig. 16). Also, many karst caverns are inaccessible for humans as they are either too small to access or infilled/blocked by clastic sediments, adding to the volumetric underestimation. The uncertainty in karst pore volume can be evaluated using fractal distributions (e.g. Curl, 1986; Pardo-Igúzquiza et al., 2018) and sedimentary thickness mapping (e.g. Lønøy et al., 2019a), and can thus be included in a reservoir model using stochastic modelling. However, this is outside the scope of this study but shows that it is difficult to establish the actual volume of a karst system and that several factors need to be considered in paleokarst reservoir modelling.

A well-known challenge in reservoir modelling is accurate and efficient modelling of complex morphologies using corner-point- or pillar-based unstructured grids (e.g. Branets et al., 2009; Mallison et al., 2014). Rendering irregular 3D shapes as geocellular bodies at a given cell size resolution will cause over- or underestimation of body volumes (Fig. 17). Even an optimal fine-tuning of the cut-off value for the "distance to objects" calculation will cause grid cell corners either to extrude beyond the periphery or fail to precisely fill in the detailed shape of the actual mapped body.

5.1. Method 1

Method 1 proved to be a time- and CPU efficient method for incorporating cave survey data into industry-standard reservoir modelling tools (Table 1). The method relies on simple datasets that might be easy

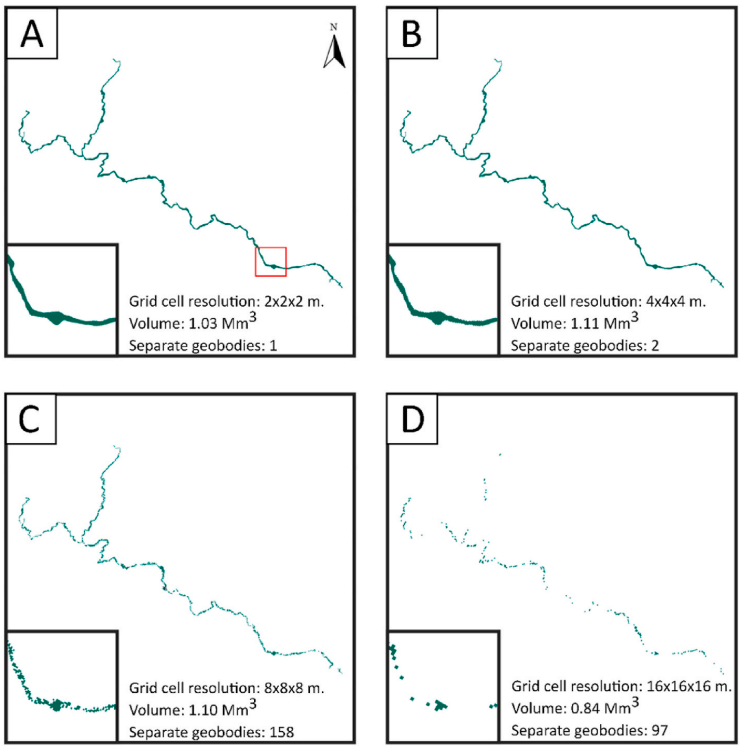

Fig. 14. Geocellular rendering at different grid cell resolution using Method 3. Filter cut-off value is kept constant at 2m for all models. Inserts show a close-up view of a section of Segment 9 (highlighted with a red square) in the same area of each model. Separate geobodies determined by image analysis. A) Grid cell resolution (2 × 2 × 2 m) equal to the cut-off value. Volumetric representation close to the "true" volume. B) Grid cell resolution (4 × 4 × 4 m) equals twice the cut-off value. Volumetric representation close to the "true" volume. C) Grid cell resolution (8 × 8 × 8 m) equals four times the cut-off value. Volumetric representation close to the "true" volume. Diminishing cell-to-cell connectivity. D) Grid cell resolution (16 × 16 × 16 m) equals eight times the cut-off value. Volume underestimated by a factor of 1.39 and cell interlinkage lost. Note that separate geobodies significantly increase when grid cell resolution increase from 4 m^3 to 8 m^3. However, in a paleokarst setting, the collapse footprint may subsume these isolated geobodies and create a coherent fluid environment if the geobodies separation distance is less than the lateral collapse propagation. (For interpretation of the references to colour in this figure legend, the reader is referred to the Web version of this article.)

and quick to collect. However, the resulting grid model lacks morphological heterogeneities often associated with karst systems, such as abrupt conduit narrowing/widening and irregular roofs and floors (Figs. 3, 9B and 11 and 15). Conduits formed along stratigraphic horizons and along fractures are expected to have different geometries (wide and low vs tall and narrow) and sedimentary infill. The nature of infill type is closely related to the local hydraulic regime, cavity breakdown and diagenesis. These factors ultimately control fluid flow. As Method 1 render all cave corridors as cylinders with a fixed and constant diameter, the method will probably work better for conduits with a circular to elliptical cross-sectional shape (e.g. phreatic conduits with low fracture density formed in homogenous limestones). Method 1 may also create morphological artifacts (e.g. Fig. 11C) as the vertical and horizontal extent of the conduit is only constrained by a fixed distance to a single reference point.

Studies have shown that some karst voids and conduit sections may remain open at great depths up to 6 km (e.g. Loucks (1999); Lu et al. (2017)). Synthetic conduits with a uniform circular geometry may prove unsuitable for establishing rules for subsequent delimited forward collapse modelling, as it would make morphological identification of cave sections prone to roof collapse difficult. Attic pockets acting as hydrocarbon traps may thus be overlooked or have an uncertain spatial distribution in the final grid model; potentially resulting in imprecise estimates of stock-tank oil original in place (STOOIP) and gas initially in place (GIIP) and probably an overestimation of recovery. Moreover, the volumetric accuracy of the resulting grid models reflects the morphological complexity of the cave system in addition to the selected cut-off value constraining the vertical- and horizontal extent of the conduits (Figs. 10, Figs. 12 and 15). In most cases, except maybe in wet caves, cave surveys comprise at least some boundary measurements (minimum LRUD). Thus, this method may prove to be oversimplified or obsolete for most cave survey data.

5.2. Method 2

Method 2 also proved to be a time- and CPU efficient method for reservoir modelling of single-tiered cave systems with simple morphology, such as Maaras (Table 1). However, studies by Ledsaak (2016) showed that, using existing industrial reservoir modelling tools, the method is intricate and time-consuming when used for multi-tiered caves with complex geometries. Method 2 captures the orientation and connectivity of the conduit and provides a better geometric approximation of the real cave morphology than Method 1 (Figs. 9B and 11). Still, Method 2 only relies on four points (for each survey station) delimiting the vertical and horizontal extent of the cave system. Thus the gridded cross-sections will comprise extrapolated rectangular shapes between stations (e.g. Fig. 9B).

In the present study, the models generated using Method 2 overestimate the total cave volume in all segments except Seg 2 (Fig. 9C). A volumetric deviation is expected as Method 2 renders all cave passages as rectangles (e.g. Figs. 4 and 18). However, the volumetric overestimation could be related to the input data. The Maaras cave survey was conducted using contemporary surveying techniques (Fig. 2B) and included multiple wall shots. In the absence of fixed LRUD points, these had to be generated from the measured wall shots by an automatic vector interpolation function in Visual Topo (2017). Following Method 2, the grid model will always comprise volumes that are either too large or small, depending on the cave survey array (e.g. the spatial distribution of the survey station relative to the conduit size and shape in Fig. 18). Although a volumetric deviation is expected, the volumetric

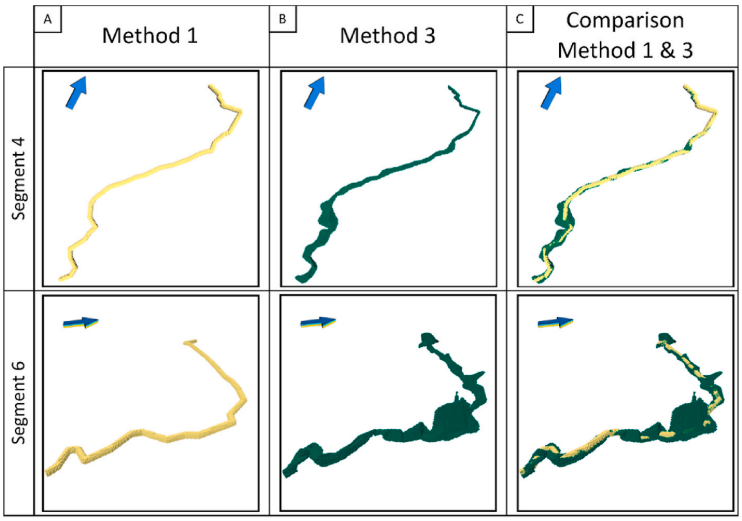

Fig. 15. Segmented grid model comparison. A) Grid model of segment 4 and 6 using Method 1. B) The same segments using Method 3. C) Grid model comparison between Method 1 and 3 with identical segmentation and angle of view. Areas shown in yellow are those where the cave predicted by the cylindrical model exceeds the volume from Method 3, whilst the green areas are areas where Model 1 underpredicts the magnitude of the passage. Note that the biggest volumetric difference (Seg 6) is in an area with a heterogeneous cave morphology, large chambers and associated high abundance of break-down related breccias (Lønøy et al., 2019a). North direction in gridded models indicated by a blue arrow. (For interpretation of the references to colour in this figure legend, the reader is referred to the Web version of this article.)

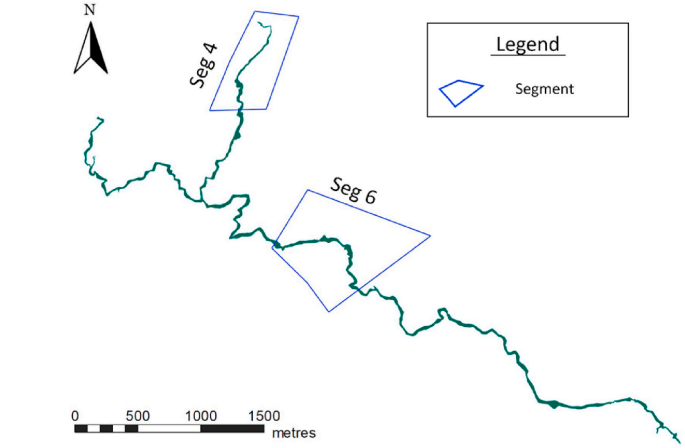

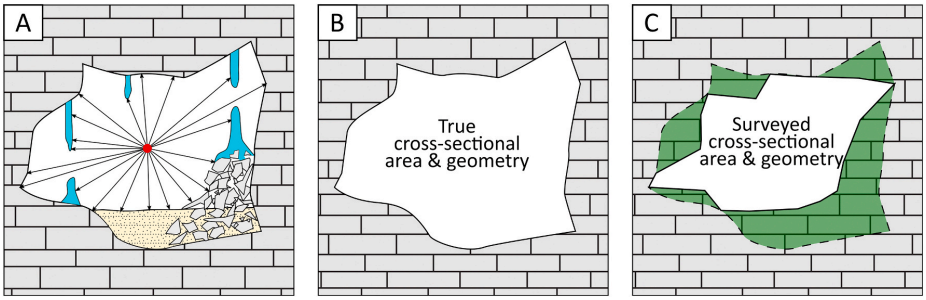

Fig. 16. Method 3 - Example of a potential coverage area using modern cave survey techniques. A) Conventional survey set-up and associated directional shots. Note that the shots only measure the distance, inclination, and azimuth to the closest obstacle (i.e. stalactites, stalagmites, breccia cones and clastic sedimentary infill). B) The true cross-sectional area and geometry (black line). C) The cross-sectional area and geometry covered by the cave survey (black line) and the true area and geometry (green area). (For interpretation of the references to colour in this figure legend, the reader is referred to the Web version of this article.)

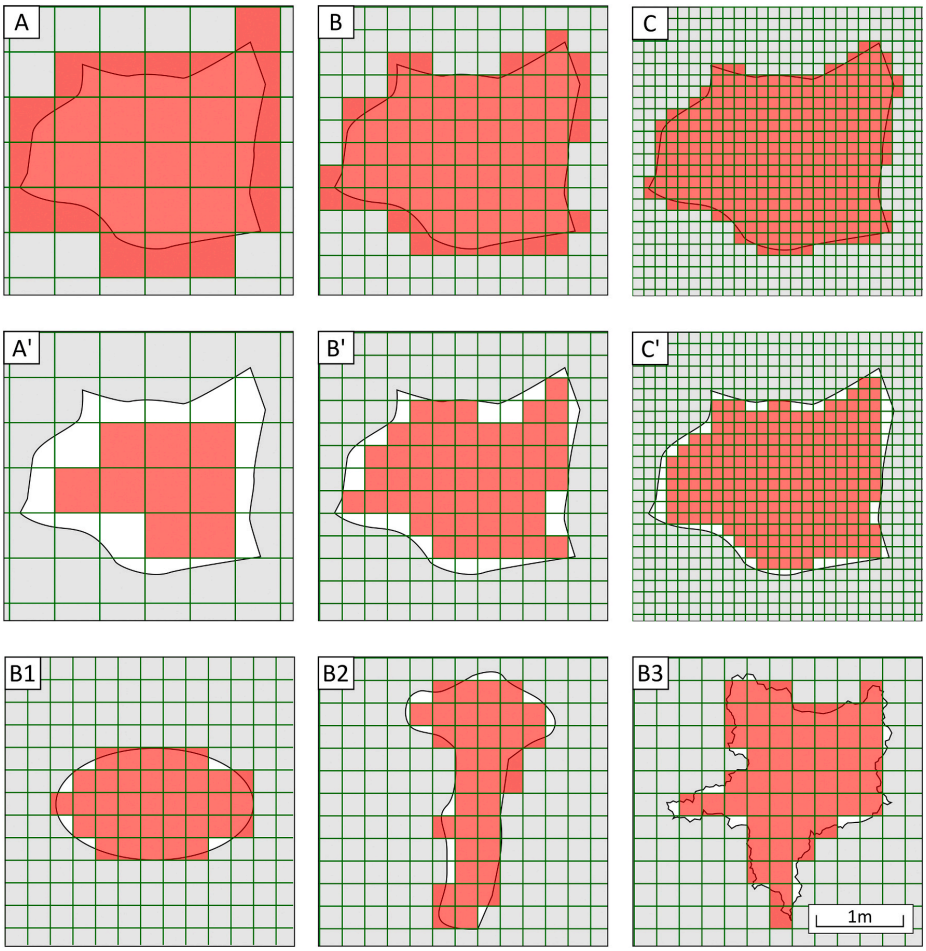

Fig. 17. Discretized area by different global grid resolutions. Note that this figure is only for illustrative purposes and that a reservoir modelling software could discretize the cave area differently. The grid cell size in this illustration is relative, and thus a unit of measure is not applied. A–C: Grid cells completely encompassing the cave perimeter. A′-C': Grid cells kept within the cave perimeter. B1–B3: Geocellular rendering of different passage shapes: phreatic conduit, vadose canyon and complex passage geometry with asperities. Grid cells kept within cave perimeter. A) Large grid cells - size 1. B) Intermediate grid cells – size 1/4. C) Small grid cells – size 1/16. As the grid framework becomes finer, the morphological resolution increases. Note that depending on whether grid cells encompass (A–C) or are kept inside the cave perimeter (A′-C′), volumetric rendering respectively decreases or increases with finer grid resolutions.

error using automatically generated LRUD points may be larger than those derived from grid models generated using reliable LRUD survey data. This inaccuracy of using LRUD data generated from multiple wall shots becomes evident in Segment 2, where there are an obvious error in the generated roof (U) and floor (D) points. In this segment, some of the floor points (D) has a higher elevation than the roof points (D) and thus the floor- and roof horizons are crossing resulting in non-discretized areas which could explain the volumetric underestimation shown in Fig. 9C.

5.3. Method 3

Method 3 involves a few additional steps and software combinations compared to the two other methods. Most of these steps are fully automated and do not require significant manual effort. In terms of time-consumption and complexity, our new method is significantly quicker and easier than Method 2, but not as fast and easy as Method 1 (Table 1). It does, however, provide a significantly improved geocellular rendering of cave morphology.

Models following Method 3 show an evident polynomial trend between the discretized volume and applied filter cut-off; with a coefficient of determination (R^2) of 1 (Fig. 13). This trend is consistent for the complete model as well as for the different segments, indicating that an optimal cut-off value can be determined if the "true" volume is known. Accurate volumetric modelling following Method 3 is then achievable by establishing an optimal geometric distance to the objects.

In this study, the applied point cloud density does not seem to have any impact on the modelling outcome in terms of volumetric rendering (Fig. 9D). Both point clouds (0.5m and 1.0m) result in models with identical volumes. However, the point densities used are below the applied global grid resolution, and thus a volumetric deviation might be expected as point density exceeds the grid resolution.

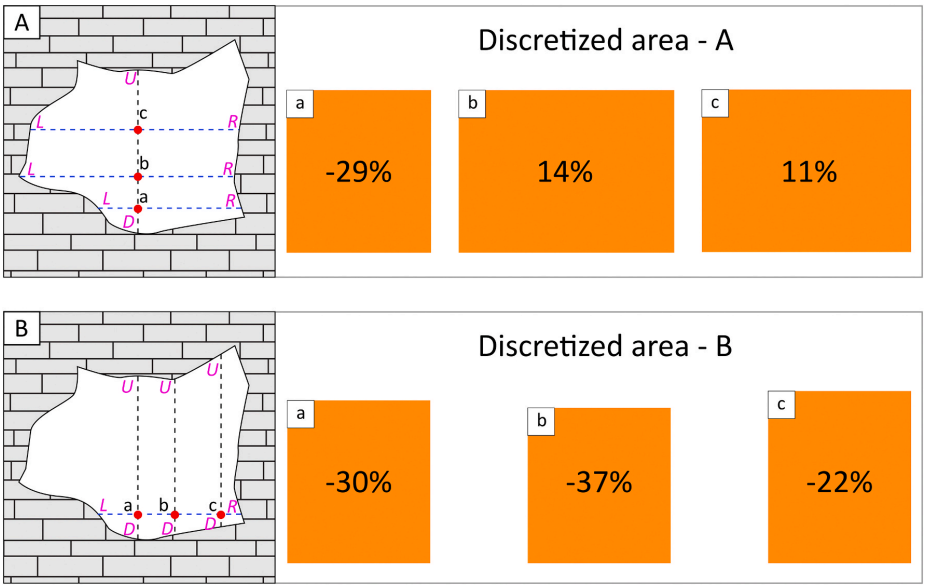

Fig. 18. Method 2 - Survey configuration and its impact on the cave representation in a geocellular framework. A) Example showing the horizontal impact of the vertical spatial distribution of the survey station. B) Example showing the vertical impact of the horizontal spatial distribution of the survey station. Right: The discretized areas (orange) and associated over-/underestimation, in percentage. Note that Method 2 renders all sections of the cave as rectangles causing significant deviation of the volumetric representation. (For interpretation of the references to colour in this figure legend, the reader is referred to the Web version of this article.)

Table 1
Methods summarized.

Method	Input data	Delineation	Rendered vol. (Mm^3)	Advantages	Disadvantages
Method 1	Center points	Geometric distance to centerline	1.13	Simple input data Time efficient	Cave geometry not captured Vol. accuracy dependant on morphological hetereogenity
Method 2	Center points + LRUD	Floor and roof horizons Wall polygon	2.66	Simple input data	Cave geometry not captured Time consuming Multi-tiered systems add complexity Overestimate vol.
Method 3	Centre points + multiple wall shots	Geometric distance to point cloud	1.55	Good geometric representation Good vol. representation	Geometric resolution reflects cave survey resolution Require "true" cave vol. to establish an optimal filter cut-off

The plot "cumulative length vs cumulative volume" (Fig. 10B) displays the continuous difference in area between the methods, which in turn reflects geometric heterogeneity. As observed in Fig. 9D, some of the Method 3 segments exhibit volumes that deviate from the "true" cave volume. However, the overall volume captured by Method 3 is close to that of the original cave survey (Fig. 10B).

5.4. Grid resolution and cut-off value

Grid resolution, as expected, influences geometric rendering and volumetric calculations in the models. The grid cell size sensitivity (Fig. 12) illustrates how rendered volume and cell-to-cell connectivity reflects the global grid resolution applied (e.g. Fig. 14). For Method 1 and 3, volumetric rendering is similar for any given cut-off value and global grid resolutions below 16 m^3. However, once the global grid resolution exceeds 8 m^3 the discretized volume decreases significantly. This could be explained by the grid cell size exceeding the conduit dimensions or that the distance to certain grid cell centre-points is surpassing the cut-off value.

Method 1 and 3 are very sensitive to the applied parameter cut-off value which must be equal to, or larger, than the grid cell resolution to ensure a coherent grid model of the cave system. On the other hand, for Method 2, grid cell connectivity is sensitive to the global grid cell resolution applied, and coherence diminishes in areas where the grid cell size exceeds the vertical and horizontal extent of the conduits (Fig. 12). Thus, all grid cells extruding the boundary surfaces and wall polygon will not be discretized.

In most cases, the use of very high-resolution grids (i.e. with cells $<2 \times 2 \times 2$m) is limited by CPU cost. However, as computer modelling and tracer tests have shown (e.g. Field and Pinsky, 2000; Hauns et al., 2001; Goldscheider, 2008; Montaron et al., 2014), morphology can substantially affect calculations of in-place volumes, fluid flow, and production behaviour and hence reserve estimates. Thus, ideally, modelling efforts should strive to incorporate as much geometric detail as possible without the model becoming unmanageable. On the other hand, the level of morphologic detail provided by using cave surveys is beyond anything achievable using seismic and well -data. In models of actual subsurface reservoirs, these morphological features must be captured using stochastic modelling methods. Constraints and guidelines for these can, however, be provided by using the kind of analogue models exemplified in the present study.

6. Conclusion

The method for implementing cave survey data into industry-standard reservoir models as presented here (Method 3), provides an significantly improved rendering compared to previous methods by Furnée (2015) and Ledsaak (2016).

The two pre-established methods systematically and significantly either overestimate or underestimate the actual cave volume. A volumetric over- or underestimation is expected when irregular shapes conform to a geocellular framework. This relates to the "edge-effect" caused by grid cell corners either extruding the cave periphery or when grid cells are not entirely infilling the cave volume. For Method 1 the accuracy of volumetric calculations is related to the accuracy of the estimated mean cave diameter employed as model input, whereas for Method 2 it is primarily related to all cave cross-sections being represented as rectangles.

As shown in this study, our proposed method (Method 3) provides a good approximation of the cave morphology and volume when employing cave surveys as input. The precision is limited by the quality of the survey, grid resolution and applied filter cut-off value. An optimal filter cut-off value can be determined if the "true" cave volume and desired global grid resolution is known, allowing geometric and volumetric accurate and coherent geocellular rendering.

A 3D geocellular model of the cave system in combination with conventional methods for gathering stratigraphic- and structural data, could be a good starting point for developing guidelines and workflows for forward collapse modelling. This combination would allow easy discretization of pre- and post-collapse infill and associated population of petrophysical properties. Moreover, using recent cave systems as analogues to paleokarst reservoir modelling may be appropriate as the tectonostratigraphic history of the cave systems is often well constrained and cave survey data ubiquitous.

CRediT authorship contribution statement

Bjarte Lønøy: Writing - original draft, Writing - review & editing, Conceptualization, Software, Data curation, Formal analysis, Investigation, Methodology, Validation, Visualization. **Jan Tveranger:** Writing - review & editing, Conceptualization, Formal analysis, Funding acquisition, Methodology, Project administration, Resources, Supervision, Validation. **Christos Pennos:** Writing - review & editing, Conceptualization, Methodology, Software, Resources, Validation. **Fiona Whitaker:** Writing - review & editing, Methodology, Supervision. **Stein-Erik Lauritzen:** Writing - review & editing, Supervision, Conceptualization.

Declaration of competing interest

The authors declare that they have no known competing financial interests or personal relationships that could have appeared to influence the work reported in this paper.

Acknowledgement

The authors would like to thank the Research Council of Norway (project number: 267634) for funding this study and Emerson Roxar for providing an academic license for RMS™. The reviewers are acknowledged for their constructive feedback and for improving the research. Jon Petter Furnee and Karina Ledsaak are acknowledged for their pioneering work in using cave survey data as input to paleokarst reservoir modelling. The scientific discussions with Gordon Coy, Mateu Esteban Cerdà and Arve Lønøy (the latter also contributed by proof-reading) are also highly appreciated, and their input has significantly benefited the research.

Appendix A. Supplementary data

Supplementary data to this article can be found online at https://doi.org/10.1016/j.marpetgeo.2020.104652.

References

Blickwede, J., Rosenfeld, J., 2010. The Greatest Oil Well in History? the Story of Cerro Azul# 4.
Borghi, A., Renard, P., Jenni, S., 2010. How to model realistic 3D karst reservoirs using a pseudo-genetic methodology–example of two case studies. Advances in Research in Karst Media 251–255.
Branets, L.V., Ghai, S.S., Lyons, S.L., Wu, X.H., 2009. Challenges and technologies in reservoir modeling. Commun. Comput. Phys. 6, 1–23.
Budaj, M., Mudrák, S., 2008. Therion–digital cave maps therion–cartographie souterraine digitale. In: Presented on the 4th European Speleological Congress. Banska Bystrica, Slovakia.
Budaj, M., Stacho, M., 2019. Therion 5.4, 4 ed.
Chaojun, Z., Chengzao, J., Benliang, L., Xiuyu, L., Yunxiang, L., 2010. Ancient karsts and hydrocarbon accumulation in the middle and western parts of the North Tarim uplift, NW China. Petrol. Explor. Dev. 37, 263–269.
Coogan, A.H., Maggio, C., Bebout, D.G., 1972. Depositional environments and geologic history of golden Lane and poza rica trend, Mexico, an alternative view. Am. Assoc. Petrol. Geol. Bull. 56, 1419–&.
Craig, D.H., 1988. Caves and Other Features of Permian Karst in San Andres Dolomite, Yates Field Reservoir. Springer, west Texas, Paleokarst, pp. 342–363.
Curl, R.L., 1986. Fractal dimensions and geometries of caves. Math. Geol. 18, 765–783.
Erzeybek Balan, S., 2012. Characterization and Modeling of Paleokarst Reservoirs Using Multiple-point Statistics on a Non-gridded Basis. The University of Texas at Austin, pp. 1–307. Ph.D. Dissertation.
Field, M.S., Pinsky, P.F., 2000. A two-region nonequilibrium model for solute transport in solution conduits in karstic aquifers. J. Contam. Hydrol. 44, 329–351.
Fikos, I., Vargemezis, G., Pennos, C., Lønøy, B., Jensen, K., Tveranger, J., EAGE, 2019. Processing 2D ERT data in 3D environment: a case study inside a karstic cave in North Greece. In: Near Surface Geoscience Conference and Exhibition. The Hauge, Netherlands.
Fournillon, A., Abelard, S., Viseur, S., Arfib, B., Borgomano, J., 2012. Characterization of karstic networks by automatic extraction of geometrical and topological parameters: comparison between observations and stochastic simulations. Geological Society, London, Special Publications 370, 247–264.
Furnée, J.P.B., 2015. Geo-modeling and Fluid Flow Simulation in Paleokarst Reservoirs. The University of Bergen.
Gallay, M., Hochmuth, Z., Kanuk, J., Hofierka, J., 2016. Geomorphometric analysis of cave ceiling channels mapped with 3-D terrestrial laser scanning. Hydrol. Earth Syst. Sci. 20, 1827–1849.
Gallay, M., Kanuk, J., Hochmuth, Z., Meneely, J.D., Hofierka, J., Sedlak, V., 2015. Large-scale and high-resolution 3-D cave mapping by terrestrial laser scanning: a case study of the Domica Cave, Slovakia. Int. J. Speleol. 44, 277–291.
Gede, M., Petters, C., Nagy, G., Nagy, A., Mészáros, J., Kovács, B., Egri, C., 2013. Laser scanning survey in the pálvölgy cave, budapest. In: Proceedings of the 26th International Cartographic Conference. International Cartographic Association, Dresden, p. 905.
Goldscheider, N., 2008. A new quantitative interpretation of the long-tail and plateau-like breakthrough curves from tracer tests in the artesian karst aquifer of Stuttgart, Germany. Hydrogeol. J. 16, 1311–1317.
Hauns, M., Jeannin, P.Y., Atteia, O., 2001. Dispersion, retardation and scale effect in tracer breakthrough curves in karst conduits. J. Hydrol. 241, 177–193.
Heeb, B., 2008. Paperless Caving-An Electronic Cave Surveying System La topo sans papier-un système électronique de topographie. IV th European speleological congress (Isére - France).
Heeb, B., 2009. An all-in-one electronic cave surveying device. Cave Radio & Electronics Group Journal 72, 8–10.
Heeb, B., 2010. PocketTopo 1.34.
Heeb, B., 2014. The next generation of the DistoX cave surveying instrument. CREG Journal 88, 5–8.
Kaiser, M.J., Pulsipher, A.G., 2007. A review of the oil and gas sector in Kazakhstan. Energy Pol. 35, 1300–1314.
Labourdette, R., Lascu, I., Mylroie, J., Roth, M., 2007. Process-like modeling of flank-margin caves: from genesis to burial evolution. J. Sediment. Res. 77, 965–979.
Ledsaak, K., 2016. Geo-modelling of Paleokarst Reservoirs-From Cave-Survey to Geocellular Paleokarst Model. The University of Bergen.
Lerma, J.L., Navarro, S., Cabrelles, M., Villaverde, V., 2010. Terrestrial laser scanning and close range photogrammetry for 3D archaeological documentation: the Upper Palaeolithic Cave of Parpallo as a case study. J. Archaeol. Sci. 37, 499–507.
Lomando, A.J., Harris, P.M., Orlopp, D.E., 1993. Casablanca Field, Tarragona Basin, Offshore Spain: a Karsted Carbonate Reservoir. Special publications of SEPM.
Lønøy, B., Pennos, C., Tveranger, J., Fikos, I., Vargemezis, G., Jensen, K., Lauritzen, S.-E., 2019a. Sediment Accumulations in Paleokarst Reservoirs - Analogues from an Active Cave System. Bathurst Meeting of Carbonate Sedimentologists 2019, Mallorca, Spain, p. 1.
Lønøy, B., Pennos, C., Tveranger, J., Lauritzen, S.-E., Furnée, J.P., Ledsaak, K., 2019b. Paleokarst Reservoir Modelling Based on Active Cave System Analogs - Implementing Cave Survey Data in Geocellular Reservoir Models. Winter conference 2019. Bergen.

Loucks, R.G., 1999. Paleocave carbonate reservoirs: origins, burial-depth modifications, spatial complexity, and reservoir implications. AAPG Bull. 83, 1795–1834.
Lu, X.B., Wang, Y., Tian, F., Li, X.H., Yang, D.B., Li, T., Lv, Y.P., He, X.M., 2017. New insights into the carbonate karstic fault system and reservoir formation in the Southern Tahe area of the Tarim Basin. Mar. Petrol. Geol. 86, 587–605.
Mallison, B., Sword, C., Viard, T., Milliken, W., Cheng, A., 2014. Unstructured cut-cell grids for modeling complex reservoirs. SPE J. 19, 340–352.
MATLAB, 2010. Version 9.4.0.813654. The MathWorks Inc, Natick, Massachusetts. R2018a.
Montaron, B., 2008. Carbonate evolution. Oil & Gas Middle East, pp. 26–31.
Montaron, B.A., Xue, F.J., Tian, W., Han, R., Ray, P., 2014. Cave Geomorphology and its Effects on Oil Recovery Factors in Tarim Karst Reservoirs, West China, International Petroleum Technology Conference. Kuala Lumpur, Malaysia, p. 13.
Mylroie, J.E., Carew, J.L., 1995. Karst Development on Carbonate Islands.
Palmer, A.N., 1991. Origin and morphology of limestone caves. Geol. Soc. Am. Bull. 103, 1–21.
Pardo-Igúzquiza, E., Dowd, P.A., Durán, J.J., Robledo-Ardila, P., 2018. A review of fractals in karst. Int. J. Speleol. 48, 2.
Pennos, C., Lauritzen, S.E., Pechlivanidou, S., Aidona, E., Haflidason, H., Sotiriadis, Y., 2016a. Decoding Clastic Sediment Sources from the Maaras Cave Northern Greece, 18th Joint Geomorphological Meeting. Chambery, France.
Pennos, C., Lauritzen, S.E., Pechlivanidou, S., Sotiriadis, Y., 2016b. Geomorphic constrains on the evolution of the Aggitis river basin Northern Greece. Bull. Geol. Soc. Greece 50.
Rongier, G., Collon-Drouaillet, P., Filipponi, M., 2014. Simulation of 3D karst conduits with an object-distance based method integrating geological knowledge. Geomorphology 217, 152–164.
Roxar, R.M.S., 2018. Roxar Software Solutions 1994-2018, 11.0.1 ed.
Soudet, H.J., Sorriaux, P., Rolando, J.P., 1994. Relationship between fractures and karstification - the oil-bearing paleokarst of Rospo Mare (Italy). B Cent Rech Expl 18, 257–297.
Sun, S.Q., Sloan, R., 2003. Quantification of uncertainty in recovery efficiency predictions: lessons learned from 250 mature carbonate fields. In: SPE Annual Technical Conference and Exhibition. Society of Petroleum Engineers, Denver, Colorado, p. 15.
Tian, F., Jin, Q., Lu, X.B., Lei, Y.H., Zhang, L.K., Zheng, S.Q., Zhang, H.F., Rong, Y.S., Liu, N.G., 2016. Multi-layered ordovician paleokarst reservoir detection and spatial delineation: a case study in the Tahe Oilfield, Tarim Basin, Western China. Mar. Petrol. Geol. 69, 53–73.
Trice, R., 2005. Challenges and insights in optimising oil production form middle eastern karst reservoirs. In: SPE Middle East Oil and Gas Show and Conference. Society of Petroleum Engineers.
Viniegra, F., Castillo-Tejero, C., 1970. Golden Lane Fields. Veracruz, Mexico.
Visual Topo, 2017. David, Eric, 5.06.
Weisstein, E.W., 2020. Polygon area, from MathWorld–A wolfram web resource. http://mathworld.wolfram.com/PolygonArea.html.
White, W.B., Culver, D.C., Herman, J.S., Kane, T.C., Mylroie, J.E., 1995. Karst lands. Am. Sci. 83, 450–459.
Yan, X., 2002. Reservoir properties of ordovician carbonate rocks in the Tahe field, Tarim Basin, China. Shiyou Yu Tianranqi Dizh (Oil and Gas Geology) 23, 262–265.
Zempolich, W.G., Cook, H.E., 2002. Paleozoic carbonates of the Commonwealth of Independent States (CIS): subsurface reservoirs and outcrop analogues, Paleozoic carbonates of the Commonwealth of Independent States (CIS): subsurface reservoirs and outcrop analogues. SEPM Society for Sedimentary Geology, Special publications of SEPM, pp. 1–3.

Paper 2

Delimiting morphological and volumetric elements of cave surveys as analogues for paleokarst reservoir modelling – A case study from the Maaras cave system, northern Greece

Marine and Petroleum Geology

Delimiting morphological and volumetric elements of cave surveys as analogues for paleokarst reservoir modelling – A case study from the Maaras cave system, northern Greece

Bjarte Lønøy[1,2], Christos Pennos[2], Jan Tveranger[1], Ilias Fikos[3], George Vargemezis[3], Stein-Erik Lauritzen[2].

[1] NORCE – Norwegian Research Centre AS, Nygårdsgaten 112, 5008 Bergen, Norway

[2] University of Bergen, Department of Earth Science, Allégaten 41, 5007 Bergen, Norway

[3] Aristotle University of Thessaloniki, Department of Geophysics, Thessaloniki 541 24, Greece

Abstract

Active karst systems can offer good analogues for paleokarst reservoir modelling as they can provide links between present karst system geometries and the final reservoir architecture. Although clastic sediments are a characteristic and commonly conspicuous component of modern karst systems, their impact on the surveyed cave morphology has received limited attention. Here we address this topic by investigating the spatial and volumetric distribution of clastic sediments in a large karst cave hosting an active fluvial channel in northern Greece and discretize these in a geocellular framework. Mapping of cave floor sediment-types was supplemented by local stratigraphic logging of relict sediment terraces and electrical resistivity tomography in parts of the cave. Four resistivity groups were identified and interpreted as low- and high-porosity siliciclastic sediments, interbedded marble clasts, and host rock (marble). Sediment infill thickness ranges from 25 m to >45 m at the time of measurement; corresponding to a minimum of 64-95% of the cross-sectional area of the karst cavity in the surveyed part. These observations demonstrate that under certain circumstances, allochthonous siliciclastic sediments can form a significant volumetric component in karst systems and, by extension, in paleokarst reservoirs originating from similar karstic systems. This highlights the importance of understanding the context, organization and development of the initial karst system when characterizing paleokarst reservoirs. Mapping of sediment thickness is not usually carried out during cave surveys, which primarily focus on recording open cavities accessible to man. This implies that survey data concerning the shape and volume of cave systems and statistics compiled and derived from them should be handled with care when applied to paleokarst reservoir modelling.

Keywords: Sediment mapping; karst; paleokarst; electrical resistivity tomography; Maaras cave

1. Introduction

A significant proportion of carbonate reservoirs worldwide exhibit features related to former surface and/or sub-surface karst processes (Fritz et al., 1993; Mazzullo and Chilingarian, 1996; Schlumberger, 2007; Burchette, 2012; Zou, 2013; Agada et al., 2014). Paleokarst is the product of preservation as well as infill, degradation, and burial of the original karst features. This involves a range of processes operating on different spatial and temporal scales, which can form very complex and highly heterogeneous subsurface reservoirs. Characterization of paleokarst reservoirs is challenging, as many features are below the current state of seismic resolution, and available well data is often too scarce to reliably assess how representative it is for the entire reservoir. These constraints also affect the handling of paleokarst in reservoir models. Current geo-modelling of paleokarst reservoirs (e.g., Strebelle, 2002; Henrion et al., 2008; Borghi et al., 2010; Erzeybek Balan, 2012; Rongier et al., 2014; Frantz et al., 2021) employ adapted or modified versions of concepts and workflows developed for siliciclastic and carbonate reservoirs (e.g., Ringrose and Bentley, 2015). However, given the constraints of well data and seismic information in paleokarst, largely data-driven modelling often fails to render the spatial distribution, morphology, volume, and, crucially, flow-connectivity characteristics of paleokarst features in a realistic manner. This highlights the importance of developing and using concept-driven rather than data-driven approaches when modelling paleokarst, as it allows populating reservoir models with realistic geological features that cannot be resolved by subsurface data acquisition. For paleokarst, these concepts involve understanding the factors and processes controlling karst formation and transformation from karst to paleokarst, and characterize and, if possible, quantify the features they produce. Modern karst forms a natural starting point for developing such concepts for paleokarst formation that can be extended to modelling of subsurface reservoirs.

Karst cave systems form spatial framework nuclei in and around which paleokarst reservoirs develop as some morphological karst elements are preserved, and others degraded, filled in and/or altered by the collapse of cavities. Active karst cave systems can therefore offer good analogues for understanding the starting configuration and initial stages of paleokarst reservoir formation . They also provide links between present karst system geometries and environmental, tectonic, and stratigraphic constraints controlling their formation and development. If known, these links can potentially be utilized for reconstructing or forecasting likely karst configurations in given settings as suggested by some workers (e.g., Feazel, 2010; Tveranger, 2019).

Most surveys of modern cave systems are constrained by line-of-sight measurements (Judson, 1974; Heeb, 2008; Albert, 2017), which implies that they often tend to underestimate cave dimensions and accurately render the morphology of karst cavities if speleothems, boulders and sediments obstruct the line of sight to ceiling walls and floor of the cavity. Although the morphological accuracy of cave surveys has improved drastically with the use of LIDAR scanners, photogrammetry etc. in the last

decade (e.g., Zlot and Bosse, 2014; Gallay et al., 2015; Fabbri et al., 2017; Pennos et al., 2018; Triantafyllou et al., 2019), they still measure the distance to the closest obstruction and thus the actual cave morphology is often concealed. Surveying of caves can also be influenced by practical and logistic constraints such as physical and regulatory access restrictions, environmental concerns and lack of light (Sasowsky and Mylroie, 2007). Many modern karst caves and passages are flooded or filled with sediments and thus inaccessible, making the complete mapping of many cave systems difficult or impossible.

Cave conduits act as traps and conveyors for clastic sediments (Bosch and White, 2004; White, 2007). Epigenic cave systems are often highly dynamic depositional environments while karstic processes remain active, and very sensitive to local factors such as re-routing of drainage as the system evolves, blocking of passages by cavity breakdown, and changing morphology of host rock cavity (Hajna et al., 2008; Ballesteros et al., 2017; Karkanas and Goldberg, 2017). This implies that depositional changes observed locally not necessarily reflect regional factors such as climate, tectonics or regional base levels, and that sediment infill may not necessarily provide information about the geometry of the karst system, in particular, if cavity and infill are separated by a time gap (Plotnick et al., 2015). The active depositional systems in caves may only represent a snapshot of the karstic evolution. Accumulations of clastic sediments can be deposited quickly, reworked, or even flushed out of the karst system (Ford and Williams, 2002; Bosch and White, 2004; White, 2007; Van Gundy and White, 2009; Farrant and Smart, 2011).

Quantification and qualification of the role sediments play as part of paleokarst reservoirs is a rather underexplored topic, although some recent studies (e.g. Tian et al., 2017; Li et al., 2018) suggest interest is growing. Preserved cave sediments forming part of paleokarst are well documented (e.g., Kerans, 1988; Lomando et al., 1993; Loucks, 1999and references therein; Tian et al., 2017; Li et al., 2018). Although a number of studies provide descriptions of, and classification systems for cave sediments and paleokarst facies (e.g., Bögli, 1980; White, 1988; Loucks and Mescher, 2002; Bosch and White, 2004; White, 2007; Springer, 2019), assessments of their volumetric significance that could be utilized for reservoir modelling purposes are largely lacking. Even in explored caves, mapping of clastic sediment infill is normally only carried out on a local scale (e.g., Kadlec et al., 2008; Martini, 2011; Bella et al., 2020) and geophysical surveys, for various reasons, are commonly conducted from the surface (e.g., Čeru et al., 2018; Hussain et al., 2020) rather than inside the cave system. However, geophysical surveys have been employed within cave systems by archaeologists to map sediment infill, but these are often high data density surveys over relatively short sections and with shallow depth of investigation (e.g., Becker et al., 2019).

Correlation and extrapolation of facies and properties, as well as inferences about the system of cavities hosting them, must be treated with care, as the representativity of individual well observations with

respect to the more extensive systems will be largely unknown. For large cave systems hosting perennial fluvial systems and exhibiting extensive upward corrosion above the sediment fill (i.e. “paragenesis” (Ford and Williams, 1989; Farrant and Smart, 2011) or “antigravitative erosion” (Pasini, 2009) this issue may be less pertinent.

Here, we present our approach for mapping clastic sediments within active karst systems using electrical resistivity tomography (ERT) combined with standard field mapping. The study aims to identify the volumetric proportion of sediment infill in the cave system, perform an approximate assessment of the sediments, and address uncertainties tied to the use of cave surveys for geocellular modelling of paleokarst using industry-standard reservoir modelling software (e.g., Lønøy et al., 2020).

The chosen demonstration case is the more than 10 km long Maaras cave system (Aggitis river springs) in northern Greece (Figs. 1, 2), which hosts an active subterranean fluvial system transporting significant volumes of sediments. The downstream part, close to the spring, consists of a 700 m long show-cave. The presence of an active depositional system, conduit dimension and ease of access make it well suited for studying sediment distribution in a karst cave using both surface mapping, logging of sections, and geophysical methods.

2. Background

2.1. Geological setting

The Aggitis river basin, located in the prefecture of Eastern Macedonia in northern Greece (Fig. 1), constitutes a well-defined Neogene tectonic graben controlled by two NW-SE trending normal faults (Vavliakis et al., 1986). It is bounded by the mountains of Falakro to the north, the Ori Lekanis to south-southeast, the Paggeon to the south, and Menikion to the east-northeast. These consist primarily of pre-Neogene metamorphic rocks (marbles, gneisses, and schists) with minor plutonic intrusions (Christanis et al., 1998). The basin is predominantly covered by alluvial sediments (Pennos et al., 2011). The western part of the basin contains lacustrine clastic sediments of Miocene age, deposited during a period of raised sea level (Papaphilippou-Pennou, 2004). Finally, the lowlands in the eastern part of the basin comprise recent deltaic deposits from the Xiropotamos-Doxato stream (Pennos et al., 2016b).

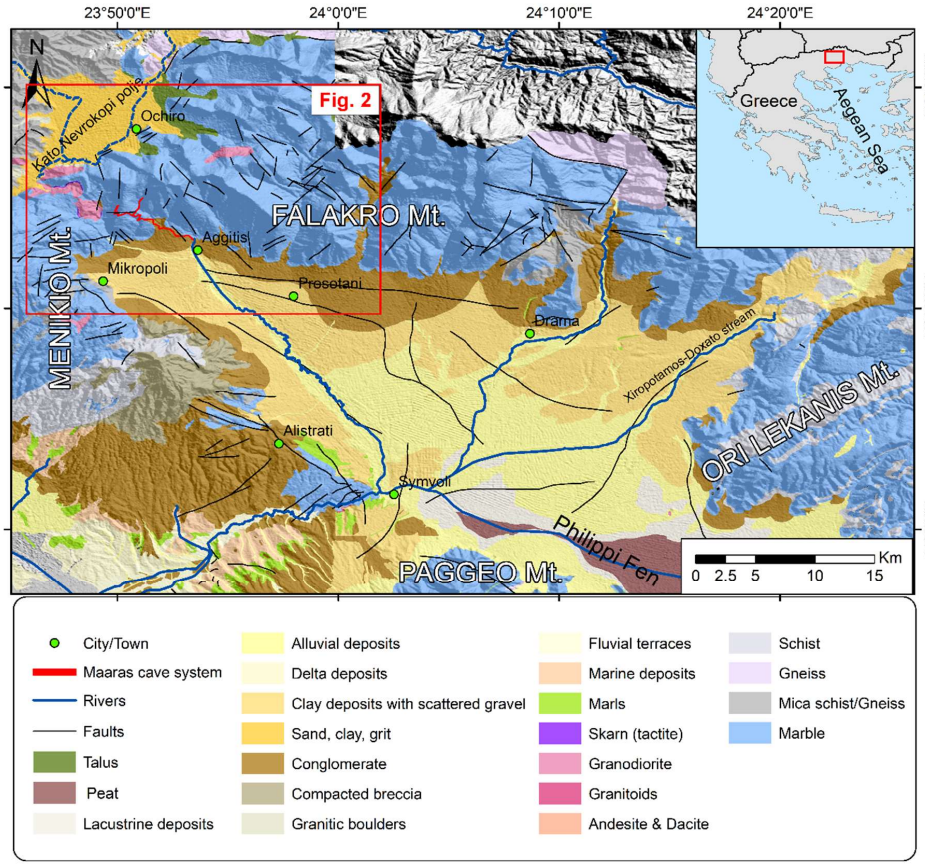

Fig. 1. Geological map of the Aggitis river basin and the broader area (modified from Papapetros, 1982; Pennos et al., 2016b) superimposed on a digital elevation model (NASA/METI/AIST/Japan Spacesystems, 2019). Rivers: GEODATA.gov.gr (2010).

2.2. Study area

The Maaras cave system is developed along the northwestern margin of the Aggitis river basin (Figs. 1, 2). It hosts an active fluvial system fed by a closed karstic basin, the Kato Nevrokopi polje, in the northwest (Petalas and Moutsopoulos, 2019). Surface water draining into the polje is stored in a multi-level aquifer comprising 3-400 m thick Quaternary deposits of stacked, interbedded breccia, conglomerate, sand, silt, marls and clays (Novel et al., 2007; Petalas and Moutsopoulos, 2019). Groundwater flow exits the polje at approximately 545 m.a.s.l. through localized inlets near the village of Ochiro (Novel et al., 2007; Petalas and Moutsopoulos, 2019), providing perennial, although seasonally fluctuating, discharge of water through the Maaras cave system (Petalas and Moutsopoulos, 2019). The river exits the subsurface through a spring located at 123 m.a.s.l. near the village of Aggitis.

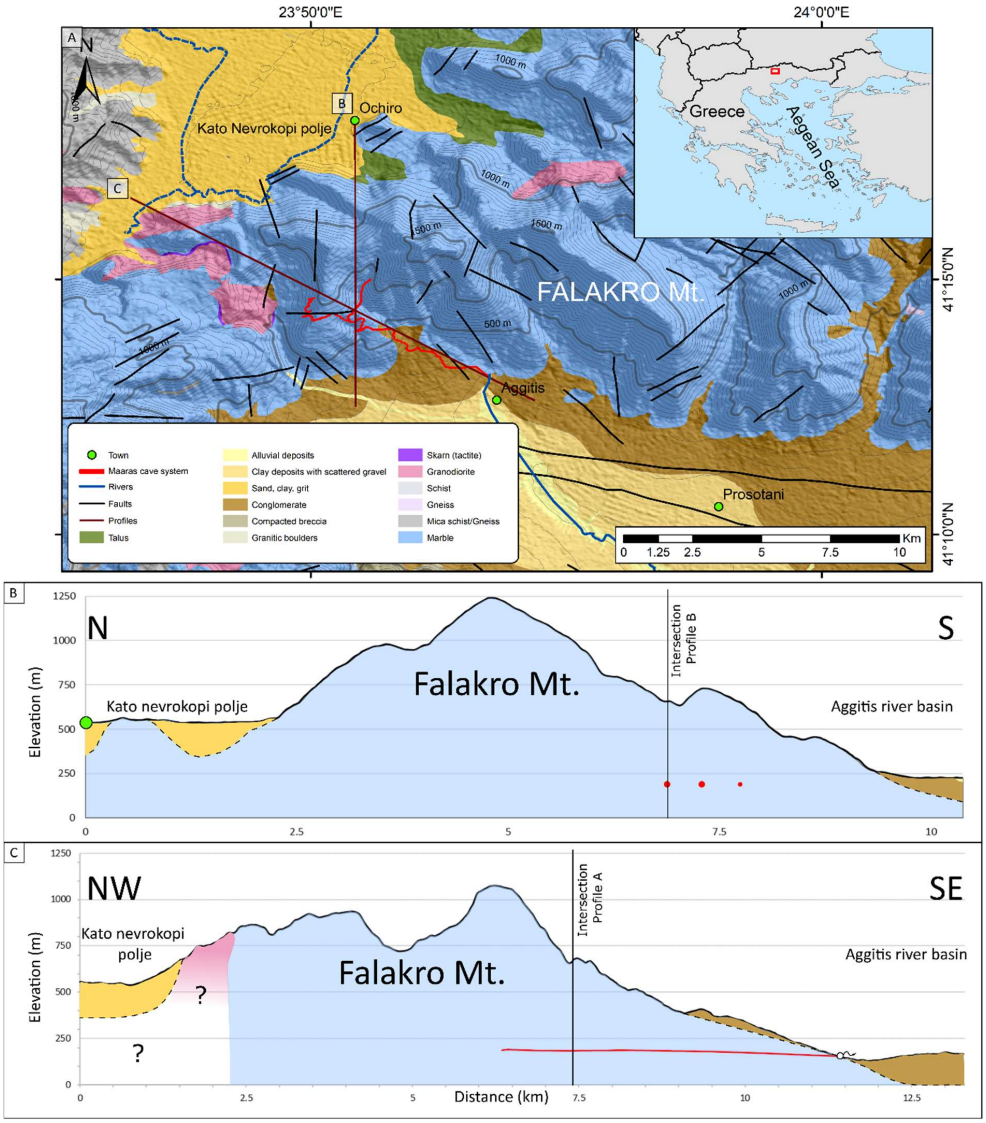

Fig. 2. Geological setting of the Maaras cave system. (A) Geological map showing the location of profile B and C. (B) N-S oriented elevation profile from the Kato Nevrokopi polje, across the Falakro Mt. and down to the Aggitis river basin. Note red circles in profile indicate where the profile intersects with the Maaras cave system. (C) NW-SE oriented elevation profile and spatial distribution of the Maaras cave-floor (red line) within the Falakro Mt. Note that the rendered Maaras profile represents the master conduit and the western branch of the cave system. Also note difference in horizontal scale between the two profiles. Cave survey and geological map modified from Pennos et al. (2016b) and Papapetros (1982), and superimposed on a Digital elevation model (NASA/METI/AIST/Japan Spacesystems, 2019). Rivers: GEODATA.gov.gr (2010).

The cave system is formed in the marbles of the Rhodope massif (Novel et al., 2007). Morphologically, it has no closed loops, and exhibits a pattern of lower-order tributaries joining to form higher-order passages. Maaras comprises two such tributaries; an eastern branch and a western branch, which

coalesce into a single master conduit running down to the spring. Following the Palmer (1991) classification, this morphology coincides with the pattern of a typical branchwork cave. Cumulative length of the system is almost 12 km, of which 10 km has been surveyed (Pennos et al., 2016b).

The thick deposits covering the cave floor have a flat top surface and consists of allochthonous sandy clastic sediments with a minimum thickness of 10 m (Pennos et al., 2016b; Petalas and Moutsopoulos, 2019). Floor altitude drops from 194 m.a.m.s.l. in the innermost part to 123 m.a.m.s.l. at the Aggitis spring over a thalweg distance of 10 km (Pennos et al., 2016b). From the confluence of the two branches and down to the spring (thalweg distance of almost 6 km), the calculated slope of the river averages 1%, steepening towards the spring. For further details see Pennos et al. (2016b). Pennos et al. (2016b) infer that the river profile is currently adapting to a lowering of base level.

Previous studies by Pennos et al. (2016a) have shown that the upper 30-40 cm of the active underground riverbed predominantly consist of silt and fine-grained sand at the time of measurement. These are locally interbedded with thin layers of coarser sand (>500 μm) (Pennos et al., 2016a). The sediments have relatively high concentrations of Si, Pb, and Fe, indicating a quartz, pyrite and galena provenance. Quartz is found in granitic intrusions north of the cave, whereas pyrite and galena occur in the skarn alterations (Figs. 1, 2). The mineralogical composition demonstrates the allogenic character of the sediment infill (Pennos et al., 2016a). However, as the cave host an active fluvial system, sediment thickness may vary over a relative short time frame.

In contrast to the low slope of the sediment floor, the cave roof has an irregular morphology with a looping pattern, and a ceiling height ranging from a few cm up to 60 m. The Maaras cave and its subsurface river system display evidence of four distinct speleogenetic phases related to changes to the local base level (Pennos et al., 2016b).

3. Methods

This study focusses on collecting data on the sub-sediment cave floor morphology and mapping thickness, grain size and spatial distribution of the sediment infill along the master conduit (Fig. 3). A cave survey of the Maaras cave system (Pennos et al., 2016b) is used as a reference for this mapping. The cave survey comprises a series of consecutive line-of-sight measurements between survey-stations combined with multiple cross-sectional measurements for each station. The measurements are anchored to a geo-referenced point at the cave entrance and form the framework of the rendered cave map.

Electrical resistivity tomography (ERT) was employed to map sediment thickness and identify resistivity signatures revealing the true cave morphology. Surveys are conducted using a linear array of electrodes, the spacing of which influences the depth of investigation and resolution; closer spacing yields high resolution but low depth of investigation and vice versa. Electric resistivity contrasts reflect

variations in sediment and pore fluid properties. These include alteration of grain size, mineralogy, porosity, pore size distribution and connectivity, water saturation (Sw), fluid chemistry, and temperature (Samouëlian et al., 2005).

Sediment distributions on the cave floor were mapped, and stratigraphic logging and sampling of fluvial sediments were carried out to link the sediment types to the resistivity responses of the ERT survey. Stratigraphic logging and sampling were carried out in a representative terrace located half-way between the passage junction and the cave entrance (Fig. 3) , as a supplement to the findings of Pennos et al. (2016a).

The fieldwork and associated data collection were carried out during the winter season as the water level is low and access is more convenient at this time of the year.

3.1. Clastic sediment-fill

The cave floor predominantly consists of fluvial sediments, locally exhibiting low, laterally continuous terraces along the active river channel. A short 1.25 m long stratigraphic section of fluvial sediments, extending to approximately 2 m above the level of the river at the time of the investigation, was logged and sampled for grain size analysis. The selected site is in the erosional slope of a raised terrace, approximately 4 km from the cave entrance.

The sediment sampling locations were chosen based on apparent contrasts in sedimentary structure or grain size and grain size analysis was performed on 13 samples from the stratigraphic section using a laser diffraction particle analyzer (Mastersizer 3000) at the EARTHLAB facilities of the University of Bergen. Sediment samples were run through the automated dispersion unit, and dispersant (Calgon) was added. Ultrasound was set to run throughout the process to ensure complete dispersion.

The spatial distribution of exposed taluses along the cave passages was mapped through the master conduit from the conduit junction to the spring. Here, talus is defined as a distinct accumulation of unconsolidated angular to subangular breakdown-derived clasts. The spatial distribution of taluses was mapped to investigate to what extent these may alter the rendered cave survey morphology.

3.2. Electrical Resistivity Tomography (ERT)

ERT surveys were conducted along four lines at the south-eastern part of Maaras (Fig. 3), within 1.5 km from the cave entrance, to map sediment thickness and resistivity patterns revealing depositional composition. The instrument used was a 10-channel resistivity meter (IRIS INSTRUMENTS) with a 48-cable multiplexing capability. The survey started inside the caves largest chamber, the Acropolis chamber (Fig. 3), measuring 60 x 140 x 40 m. The first line, ERT 1, was measured crossing the main

axis of the conduit taking advantage of the maximum opening from one side of the cave to the other and trying to map the walls of the cave dipping towards the middle of the cave. Electrode spacing was 3 m and the total length 69 m. The second line (ERT 2) was measured parallel to the conduit using 5 m spacing between the electrodes, taking advantage of the total length of the cable (115 m) and thus providing maximum depth of investigation close to 40 meters. The ERT lines intersect at 60 m (ERT 2) and 40 m (ERT 1). On-site evaluation of the acquired data from the two lines suggested that the depth to the cave floor was surprisingly great and therefore an electrode spacing of 5 m was the optimal for the rest of the survey. Due to the geometry of the cave towards the exit, ERT 3 and ERT 4 were positioned centred and parallel to the conduit orientation with 115 meters length for each one. The entire survey covers a total length of 414 m and the lines are surveyed while moving downstream and labelled in chronological order from ERT 1 to ERT 4. The depth of investigation of the lines using 5 m electrode spacing (ERT 2, 3 & 4) is approximately 40 - 45 m, with a horizontal and vertical resolution of 2.5 – 3 m. For ERT 1, employing a 3 m spacing, the depth of investigation is around 25 m, with a horizontal and vertical resolution of 1.5 m.

In order to generate 2D representations of the resistivity responses along the survey lines, the raw data of the acquired signal is inverted following the methodology proposed by Tsourlos (1995) and Tsourlos et al. (1998). A 3D model of the cave (Pennos et al., 2016b) was introduced as apriori data into the DC3DPRO software (Kim and Yi, 2010) and used to restrain any potential masking of the clastic sediments caused by the highly resistive host rock.

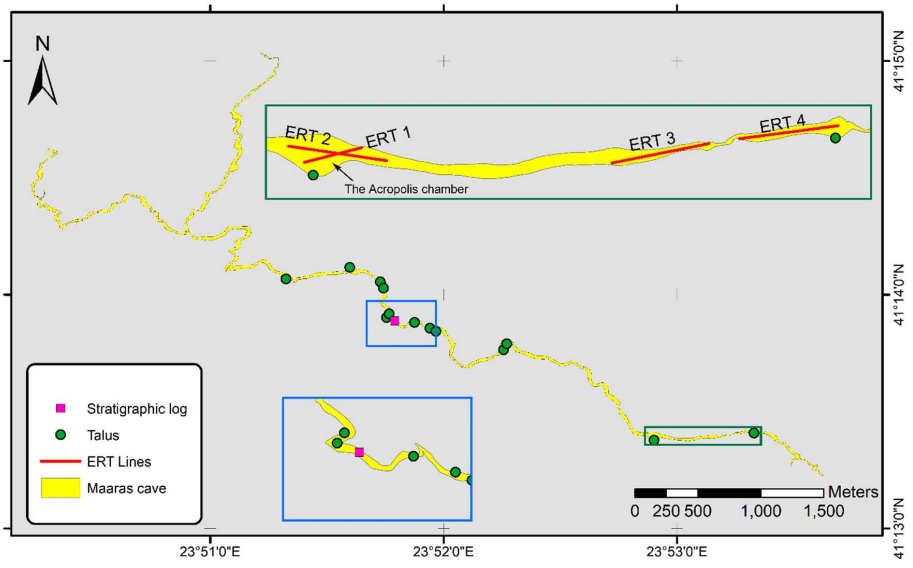

Fig. 3. Overview map of Maaras cave system showing the location of all collected data: stratigraphic log (blue insert), talus and ERT lines (green insert). Cave map from Pennos et al. (2016b).

3.3. Geocellular rendering

The reservoir modelling software RMS 11™ was used for the geocellular rendering of the clastic sediment distribution in the Maaras cave system. A pre-built grid model of the cave (Lønøy et al., 2020) was used as a framework, and a depth shifted cave floor horizon were generated along the ERT lines using a local B-spline algorithm. The newly generated horizon was used for geometric modelling ("assign values between horizons") to discretize the siliciclastic sediments. The precise sub-sediment extent of the taluses was not mapped, and consequently not rendered explicitly in the grid model. The purpose of the geocellular rendering was to visualize the results, estimate the volumetric proportion of sediment infill in the cave and, if possible, discretize the sub-sediment cave floor morphology.

4. Results

4.1. Sediment-fill

The log through the fluvial sediments (Fig. 4) starts with ~40 cm trough cross-bedded sand with 10-15 cm deep troughs and shows a coarsening upward trend from fine- to coarse-grained sand. This is indistinctly overlain by a ~25 cm succession of planar and ripple laminated sediments with mud clasts (5-15 cm in diameter), fining upward from medium-grained sand to sandy silt and capped by a set of small-scale ripples. The ripples are draped by a 9 cm thick laminated silt layer with traces of oxidation, seen as localized orange/brown patches, and in thin orange/brown laminae along the base of the bed (Figs. 4, 5E). This bed appears to be laterally extensive and can be traced over long stretches of the cave system (e.g., Fig. 5E). The top of the silt bed is truncated by an erosional unconformity overlain by 32 cm of indistinct ripple and trough cross-bedded medium to coarse-grained sand. Near the base of this bed, thin, organic-rich distorted laminae, angular rip-up clasts (4-7 cm in diameter) can be seen. This section is truncated by an erosional unconformity and overlain by 3 cm of fine-grained sand with an indistinct/massive structure.

Grain-size analyses of the logged stratigraphic sequence suggest that the sediment terrace predominantly consists of poor- to moderate-sorted coarse-grained sand (Fig. 4B, C). Three samples show a higher abundance of silts; two samples (md-s-7, md-s-12) in beds overlying the unconformity and the sharp bedding contact towards the top and one (md-s-5) in a bed comprising interbedded mud clasts. The logged section shows similar sedimentary structures and grain size distributions as other sediment terraces (Fig. 5) and grain sizes are comparable to the findings of Pennos et al. (2016a). Thus, the logged section is assumed to be representative of allochthonous sediments being funnelled through the Maaras cave system.

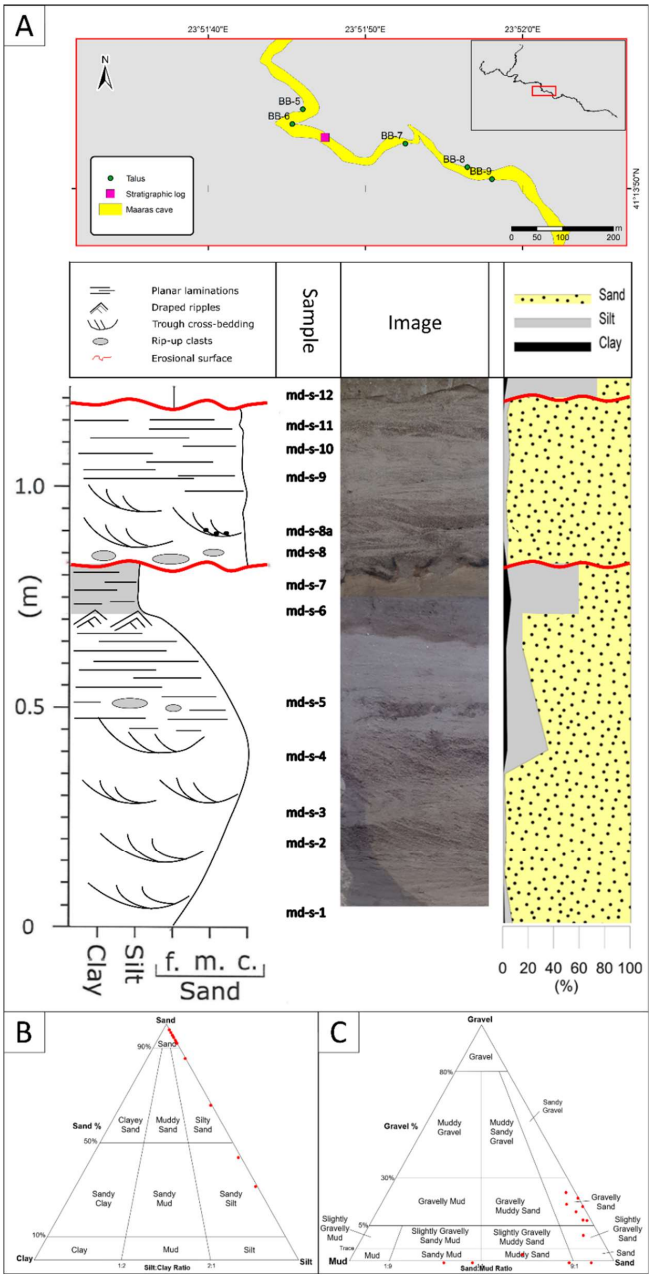

Fig. 4. Logged sediment terrace (A) Composite log: Stratigraphic log, photo of logged section and cumulative log of sand, silt and clay distribution (from grain size analysis). Note the colour difference of the laminated silt in the photo (at approx. 0.75 m) is related to image compilation. (B) Textural grouping of sampled sediments according to sand, silt, and clay content (C) Textural grouping of sampled sediments according to gravel, sand, and mud content. Textural grouping according to Blott and Pye (2001).

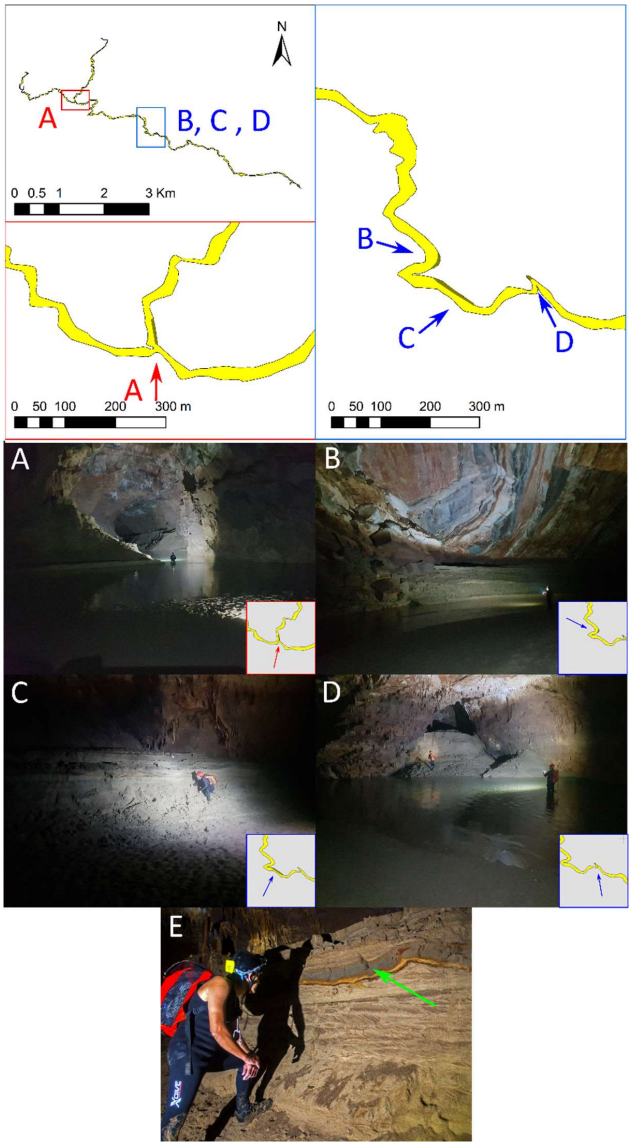

Fig. 5. Selected photos from sediment terraces. Top: Overview map showing location of image A-D, angle of view (arrows), location of sediment terraces (brown areas). Note that the sketched sediment terraces (brown areas) are only for illustrative purposes and not to scale. Bottom: Images from selected sediment terraces and inserts highlighting location and angle of view (arrows). (A) The intersection point between the eastern and western branches. Eastern tributary (centre) comprising a thick remnant sediment terrace comprising fine-grained sediments such as silt and clays. (B) Sediment terrace and break down morphology showing the previous level of sediment fill and potential incipient cave roof collapse. Note the lack of talus on the floor, suggesting these are either removed by fluvial processes or hidden by thick accumulations of siliciclastic sediments. (C) Overview photo showing the dimensions of the logged and sampled section (i.e. Fig. 4). (D)Truncated tributary fill. Cavity along the cave wall located near BB-7 (in Fig. 6). The cavity is filled with medium to coarse-grained siliciclastic sediments. (E) A laterally extensive bed of fine silt (green arrow) with thin orange/brown laminae at the base of the bed. The depicted cross-section is from a different locality than the logged section (C) but shows a similar stratigraphy. Note that this bed can be traced for more than 2.5 km. Photo by Aristeidis Zacharis.

4.2. Talus mapping

All major visible taluses along the master conduit were mapped. Each point on the map (Fig. 6) represents large distinct talus (e.g., Fig. 7). Taluses are mainly observed at the inner bends of the conduits (BB-3, 4, 5, 6, 10 & 11 in Fig. 6) and where the conduit widens (BB-1, 2, 8, 9, 12 & 13 in Fig. 6). The taluses predominantly comprise angular marble clasts that vary in size (from >2 mm to 20 m) between localities, but also locally within the same accumulation (Fig. 7). In many of the talus accumulations, the clasts are partially covered by speleothems (e.g., Fig. 7B), and thus the true extent and clast size distribution are difficult to map.

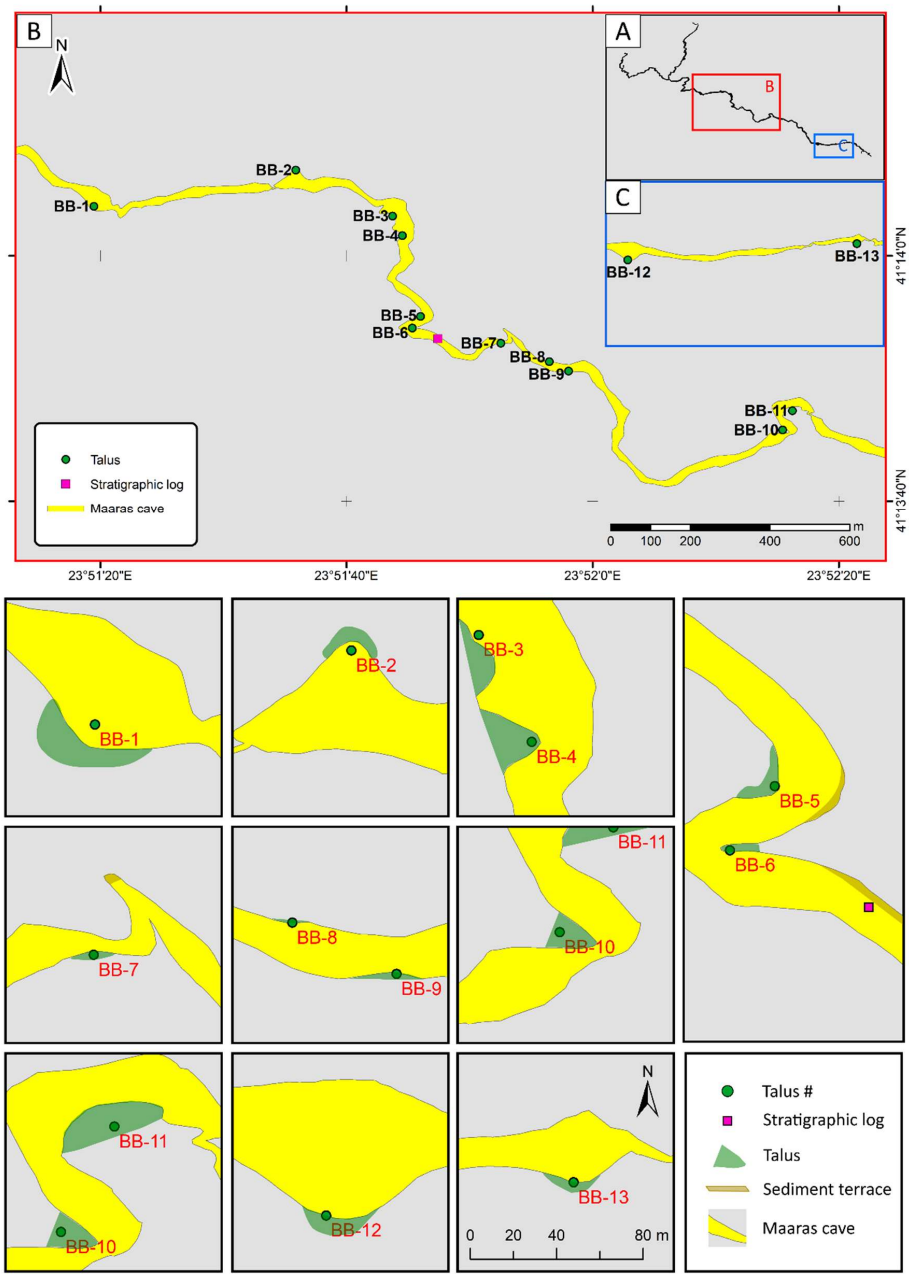

Fig. 6. Overview of outcropping talus in Maaras. (A) Overview of Maaras and location of insert (B) and (C). (B) Map section showing location of BB-1 to BB-11. (C) Map section showing location of BB-12 and BB-13. Most of the taluses are located within, or proximal to, conduit widenings or in the inner bend of the conduits (e.g. BB-3, BB-4, BB-5, BB-6, BB-10 & BB-11). Note that all conduit inserts are displayed with identical scale and orientation (last insert for reference) whereas the relative size of taluses and sediment terraces are not to scale and only for illustrative purposes.

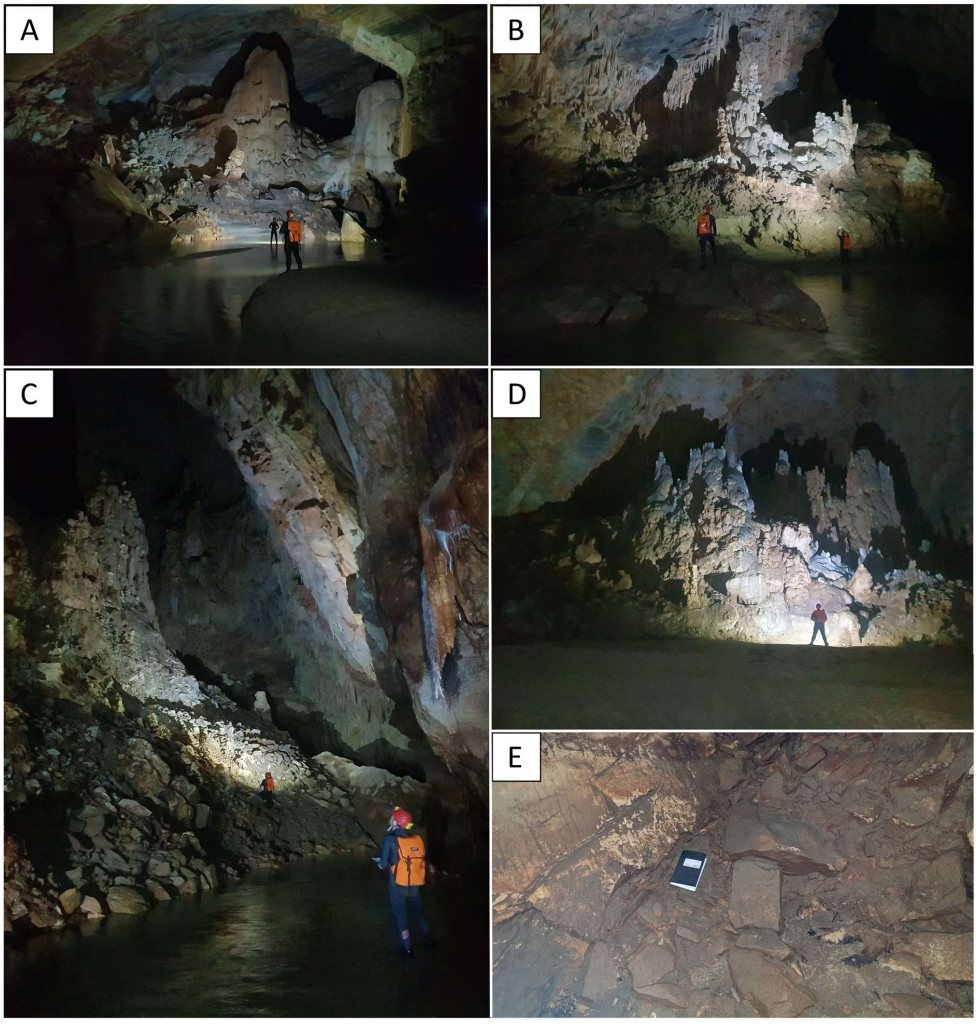

Fig. 7. Photos of talus accumulations in Maaras. (A) BB-1 in Fig. 6 - The "Ghost´s chamber". Note the thick speleothems coating the taluses. (B) BB-3 in Fig. 6 - The "Chamber of Giants". (C) BB-4 in Fig. 6 A massive chamber with lateral talus accretions building into the active river system. (D) BB-12 in Fig. 6 - The "Acropolis chamber" with breakdown derived talus covered by speleothems. (E) Close up of a collapse-related talus comprising homogenous and angular clasts. Clasts have a diverse grain size distribution, ranging from a few cm to several meters.

4.3. Electrical resistivity tomography (ERT)

ERT proved to be a quick and efficient method for estimating minimum sediment thickness and longitudinal sub-sediment cave-floor morphology within an active karst system. However, in Maaras, the thickness of the allochthonous clastic sediment infill was significantly larger than expected; at three

locations, even a survey line length of 115 m (with a maximum depth of investigation of 45 m) didn't have sufficient depth of investigation to reach the bedrock. However, the electrode array provided adequate resolution for identifying macro resistivity contrasts set up by the sediment infill and surrounding host rock (Fig. 8).

Four distinct resistivity groups, RF-1 – RF-4, are defined (Table I) based on the spatial distribution and magnitude of resistivity responses in the processed survey stations and field observations of sediment infill (Fig. 8). RF-1 comprise resistivity responses of <100 Ωm and is evident in all ERT lines, except ERT 1 (Fig. 8A). RF-2 is ranging from 100 to 350 Ωm and form the bulk of resistivity responses in all ERT lines. RF-3 is ranging from 350 to 900 Ωm and observed in all ERT lines, except ERT 4. In ERT 1, RF-3 is observed in a large talus cone extruding the underlying siliciclastic sand (southwestern part in Fig. 8A). The relatively high resistivity of RF-3 could relate to masking effects caused by encompassing lithology (cave walls/host rock). However, the array proximity to the cave walls does not seem to influence the resistivity response significantly. RF-4 comprise the highest resistivity responses (>900 Ωm) and is only observed in the lower part of ERT 4.

All resistivity groups are anticipated to be water-saturated and resistivity differences between RF-1 and RF-2 are expected to relate to porosity and water saturation primarily. In contrast, differences in RF-1/RF-2 vs. RF-3/RF-4 are assumed to be controlled by the mineralogical composition and grain size (siliciclastic sand and silt vs. marble clasts and -host rock). The ERT survey was used to estimate minimum clastic sediment thicknesses and, based on the associated roof height, calculate relative proportions on infill (Table II).

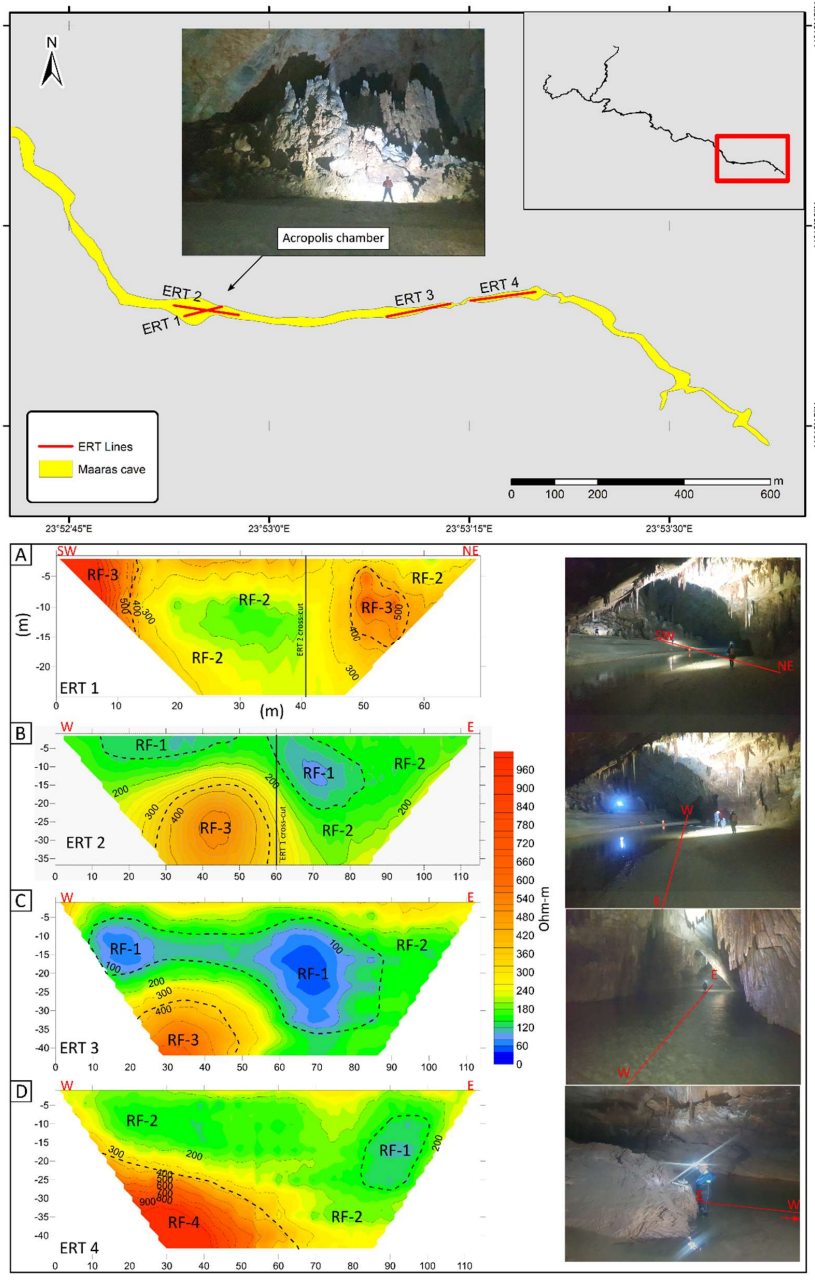

Fig. 8. ERT survey results. Upper: Plan view map of Maaras showing the spatial distribution of the ERT survey. Lower: Resistivity values and associated ERT line positioning (photos). (A) ERT 1 with a total length of 69 m and 3 m electrode spacing. (B) ERT 2 with a total length of 115 m and 5 m electrode spacing. (C) ERT 3 with a total length of 115 m and 5 m electrode spacing. (D) ERT 4 with a total length of 115 m and 5 m electrode spacing. Note that the red arrow in the photo indicates that the ERT line continuous upstream, and that vertical- and horizontal scale of ERT 1 differs from the other profiles.

ERT 1

The ERT 1 line is 69 m long and was placed with a 60˚ azimuth, running from WSW to ENE (Fig. 8A). It starts at the base of a sizeable talus cone, crosses the active stream channel, and ends on a relatively long and wide sandbar attached to the channel margin. The line intersects the ERT 2 line at the 40 m mark. Resistivity values are in the range of 100 – 1000 Ωm, with readings predominantly in the lower part of the spectrum (~100 – 350 Ωm). Elevated resistivities, up to 1000 Ωm, are evident at the western end, close to the large talus cone (SW). In contrast, relatively low resistivities are measured around and beneath the active fluvial channel. At the eastern end of the survey line, a field of intermediate resistivity surrounded by low resistivity is evident in the sub-surface.

ERT 2

The ERT 2 line is 115 m long and was placed with a 95˚ azimuth, running from W to E (Fig. 8B). It starts in the west at the toe of the talus cone, follows the river channel downstream, and ends on a relatively small sandbank. The survey intersects ERT 1 at 60 m. Resistivity values are in the range of 50 – 550 Ωm with a predominance of low resistivity readings. The lower resistivities that appear near the surface reveal a horizontal layer with a thickness that varies from 10 m to 15 m on the western half of the line. In the same area in greater depths and down to 35 m higher resistivity formations are identified indicating a change in the geology. However, near the centre of ERT 2 and toward the east, the thickness of the lower resistivity formations increases rapidly revealing an almost vertical geological boundary between different formations. Moreover, in the group of lower resistivities, we can identify areas with variations of the resistivity values that could be related to changes in the lithology.

ERT 3

The ERT 3 line is 115 m long and was placed with a 77˚ azimuth, running from W to E (Fig. 8C). It runs along the middle of the conduit from the west following the river downstream and ending near a siphon. Resistivity readings range from 40 - 650 Ωm. The results are similar to the previous case of ERT 2. Once again, we can clearly identify a low resistivity horizontal layer on the west part, with a thickness of 15 m to 20 m, that lies on top of a more resistive body that appears in depths greater than 25 m. Also, as in the previous case, a sudden increase of the low resistivity formations is revealed toward the east (downstream) forming an almost vertical boundary between the different geological formations. The variability of the resistivities can be attributed to changes in the lithology as in the previous case.

However, in ERT 3, we can clearly identify a thin layer with a small resistivity increase that lies on the surface and has a thickness that varies from 2 to 9 – 10 m.

ERT 4

The ERT 4 line is 115 m long and was placed with a 76˚ azimuth, running from W to E (Fig. 8D). The survey starts downstream of the siphon at the end of ERT 3 and runs along the centre of the conduit downstream of the river channel. The line ends on a laterally extensive sandbank with minor deposits of bat guano, proximal to a new siphon. Resistivity responses are in the range of 80 – 1050 Ωm, with a predominance of low resistivity readings <350 Ωm. A prominent resistivity contrast with an apparent dip towards the east is observed at approximately 17-45 m depth. On top of that a layer of lower resistivity formations is identified with thickness that increases downstream toward the east end of the line. A significant finding of this result is also the reversed cone shaped high resistivity anomaly that is identified close to the surface approximately at 75 m from the start of the line that is attributed to the massive body that collapsed from the roof (respective photo in Fig. 8D) that appears to continue below the surface for 5 m or even more.

Table I. Electrical resistivity groups. Resistivity ranges are in Ωm.

Electrical resistivity groups			
Group	*Resistivity*	*Resistivity range*	*Interpretation*
RF-1	Very low	<100	Highly porous fine-coarse grained siliciclastic sediments
RF-2	Low	100 - 350	Porous fine-coarse grained siliciclastic sediments.
RF-3	Intermediate	350 - 900	Autochthonous clasts (marble)
RF-4	High	>900	Host rock (marble)

4.4. Geocellular model

Figure 9 shows the grid model of the Maaras cave system modified from Lønøy et al. (2020). The orange part of the model is a 3D rendering of the open cavity based on a conventional survey of the cave. The green part of the model represents the sediment infill. In the grid model, the sediment thickness estimated from the ERT (Fig. 8) was used to discretize the minimum sediment-fill and, if possible, constrain the sub-sediment cave floor morphology (Fig. 9). The sediment-fill make up 67 – 79% of gridded volume of each segment (Fig. 9). As the cave floor was only identified in parts of ERT 4 (Fig. 8D), all clastic sediment thicknesses represent minimum thicknesses.

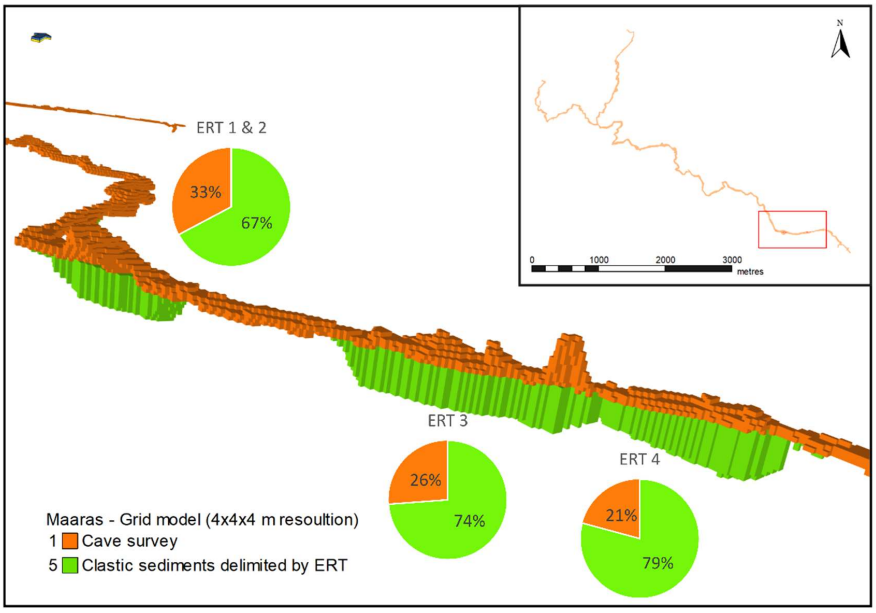

Fig. 9. Geocellular model of the Maaras cave system with a 4 x 4 x 4 m global grid resolution. The model shows a geocellular representation of the cave survey (orange grid cells), associated clastic sediment fill (green grid cells) mapped by ERT and relative proportions in percentage (pie charts). Note that most sediment thicknesses are minimum thicknesses since only ERT 4 (SE-part of grid model) had sufficient depth of investigation to reach the cave floor/host rock. Also, taluses are not discretized in the grid model as their true extent above and below the sediment surface was not mapped. Relative volume proportions (open cavity vs. clastic sediment) may thus deviate from the pie charts. Geocellular cave model modified from Lønøy et al. (2020).

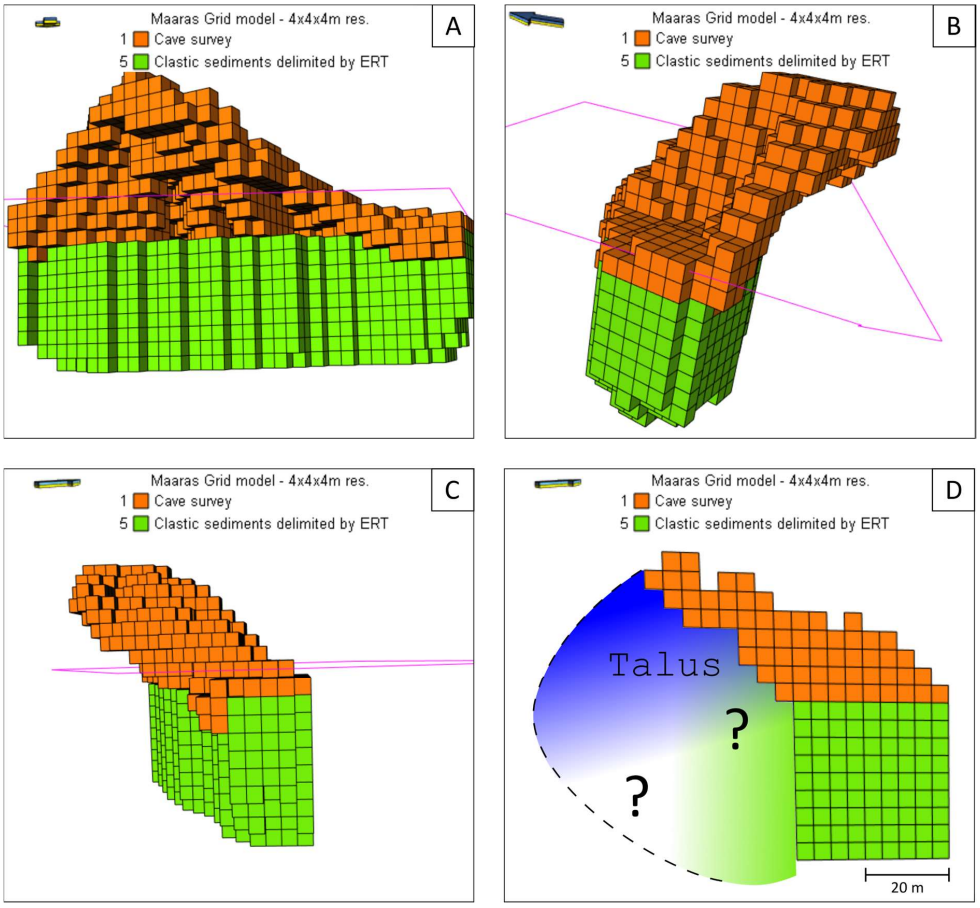

Fig. 10. Segmented grid model with a 4 x 4 x 4 m global grid resolution viewed from different angles. The segment represents the Acropolis chamber (ERT 1 & 2) and highlights the impact of inaccurate morphological rendering. Elements obstructing direct line-of-sight measurements, such as a talus cone, may cause volumetric underestimation and erroneous rendering of the conduit morphology. (A) View towards the N, from behind the talus cone (not rendered). (B) View towards the NW. Note that the geocellular rendering of the cave survey creates an "overhang" where the talus cone (not rendered) is supposed to be. (C) View towards NE. The "overhang" also evident. (D) 2D cross-section of the grid model with interpreted morphology (dashed line) and facies distribution (blue and green area). Note that siliciclastic sediments (from ERT) are only discretized directly below the surveyed cave floor and not below the talus cone (blue area). Also, note that the cross-sectional shape of the conduit is not resolved due to insufficient depth of investigation of the ERT.

5. Discussion

Maaras hosts an active fluvial system connecting the Kato Nevrokopi polje with the Aggitis river basin. Under present conditions the cave system acts as a sediment trap. The ERT survey shows that, along the mapped sections, a substantial proportion of the Maaras cave is filled in by fluvial sediments. The logged section is considered a representative sample of these deposits as it exhibits comparable grain size

distributions to the findings of Pennos et al. (2016a), and grain sizes, sorting, and sedimentary structures matching “Channel facies” as described by Bosch and White (2004). The log reflects periods of low current velocity manifested as small-scale ripples and planar lamination of fine sand and silt alternating with episodes of increased discharge reflected by trough cross-bedded and planar-bedded medium- to coarse sand, erosional contacts and mud-clasts potentially deriving from bank-collapse or basal erosion. The depositional pattern appears repetitive. The clastic sequence likely reflects the well-known fluctuations in discharge inside the cave system (Reile, 2005; Petalas and Moutsopoulos, 2019).

The mapping of exposed taluses along the master conduit shows that autochthonous breakdown material in Maaras is confined to two specific areas (Fig. 6). Inside Maaras, taluses seem predominantly located along the inner bend of the conduits (e.g., BB-3, 4, 5, 6, 10 & 11 in Fig. 6) or where passages widen (e.g., BB-1, 2, 12 & 13 in Fig. 6). The spatial arrangement of taluses relative to the conduit morphology suggests that roof and wall collapse redirect water flow, forcing lateral dissolution. However, this apparent relation may simply be related to survey bias as caves cross-sectional morphology is mapped by measuring the line-of-sight distance from the survey station to the closest obstruction. Thus, measurements may not represent the actual distance to the cave wall/roof, but rather the distance to a talus cone or fan, sediment terrace, stalactite, or other objects covering the wall/roof perimeter of the host-rock cavity. Even if the depicted cave wall represents a talus surface, it is evident that, for Maaras, the conduits are wider in most areas comprising lateral talus accretions than in proximal areas absent of talus (Fig. 6). Talus is therefore believed not to be preferentially deposited at the inner bend of the conduits, but that its presence force lateral dissolution which will be mapped as an apparent inner bend on the cave map (Fig. 6).

3D inverted resistivity data indicate that the cave fill predominantly consists of very low-to-low resistive material (RF-1 & 2 in Table I); ubiquitous in all ERT lines (Fig. 8). The details observed in the sediment terrace section are below the resolution of the ERT survey, but sediments with similar grain sizes (cf., Pennos et al., 2016a) are believed to form the bulk of the allochthonous infill deposited by the active stream, and are here correlated with RF-1 and RF-2 in the ERT data (Table I). RF-1 predominantly occur below or in the vicinity of the active stream channel, frequently enclosed by RF-2, and is accordingly interpreted to comprise a similar composition as RF-2, but with higher porosity and water saturation. The absence of RF-1 in ERT 1 and elevated resistivity observed along the sediment surface (compared to ERT 2) may relate mainly to the different orientation of the line but also to the difference in the electrode spacing, thus the resolution and the depth of investigation. In addition, most sand deposits in ERT 1 (compared to ERT 2) are above the present level of the river and likely to be partially drained, thus potentially causing higher resistivity readings. RF-2 has a similar resistivity signature to exposed allochthonous sediments, suggesting that RF-2 is composed of siliciclastic sand. The irregular geometry, spatial arrangement, and enclosing resistivity responses (mainly RF-2) indicate that RF-3 may represent accumulations of marble clasts (talus). The abundance of clasts may, however, be considerably higher

than what is evident from the ERT. Suppose the size of individual clasts or accumulation of clasts is below the resolution of the survey. In that case, the resistivity signal may be smeared out or masked by surrounding low-resistivity clastic infill. A highly resistive zone, classified as RF-4, can be observed along the base of ERT 4. This resistivity response differs from RF-3 both in geometry and partially in resistivity and is interpreted to represent the cave floor/host rock lithology.

The ERT survey shows that siliciclastic sediments in Maaras, represented by RF-1 and RF-2, vary in thickness from approximately 25 m to >45 m (Fig. 8). Assuming that the cave system comprises a typical phreatic conduit morphology (elliptical), the depicted resistivity groups representing siliciclastic sediments occupy more than 64 – 95% of the available space (Table II). The cave floor, represented by RF-4 and observed in ERT 4 (Fig. 8D), has a downstream dipping trend, indicating that sedimentary thickness variations might be controlled by inherent conduit morphology and associated accommodation space (Fig. 11). Furthermore, the floor- relative to the roof morphology (Fig. 11) suggests that the conduits have an overall intrinsic looping morphology supporting the interpretation by Pennos et al. (2016b) of conduits initially formed as deep phreatic loops.

Termination of current fluvial deposition in the Maaras system, through blockage or redirection of the river system, would preserve the sediments during future burial. Similar infills as observed in the Maaras cave system have been reported from paleokarst in some areas of the Tarim basin (China). A study by Tian et al. (2017) showed that wells penetrating karst slopes and -depressions in the Tarim basin tended to comprise paleokarst intervals with a high degree of sediment-fill (52 - 100%), whereas the former karst highland areas exhibited significantly lower values (3 - 17%).

Table II. Clastic sediment thicknesses from ERT. The maximum (blue) and minimum (red) distance from the sediment top to the roof along the individual ERT-line and associated calculated proportions of clastic sedimentary infill. Note that relative proportion clastic sedimentary infill is calculated based on the assumption that the conduits comprise a typical phreatic conduit morphology.

Minimum clastic sedimentary infill				
ERT	*Estimated min. sed. thickness (m)*	*Max. dist. Sed. top – cave roof (m)*	*Min distance sediment top – cave roof (m)*	*Proportion clastic sedimentary infill (min/max. %)*
1	24	20	5	64/90
2	35	20	5	69/88
3	40	5.7	4.2	88/90
4	45	9.7	2.2	82/95

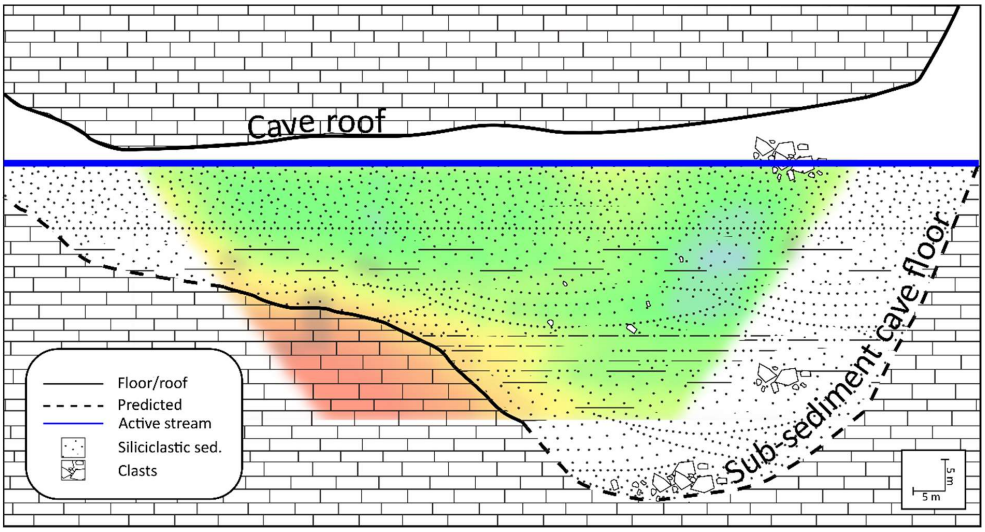

Fig. 11. Illustration showing predicted conduit morphology. The illustration shows how traditional cave surveys can be used in combination with ERT surveys (in this case, ERT 4) to estimate conduit morphology, sedimentary thicknesses, and compositional variations. Note that outcropping clast accumulations shown in the illustration were identified during talus mapping and not depicted by the ERT survey. However, the absence of interbedded breakdown material could relate to the size of clast accumulation being below ERT resolution.

Our findings show how allochthonous clastic sediments can fill substantial parts of the initial cavern void. If preserved during subsequent de-activation of the fluvial system and burial (i.e., transformation to paleokarst), the sediment infill is likely to influence the resulting reservoir architecture and properties in several ways. The ERT surveys and field observations suggest that clastic sediments inside Maaras have not experienced extensive compaction. Clastic sediments within intact cavities may thus potentially retain high porosity during burial unless cemented or compacted under a subsequently collapsing roof.

Gravity-induced collapse propagation during burial is largely constrained by available accommodation and compaction of the sediments during roof collapse. The ERT surveys combined with the cave survey show that the accommodation available for breakdown-derived material may, in some cases, constitute only a small proportion of the actual cave volume. Thus, the presence of pre-collapse sediment infill will affect collapse propagation, and eventually the reservoir architecture, by reducing accommodation. For multi-level systems of cavities, this is likely to affect the extent to which superimposed cavities coalesce during a collapse. Moreover, the sediments can provide lithostatic pressure to the cave walls and impede or prevent wall spalling. Even if the sediments are unconsolidated, as present in Maaras, tension release along cave walls will only result in a local rearrangement of the sediments without influencing bulk porosity.

The grid model (Figs. 9, 10) illustrates how elements in karst systems may impact the morphological and volumetric rendering of a cave survey. It is evident that the volume and wall morphology concealed by the talus cone (Figs. 7D, 8A) are not rendered by the cave survey (e.g., Fig. 10), causing an underestimation of the actual cave dimensions. Consequently, the volume of the talus cone and the cave wall morphology is reproduced erroneous. Also, the width of the cave floor is rendered narrower than it actually is, resulting in clastic sediments not being fully discretized along the sub-sediment cave floor (e.g., Fig. 10D). ERT proved to be an efficient method, if depth of investigation is sufficient, for constraining the longitudinal sediment thickness in a geocellular framework. However, delimiting the cross-sectional conduit morphology and associated sediment distribution may prove difficult as depth of investigation is limited by the survey array length. In narrow conduits with thick sediment accumulations, the passage width may not provide enough space for setting up perpendicular ERT surveys with a depth of investigation reaching the bedrock. Consequently, the true extent of the clastic sediments may not be fully discretized. Although not verified by this study, this could potentially be resolved by running multiple parallel ERT lines for each section (e.g., two lines along the walls and one conduit centered) and infer the cross-sectional sub-sediment cave-floor morphology by extrapolation between the ERT lines. In the grid model, the discretized siliciclastic sediments occupy 67% (ERT 1 & 2), 74% (ERT 3) and 79% (ERT 4) of the total grid volume for each segment (Fig. 9); which is comparable but lower than the estimated minimum percentage infill (Table II). A deviation between the estimated- and gridded proportion is expected and can be explained by:

- Estimated proportions are based on single min/max values (Table II), whereas the grid model calculations represent the entire segment (Fig. 9).

- Estimated proportions (Table II) are based on a circular cross-sectional morphology, whereas the gridded siliciclastic sediments are rendered rectangular for all of ERT lines due to insufficient depth of investigation (e.g., Fig. 10D), except ERT 4 (Fig. 9).

- Narrowing of the “cave floor” (sediment top) due to the presence of a talus cone result in erroneous discretization of clastic sediments and sub-sediment cave floor morphology.

- Grid cell resolution controls the geometric accuracy the rendered morphology, eventually impacting volumetric calculations.

Although cave surveys comprise the bulk of available observations on cave dimensions and configurations, they do not register sediment thickness (Fig. 12). Consequently, if sediment infills are present, conventional cave surveys can severely underestimate the dimensions of karst cavities (Figs. 10, 11, 12), which in turn affects the use of statistical information derived from them for modelling purposes. Inaccuracies may be amplified if statistical data is used for forward collapse modelling and subsequent forecasting of the final reservoir architecture. This shows that recognizing the presence of allochthonous clastic sediments in karst systems could offer better constraints to forecast the paleokarst reservoir architecture and associated facies distribution, and potentially improve calculations of in-place volumes, fluid flow and reserve estimates.

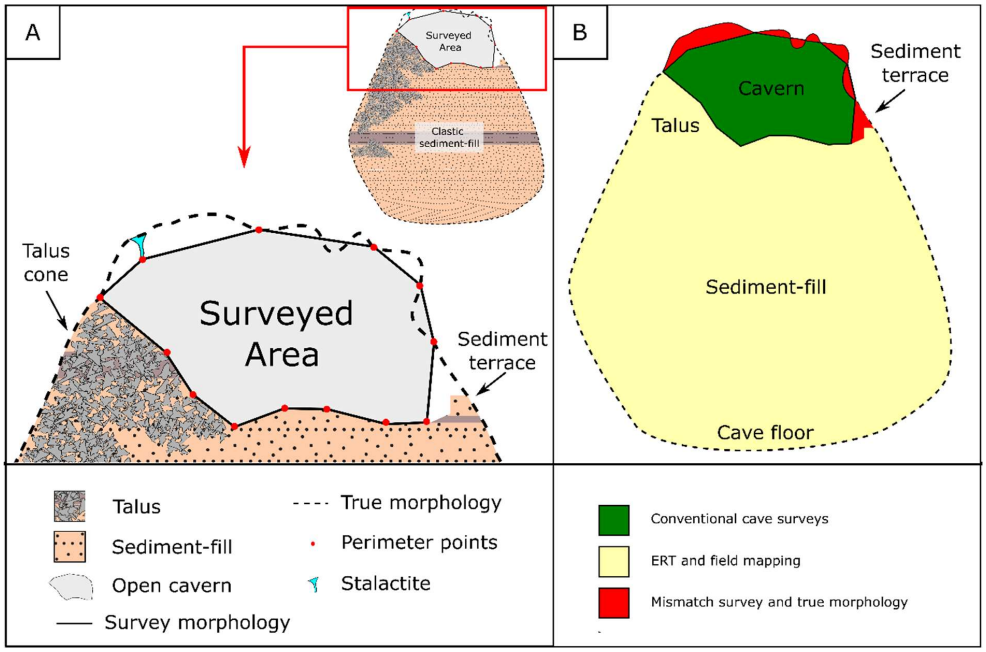

Fig. 12. Simplified conceptual sketch of rendered cave morphology and associated areas not mapped by conventional surveying techniques. (A) Surveyed cross-sectional morphology relative to the true cave morphology. Infilling of clastic sediments is a volumetrically significant component not captured by the survey. Note that the surveyed morphology is represented by the Euclidian distance between the perimeter points. Therefore, there is a mismatch between the survey and true cross-sectional morphology. The morphology is delineated by line-of-sight measurements and obstructions (e.g., a stalactite) may be treated as a cave wall or roof. (B) The cross-sectional area of the true cave morphology and associated methods for delimiting various karst elements. The cave survey may fail to discretize the true cross-sectional morphology of conduits even though wall- and roof shots (measurements) are not obstructed. This is due to the perimeter being constrained by the Euclidean distance between survey points. Thus, volumes may either be over- or underestimated in conduits with highly complex morphologies with asperities. This unresolved area may be delimited by using a Lidar scanner for surveying, but this is not verified by this study. Note that the illustration is not to scale.

6. Conclusions

This study is the first to estimate large scale sedimentary thickness variations using ERT-surveys inside active cave systems. The use of ERT proved to be useful for identifying and benchmarking macro-scale resistivity contrasts to outcropping infill. However, a trade-off between resolution and depth of investigation proved to be difficult. Comprehensive research and optimization of electrode spacing should be carried out to understand the extent of clastic sediments in karst systems. Also, the spatial distribution and density of ERT surveys should be carefully evaluated to ensure adequate morphological and volumetric constraints are achieved.

Results show that significant volumes of clastic sediments can accumulate in active karst systems and potentially be preserved during burial. In the studied sections of Maaras, the clastic sedimentary thickness varied from 25 m to >45 m, occupying a minimum of 64-95% of the karst cavity volume in the part of the cave surveyed by ERT. A high degree of pre-burial infill will result in less accommodation space available for subsequent breakdown-derived material. Thus, a high abundance of pre-burial infill can have a significant impact on the overall reservoir geometry and will significantly affect the architecture of coalesced cave collapses. Moreover, clastic sediments may have considerably different petrophysical properties than later breakdown material or disturbed host rock. Volumetric underestimation and incorrect spatial distribution of clastic sediments in paleokarst reservoirs can thus largely affect resource calculations, fluid flow analyses, subsequent recovery factors, and associated prospect evaluations. This study has also shown that geostatistical analyses based on active karst systems may have to be reconsidered as cave dimensions are most likely highly underestimated, and true cave morphology is often concealed by present sediment level.

Our study has demonstrated the viability of supplementing conventional survey methods with ERT to obtain more accurate data on cave dimensions in sediment-filled conduits. We hope this may encourage adding non-destructive geophysical investigation of cave sediment infill to the toolbox of cave surveyors as delimiting elements concealing the true cave morphology can significantly improve volumetric and geometric accuracy of paleokarst reservoir models based on recent karst systems.

Acknowledgments

The authors would like to thank the Research Council of Norway (project number: 267634) for funding this study and Emerson Roxar for providing an academic license for RMS™. The Hellenic Ministry of Culture is acknowledged for providing permission to perform the study and allowing the execution of the fieldwork. Permission is granted to Christos Pennos (reference number: ΥΠΠΟΑ/ΓΔΑΠΚ/ΕΠΣ/ΤΑΠΠΠ/307618/181597/5084/2126). The reviewers are acknowledged for their constructive feedback. The authors are also grateful for the facilities made available by the Maaras tourist center team (Dimitris Stergiakos and Nikos Diafas) allowing us to prepare the fieldwork. Stavros Zachariadis, Eugenia Kiourexidou, Kristian Jensen and Tasos Polihroniadis are acknowledged for assisting the fieldwork. The scientific discussions with Arve Lønøy are also highly appreciated.

References

Agada, S., Chen, F., Geiger, S., Toigulova, G., Agar, S., Shekhar, R., Benson, G., Hehmeyer, O., Amour, F., Mutti, M., Christ, N., and Immenhauser, A., 2014, Numerical simulation of fluid-flow processes in a 3D high-resolution carbonate reservoir analogue: Petroleum Geoscience, v. 20, no. 1, p. 125-142.

Albert, G., 2017, Aspects of cave data use in a GIS: Cave Investigations, Intech, Rijeka. https://doi. org/10.5772/intechopen, v. 68833, p. 25-44.

Ballesteros, D., Jiménez-Sánchez, M., Giralt, S., DeFelipe, I., and García-Sansegundo, J., 2017, Glacial origin for cave rhythmite during MIS 5d-c in a glaciokarst landscape, Picos de Europa (Spain): Geomorphology, v. 286, p. 68-77.

Becker, R. J., Janković, I., Ahern, J. C., and Komšo, D., 2019, High data density electrical resistivity tomography survey for sediment depth estimation at the Romuald's Cave site: Archaeological Prospection, v. 26, no. 4, p. 361-367.

Bella, P., Gradziński, M., Hercman, H., Leszczyński, S., and Nemec, W., 2020, Sedimentary anatomy and hydrological record of relic fluvial deposits in a karst cave conduit: Sedimentology.

Blott, S. J., and Pye, K., 2001, GRADISTAT: A grain size distribution and statistics package for the analysis of unconsolidated sediments: Earth Surface Processes and Landforms, v. 26, no. 11, p. 1237-1248.

Bögli, A., 1980, Karst hydrology and physical speleology: Springer-Verlag, Berlin, p. 284.

Borghi, A., Renard, P., and Jenni, S., 2010, How to Model Realistic 3D Karst Reservoirs Using a Pseudo-Genetic Methodology–Example of Two Case Studies: Advances in Research in Karst Media, p. 251-255.

Bosch, R. F., and White, W. B., 2004, Lithofacies and transport of clastic sediments in karstic aquifers, Studies of cave sediments, Springer, p. 1-22.

Burchette, T. P., 2012, Carbonate rocks and petroleum reservoirs: a geological perspective from the industry: Geological Society, London, Special Publications, v. 370, no. 1, p. 17-37.

Čeru, T., Šegina, E., Knez, M., Benac, Č., and Gosar, A., 2018, Detecting and characterizing unroofed caves by ground penetrating radar: Geomorphology, v. 303, p. 524-539.

Christanis, K., Georgakopoulos, A., Fernandez-Turiel, J. L., and Bouzinos, A., 1998, Geological factors influencing the concentration of trace elements in the Philippi peatland, eastern Macedonia, Greece: International Journal of Coal Geology, v. 36, no. 3-4, p. 295-313.

Erzeybek Balan, S., 2012, Characterization and modeling of paleokarst reservoirs using multiple-point statistics on a non-gridded basis: Ph.D. Dissertation, The University of Texas at Austin, p. 1-307.

Fabbri, S., Sauro, F., Santagata, T., Rossi, G., and De Waele, J., 2017, High-resolution 3-D mapping using terrestrial laser scanning as a tool for geomorphological and speleogenetical studies in caves: An example from the Lessini mountains (North Italy): Geomorphology, v. 280, p. 16-29.

Farrant, A. R., and Smart, P. L., 2011, Role of sediment in speleogenesis; sedimentation and paragenesis: Geomorphology, v. 134, no. 1-2, p. 79-93.

Feazel, C., 2010, Using modern cave systems as analogs for paleokarst reservoirs: AAPG Search and Discovery Article, v. 50252.

Ford, D. C., and Williams, P. W., 1989, Karst geomorphology and hydrology, Unwin Hyman London.

-, 2002, Karst geomorphology and hydrology, Unwin Hyman London.

Frantz, Y., Collon, P., Renard, P., and Viseur, S., 2021, Analysis and stochastic simulation of geometrical properties of conduits in karstic networks: Geomorphology, v. 377, p. 107480.

Fritz, R. D., Wilson, J. L., and Yurewicz, D. A., 1993, Paleokarst related hydrocarbon reservoirs, SEPM, v. 18.

Gallay, M., Kanuk, J., Hochmuth, Z., Meneely, J. D., Hofierka, J., and Sedlak, V., 2015, Large-scale and high-resolution 3-D cave mapping by terrestrial laser scanning: a case study of the Domica Cave, Slovakia: International Journal of Speleology, v. 44, no. 3, p. 277-291.

GEODATA.gov.gr, 2010, Network of rivers and streams of Greece, Network of rivers and streams of Greece.

Hajna, N. Z., Pruner, P., Mihevc, A., Schnabl, P., and Bosák, P., 2008, Cave Sediments from Postojnska–Planinska Cave System (Slovenia): Evidence of Multi-Phase Evolution in Epiphreatic Zone: Acta carsologica, v. 37, no. 1.

Heeb, B., 2008, Paperless Caving-An Electronic Cave Surveying System La topo sans papier-un système électronique de topographie, IV th European speleological congress: Isére - France.

Henrion, V., Pellerin, J., and Caumon, G., A stochastic methodology for 3D cave systems modeling2008.

Hussain, Y., Uagoda, R., Borges, W., Nunes, J., Hamza, O., Condori, C., Aslam, K., Dou, J., and Cárdenas-Soto, M., 2020, The potential use of geophysical methods to identify cavities, sinkholes and pathways for water infiltration: Water, v. 12, no. 8, p. 2289.

Judson, D., 1974, Cave surveying for expeditions: Geographical Journal, p. 292-300.

Kadlec, J., Chadima, M., Lisa, L., Hercman, H., Osintsev, A., and Oberhaensli, H., 2008, Clastic cave deposits in Botovskaya cave (Eastern Siberia, Russian federation): Journal of Cave and Karst Studies, v. 70, no. 3, p. 142-155.

Karkanas, P., and Goldberg, P., 2017, Cave settings: Encyclopedia of Geoarchaeology; Gilbert, AS, Ed.; Springer: Dordrecht, The Netherlands, p. 108-118.

Kerans, C., 1988, Karst-Controlled Reservoir Heterogeneity in Ellenburger Group Carbonates of West Texas: Aapg Bulletin-American Association of Petroleum Geologists, v. 72, no. 10, p. 1160-1183.

Kim, J., and Yi, M., 2010, DC3DPRO-3D Geoelectrical Modelling and Inversion, User's Manual: KIGAM, Korea.

Li, Y. Q., Hou, J. G., Sun, J. F., Kang, Z. J., Liu, Y. M., Song, S. H., and Han, D., 2018, Paleokarst reservoir features and their influence on production in the Tahe Oilfield, Tarim basin, China: Carbonates and Evaporites, v. 33, no. 4, p. 705-716.

Lomando, A. J., Harris, P. M., and Orlopp, D. E., 1993, Casablanca field, Tarragona Basin, offshore Spain: a karsted carbonate reservoir: Special publications of SEPM.

Lønøy, B., Tveranger, J., Pennos, C., Whitaker, F., and Lauritzen, S.-E., 2020, Geocellular rendering of cave surveys in paleokarst reservoir models: Marine and Petroleum Geology, p. 104652.

Loucks, R. G., 1999, Paleocave carbonate reservoirs: Origins, burial-depth modifications, spatial complexity, and reservoir implications: Aapg Bulletin-American Association of Petroleum Geologists, v. 83, no. 11, p. 1795-1834.

Loucks, R. G., and Mescher, P. K., 2002, Paleocave facies classification and associated pore types: American Association of Petroleum Geologists.

Martini, I., 2011, Cave clastic sediments and implications for speleogenesis: new insights from the Mugnano Cave (Montagnola Senese, Northern Apennines, Italy): Geomorphology, v. 134, no. 3-4, p. 452-460.

Mazzullo, S., and Chilingarian, G., 1996, Hydrocarbon reservoirs in karsted carbonate rocks: Developments in Petroleum Science, v. 44, p. 797-865.

NASA/METI/AIST/Japan Spacesystems, a. U. S. J. A. S. T., 2019, ASTER Global Digital Elevation Model V003, *in* DAAC, N. E. L. P., ed.

Novel, J. P., Dimadi, A., Zervopoulou, A., and Bakalowicz, M., 2007, The Aggitis karst system, Eastern Macedonia, Greece: Hydrologic functioning and development of the karst structure: Journal of Hydrology, v. 334, no. 3-4, p. 477-492.

Palmer, A. N., 1991, Origin and Morphology of Limestone Caves: Geological Society of America Bulletin, v. 103, no. 1, p. 1-21.

Papapetros, P., 1982, Geological map of Greece, scale 1:50000.

Papaphilippou-Pennou, E., 2004, Dynamic evolution and recent exogenic processes of Strymon river network in Serres graben (North Greece) [Ph.D.: Aristotle University of Thessaloniki, 212 p.

Pasini, G., 2009, A terminological matter: paragenesis, antigravitative erosion or antigravitational erosion?: International Journal of Speleology, v. 38, no. 2, p. 4.

Pennos, C., Astaras, T., Vouvalidis, K., Papaphilippou-Pennou, E., and Pechlivanidou, S., 2011, Geomorphological and morphotectonic features of the alluvial fans of the nortern part of the Aggitis river: Bulletin of the Geological Society of Greece, v. 44, p. 29-36.

Pennos, C., Lauritzen, S.-E., Lonoy, B., and Tveranger, J., 2018, A 3D model of a cave collapse from Peristerionas cave, northern Greece: EGUGA, p. 17322.

Pennos, C., Lauritzen, S. E., Pechlivanidou, S., Aidona, E., Haflidason, H., and Sotiriadis, Y., 2016a, Decoding clastic sediment sources from the Maaras Cave Northern Greece, 18th Joint Geomorphological Meeting: Chambery, France.

Pennos, C., Lauritzen, S. E., Pechlivanidou, S., and Sotiriadis, Y., 2016b, Geomorphic constrains on the evolution of the Aggitis river basin Northern Greece (a preliminary report): Bulletin of the Geological Society of Greece, v. 50.

Petalas, C. P., and Moutsopoulos, K. N., 2019, Hydrogeologic Behavior of a Complex and Mature Karst Aquifer System under Drought Condition: Environmental Processes, v. 6, no. 3, p. 643-671.

Plotnick, R. E., Kenig, F., and Scott, A. C., 2015, Using the voids to fill the gaps: caves, time, and stratigraphy: Geological Society, London, Special Publications, v. 404, no. 1, p. 233-250.

Reile, P., Le Karst du Massif du Falakro et la Résurgence de Maaras Résultats des travaux hydrogéologiques et Topographiques, *in* Proceedings 14th International congress of Speleology, Athens, Kalamos, Greece, 2005.

Ringrose, P., and Bentley, M., 2015, Reservoir model design - A practioner´s guide, Springer.

Rongier, G., Collon-Drouaillet, P., and Filipponi, M., 2014, Simulation of 3D karst conduits with an object-distance based method integrating geological knowledge: Geomorphology, v. 217, p. 152-164.

Samouëlian, A., Cousin, I., Tabbagh, A., Bruand, A., and Richard, G., 2005, Electrical resistivity survey in soil science: a review: Soil and Tillage research, v. 83, no. 2, p. 173-193.

Sasowsky, I. D., and Mylroie, J., 2007, Studies of cave sediments: physical and chemical records of paleoclimate, Springer Science & Business Media.

Schlumberger, 2007, Carbonate Reservoirs - Meeting unique challenges to maximize recovery.

Springer, G. S., 2019, Clastic sediments in caves, Encyclopedia of Caves, Elsevier, p. 277-284.

Strebelle, S., 2002, Conditional simulation of complex geological structures using multiple-point statistics: Mathematical geology, v. 34, no. 1, p. 1-21.

Tian, F., Lu, X. B., Zheng, S. Q., Zhang, H. F., Rong, Y. S., Yang, D. B., and Liu, N. G., 2017, Structure and Filling Characteristics of Paleokarst Reservoirs in the Northern Tarim Basin, Revealed by Outcrop, Core and Borehole Images: Open Geosciences, v. 9, no. 1, p. 266-280.

Triantafyllou, A., Watlet, A., Le Mouélic, S., Camelbeeck, T., Civet, F., Kaufmann, O., Quinif, Y., and Vandycke, S., 2019, 3-D digital outcrop model for analysis of brittle deformation and lithological mapping (Lorette cave, Belgium): Journal of Structural Geology, v. 120, p. 55-66.

Tsourlos, P., 1995, Modelling, interpretation and inversion of multielectrode resistivity survey data: University of York.

Tsourlos, P., Szymanski, J., and Tsokas, G., 1998, A smoothness constrained algorithm for the fast 2-D inversion of DC resistivity and induced polarization data: Journal of the Balkan Geophysical Society, v. 1, no. 1, p. 3-13.

Tveranger, J., Disentangeling paleokarst reservoirs (presentation), *in* Proceedings The FORCE Carbonate and Chalk Reservoirs Network Group, Lundin Norway, Oslo, 2019.

Van Gundy, J. J., and White, W. B., 2009, Sediment flushing in Mystic Cave, West Virginia, USA, in response to the 1985 Potomac Valley flood: International Journal of Speleology, v. 38, no. 2, p. 2.

Vavliakis, E., Psilovikos, A., and Sotiriadis, L., 1986, The epigenetic valley of the Aggitis river and its relation with the evolution of Drama and Serres basins: Geological and Geophysical studies (IGME), v. 6, p. 5-14.

White, W. B., 1988, Geomorphology and hydrology of karst terrains, Oxford University Press, v. 551.447 W4, 464 p.:

White, W. B., 2007, Cave sediments and paleoclimate: Journal of Cave and Karst Studies, v. 69, no. 1, p. 76-93.
Zlot, R., and Bosse, M., 2014, Three-dimensional mobile mapping of caves: Journal of Cave & Karst Studies, v. 76, no. 3.
Zou, C., 2013, Carbonate Fracture-Cavity Reservoir, Elsevier, 1-2 p.:

APPENDICES

Data repository

Forward collapse modelling tool

- https://www.researchgate.net/publication/350090407_Forward_collapse_simulation_using_cave_surveys

RMS™ reservoir model

- https://dataverse.no/dataset.xhtml?persistentId=doi:10.18710/QNERVT
- https://www.researchgate.net/publication/350174737_Paleokarst_reservoir_model_of_the_Agios_Georgios_cave_system_in_northern_Greece

Graphic design: Communication Division, UiB / Print: Skipnes Kommunikasjon AS

uib.no

ISBN: 9788230848227 (print)
9788230846865 (PDF)